

1 **Data use policy**

2 We request that the present study be specifically and clearly acknowledged when data sets
3 or data samples are used for data analyses and visualizations in publications, posters, oral
4 presentations, reports, Web pages, and any other types of scientific media. Please cite also the
5 relevant original studies of each used specific data samples

6

7 **1. Supplementary material summary**

8 **1.1. Information detailed in the description of the experimental data sets**

9 To facilitate the use of the soft tissue artifact (STA) data sets provided in the supplementary
10 material, the following information are summarized in paragraph 2 for each data set sample.

11 a) *Data samples name and scientific article\s of reference;*

12 a) *Subject or specimen characteristics* - available information aimed at describing subject
13 characteristics (age, mass, height, body mass index, etc.);

14 b) *Motor task description* - available information aimed at describing the motor task
15 analyzed (e.g. type of motion, gait speed, range of joint motion, tread and rise when step or
16 seat are used, type of footwear, etc.);

17 c) *Experimental data description* - list of the body segments under analysis, skin marker
18 locations, anatomical landmarks (ALs) used (their acronyms are listed in section 3.3, Table
19 {anat_landmk}),

20 d) *Anatomical coordinate system definitions (ACS)*

21 e) *Measurement specifications* - description of the measurement systems and techniques
22 used to process the position data (number of cameras, capture volume, sample frequency,
23 measurement accuracy, etc.);

24 f) *Ground truth* - description of the technique used to determine the ground truth bone pose
25 (measurement accuracy, procedures for calibration, registration, and synchronization
26 between instruments, etc.).

27 g) *STA characterization* - for each marker, a statistical description of the relevant STA is
28 provided according to the proposed metrics. The dispersion of each STA parameter over all
29 available markers is described using a five-number summary technique (minimum, lower
30 quartile, median, upper quartile, and maximum).

31 A total of 31 data sets are described and made available in the supplementary material. When
32 more than a motor task is obtained from the same experimental set-up, the relevant data sets
33 are grouped in a single database and information relative to points *c*, *d*, and *e* are provided
34 only once. If all data sets in a database are relative to the same specimen/subject, also point *a*
35 is reported only once.

36 **1.2. Data storing and exchange: the lexicon**

37 A lexicon is described in paragraph 2 that was used as format for the benchmark data sets
38 shared as supplementary material. It has its roots in a previous lexicon based on the syntactic
39 lexicon, CAMARC DST (Data Storage and Transfer), first proposed for storing and data
40 exchange between laboratories involved in the CAMARC II project (Paul and Morris, 1992;
41 Cappozzo and Della Croce, 1994) and developed within the IST Project (IST-1999-10954),
42 Virtual Animation of the Kinematics of the Human for Industrial, Educational and Research
43 Purposes.

44 The lexicon was devised to store the data in a common data format, relative to position and
45 orientation of upper or lower limb body segments while aiming at a complete description of
46 the kinematics of a motor task. The lexicon is detailed in terms of:

- 47 • Data set storing description (Dataset name; Data information; Measurement Units).
- 48 • Subject description (Subject name; Subject information; Warning; Subject data).
- 49 • Legend tables (owner, motor task, footwear, pathology, side, segment, anatomical
50 landmarks)

51 Data are stored at a pre-elaboration level, to acknowledge the fact that each laboratory used its
52 own experimental protocol to acquire and process the data, described in the following section,
53 and to allow different possible further processing procedures. This format was designed so
54 that data could be exchanged and compared without forcing different laboratories to uniform
55 all protocols and procedures for data processing. This choice does not preclude a user to
56 obtain a final data representation according to his/her interests, without knowing the
57 experimental set-up of the laboratory where data were acquired. A software that reads and
58 processes data coming from different set-ups can be developed and used without any change.
59 For some variables and parameters, to be included in the file, standard names were used
60 (listed in *ad hoc* tables, reported at the end of this document). For further uses of this lexicon,
61 these values can of course be modified or added, if required.

62

63 **2. Description of the experimental data sets**

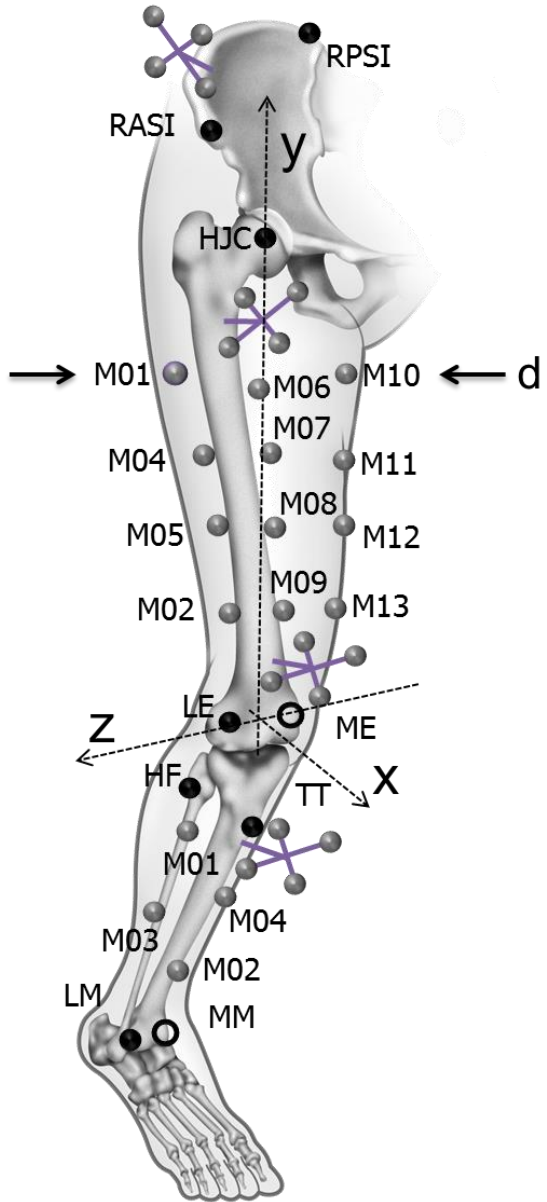
64 **2.1. Ex-vivo data from FOROIT**

65 *Scientific articles of reference* - A detailed description of the original data set can be found
66 in Cereatti et al. (2009), Camomilla et al. (2013) and Bonci et al. (2014).

67 *Experimental data description* - Twelve markers were glued on the thigh skin along two
68 longitudinal lines in antero-lateral and antero-medial positions avoiding the quadriceps
69 muscle bellies. (Fig. 1). The following ALs were calibrated using a pointer equipped with a
70 cluster of four markers: ASIS, PSIS, LE and ME. The hip joint centre (HJC) was determined
71 using a functional approach as described in Cereatti et al. (2009).

72 *Anatomical coordinate system definitions* - Both the pelvic and femoral ACSs were
73 determined according to the definitions proposed in Cappozzo et al. (1995).

74



75

76 **Figure 1** – Thigh markers were positioned along three longitudinal lines in antero-lateral (M01-M04),
 77 anterior (M06-M09), and antero-medial positions (M10-M013). Shank markers were positioned in
 78 frontal (M01, M03) and medial positions (M04, M02). The following ALs (dark circles) were
 79 calibrated using a pointer equipped with a cluster of four markers: RASIS, LASIS, RPSIS, LPSIS, LE,
 80 ME, HF, TT, LM, MM (see definitions in Table 3.3). d is the thigh diameter at the proximal level. The
 81 HJC was determined using a functional approach as described in Cereatti et al. (2009) and the pin
 82 markers.

83

84 *Measurement specifications* - The instantaneous markers position was reconstructed using
 85 a 9-camera stereophotogrammetric system (VICON MX) acquiring at 120 sample/s. The
 86 measurement volume was a 1.5-m-sided cube. A spot-check was performed to assess the
 87 accuracy of the stereophotogrammetric system according to Della Croce and Cappozzo

88 (2000). The marker cluster coordinate system poses relative to the global system of reference
89 were estimated using a SVD technique (Soderkvist and Wedin, 1993).

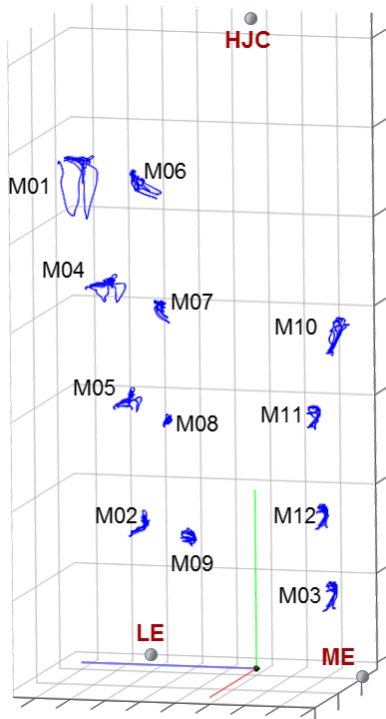
90 *Ground truth* - Two pins equipped with a four marker cluster were implanted into the
91 femur and two into the pelvis. Cruciform incisions were made through the skin and soft issue
92 to reduce forces applied to the pins. Relative angular and linear displacements between pin
93 clusters inserted in the same bone exhibited root mean square values lower than 0.31 deg and
94 0.1mm, respectively.

95 *2.1.1. Data sample 1: Hip joint centre functional movement (Star-Arc)*

96 *Specimen characteristics* - A whole body 75 y.o. adult female cadaver. The diameters of
97 the proximal and distal sections of the thigh were 190 mm and 123 mm, respectively.

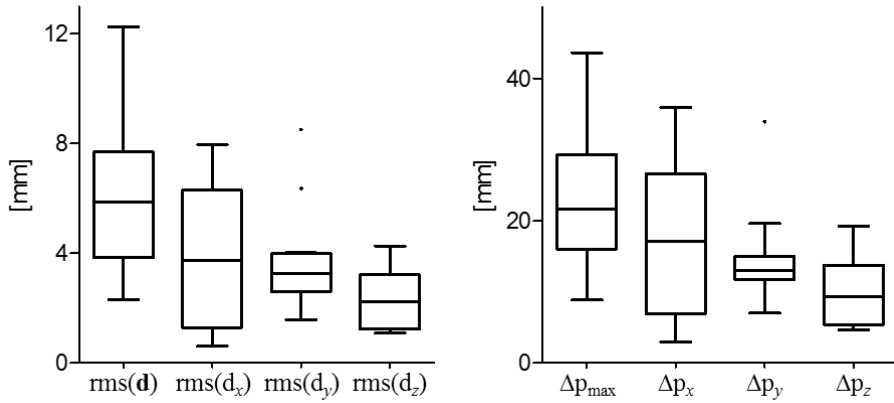
98 *Motor task description* - While the cadaver was lying supine on a table, an operator rotated
99 the right femur with respect to the pelvis. The movements consisted of rotations in the sagittal
100 plane, and in three planes externally rotated about the crano-caudal axis by about 20 deg.
101 This was followed by a half circumduction.

102 *STA characteristics* - Skin-marker trajectories in the thigh ACS are depicted in Fig. 2.
103 Trajectories were filtered with a 2nd-order lowpass Butterworth filter with a cutoff frequency
104 of 10 Hz. Statistical data describing the relevant STAs are shown in Fig. 3. Magnitude of the
105 instantaneous displacement of thigh skin-markers along with the hip joint angular kinematics
106 are depicted in Fig. 4.

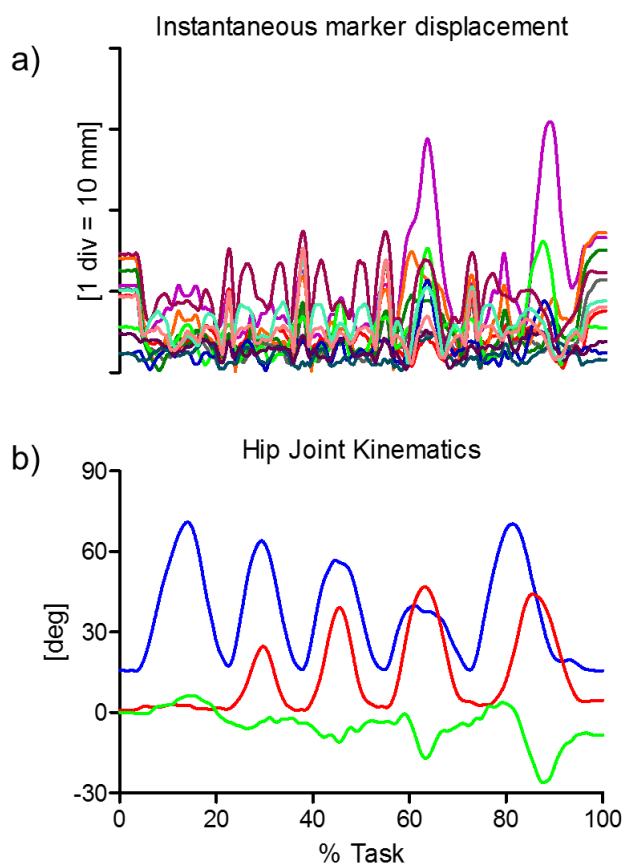


107
108 **Figure 2 – HIP JOINT CENTRE FUNCTIONAL MOVEMENT** Femur ACS, relevant ALs,
109 and skin-marker trajectories (represented in blue). The axes of the ACS are represented in red, green, and blue

110 for the x (antero/posterior, div = 50 mm), y (superior/inferior, div = 50 mm), and z (right/left, div = 20
 111 mm) directions, respectively.



112
 113 **Figure 3 – HIP JOINT CENTRE FUNCTIONAL MOVEMENT** Box-plots of the eight parameters
 114 (rms(d), rms(d_x), rms(d_y), and rms(d_z), in the left panel; Δp_{max}, Δp_x, Δp_y, and Δp_z, in the right panel)
 115 that describe the STA affecting the twelve skin-markers on the thigh during the movement. Outliers
 116 are also depicted.
 117



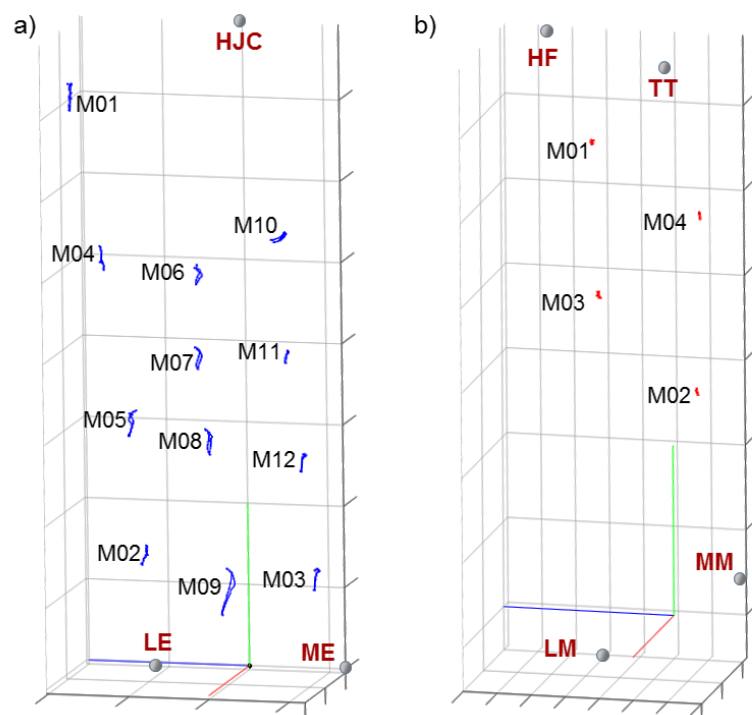
118
 119 **Figure 4 – HIP JOINT CENTRE FUNCTIONAL MOVEMENT** a) Magnitude of the instantaneous
 120 displacement of the twelve skin-markers glued on the thigh and represented in the femur ACS. b)
 121 Relevant hip joint kinematics computed according to the convention proposed by Grood and Suntay
 122 (1983) (flexion/extension, ab/adduction and internal/external rotation in blue, red and green,
 123 respectively; flexion, abduction and internal rotation are positive).
 124

125 2.1.2. Data sample 3: Hip and knee flexion/extension

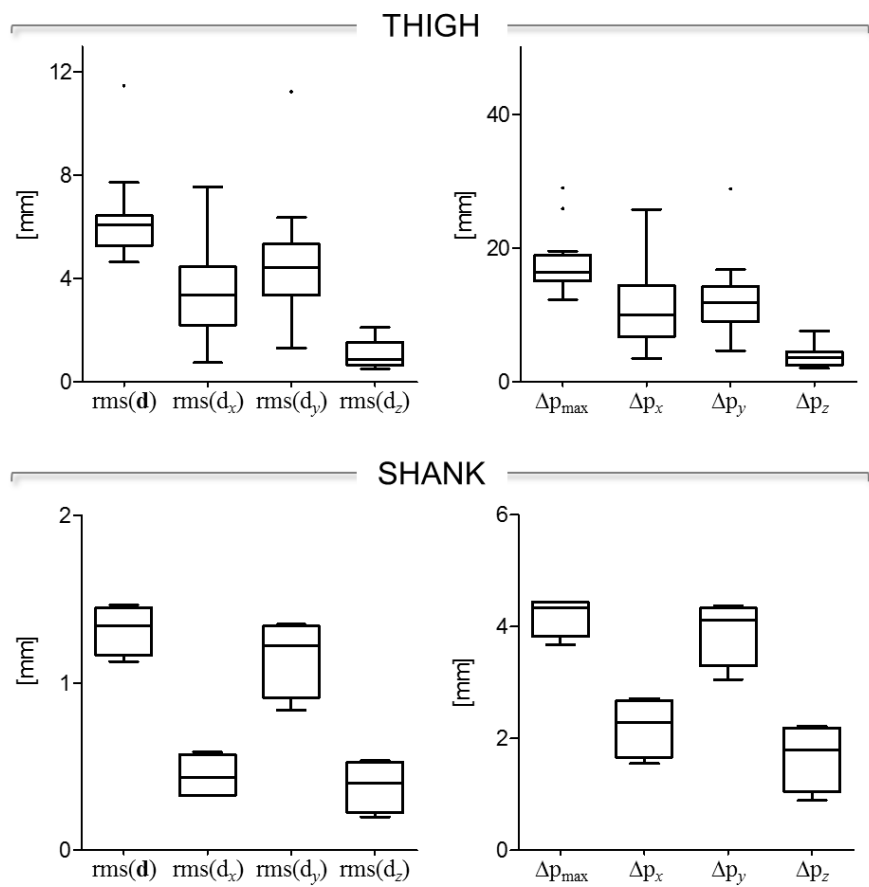
126 *Specimen characteristics* - A whole body 80 y.o. adult male cadaver. The diameters of the
 127 proximal and distal sections of the thigh were 161 mm and 105 mm, respectively.

128 *Motor task description* - While the cadaver was lying supine on a table, an operator moved
 129 the foot with respect to the pelvis, making the hip and knee to flex and the extend back.

130 *STA characteristics* - Skin-marker trajectories in the thigh and shank ACSs are depicted in
 131 Fig. 5. Trajectories were filtered with a 2nd-order lowpass Butterworth filter with a cutoff
 132 frequency of 10 Hz. Statistical data describing the relevant STAs are shown in Fig. 6.
 133 Magnitude of the instantaneous displacement of thigh and shank skin-markers along with the
 134 hip and knee joint angular kinematics are depicted in Fig. 7.

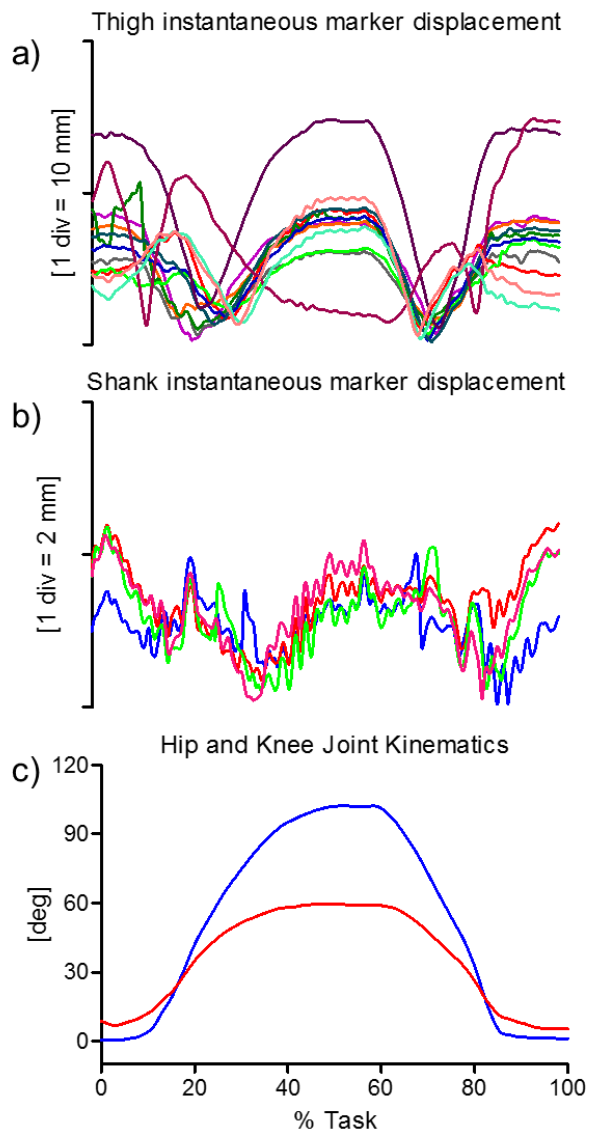


137 **Figure 5 – HIP AND KNEE FLEXION/EXTENSION** Femur (a) and tibial (b) ACSs, relevant ALs,
 138 and thigh and shank skin-marker trajectories (represented in blue and red, respectively). The axes of
 139 the ACSs are represented in red, green, and blue for the x (antero/posterior, div = 50 mm), y
 140 (superior/inferior, div = 50 mm), and z (right/left, a) div = 50 mm; b) div = 20 mm) directions,
 141 respectively.



143

144 **Figure 6 – HIP AND KNEE FLEXION/EXTENSION** Box-plots of the eight parameters ($\text{rms}(\mathbf{d})$,
145 $\text{rms}(\mathbf{d}_x)$, $\text{rms}(\mathbf{d}_y)$, and $\text{rms}(\mathbf{d}_z)$, in the left panel; Δp_{\max} , Δp_x , Δp_y , and Δp_z , in the right panel)
146 that
147 describe the STA affecting the twelve and four skin-markers on the thigh and the shank, respectively,
148 during the movement. Outliers are also depicted.



149

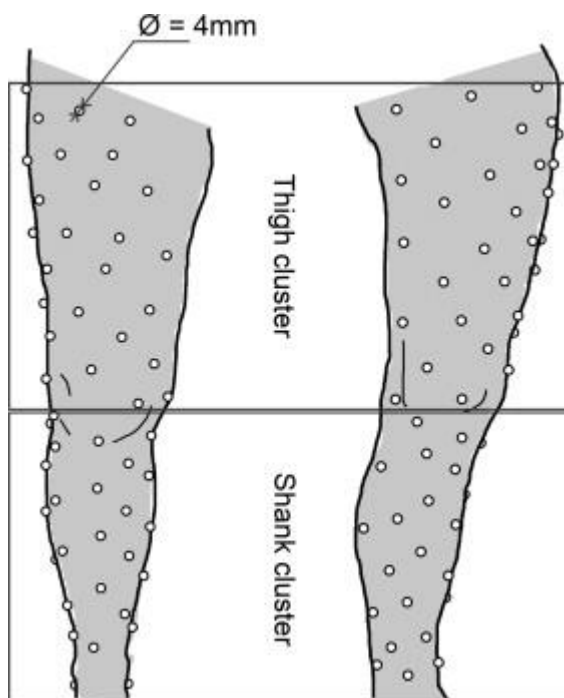
150 **Figure 7 – HIP AND KNEE FLEXION/EXTENSION** Magnitude of the instantaneous displacement
 151 of the twelve and four skin-markers glued on the thigh (a) and shank (b) represented in the relevant
 152 ACS. c) Relevant hip and knee joint kinematics computed according to the convention proposed by
 153 Grood and Suntay (1983) (hip and knee flexion/extension in red and blue, respectively; flexion is
 154 positive).

155

156 **2.2. In-vivo data from LMAM**

157 *Scientific articles of reference* - A detailed description of the original data set can be found
158 in Barré et al. (2013) and Barré et al. (2015).

159 *Experimental data description* - 80 markers were attached to thigh and shank, with at least
160 35 markers for each body segment. The reciprocal distance between markers (diameter = 4
161 mm) varied between 25–40 mm (Fig. 8).



162
163 **Figure 8** – Frontal (left) and sagittal (right) representation of the marker distribution for one specific
164 subject. Some shank markers were also apposed on the medial part.
165

166 *Anatomical coordinate system definitions* - ACSs were defined using the prosthesis
167 coordinate systems of the femoral and tibial components: the horizontal lateral axis of the
168 femoral component, the vertical axis of the tibial component, designed to support the
169 polyethylene rotating platform (Barré et al., 2013).

170 *Measurement specifications* - The instantaneous markers position was reconstructed using
171 a 7-camera stereophotogrammetric system (VICON MX3+) acquiring at 240 sample/s. The
172 measurement volume was a 2-m-sided cube. A spot-check was performed to assess the
173 accuracy of the stereophotogrammetric system according to Della Croce and Cappozzo, 2000.

174 *Ground truth* - Two fluoroscopes (BV Pulsera 300, Philips, NL) were configured to
175 acquire X-ray images at a maximal frame rate of 30 sample/s. To correct for distortions in the
176 X-ray images, a calibration was performed using a calibration plate. Synchronization between
177 fluoroscopes and stereo-photogrammetric systems was performed a posteriori using an

178 additional X-ray detector providing a synchronous signal (delay of less than 0.4 ms between
179 samples for both systems). To compute the transformation between both systems, calibration
180 was performed with three reflective markers attached to a box located at the centre of the
181 system and visible by each system using a least squares method. Applied on the dataset of this
182 study, the average residual for this method is less than 0.08 mm with a SD below 0.03 mm.

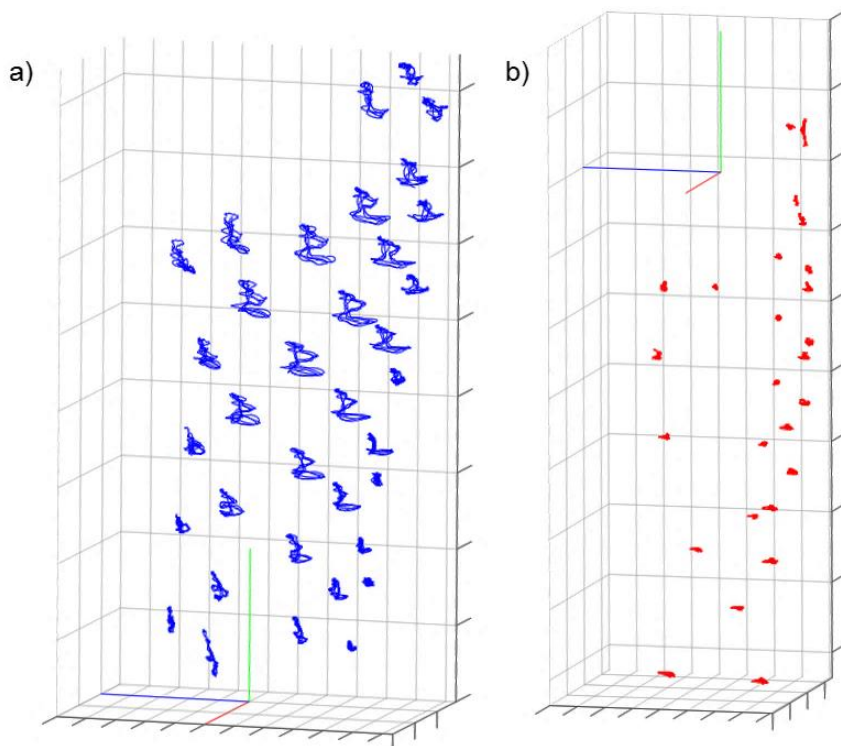
183 2.2.1. *Data sample 8: Treadmill waking*

184 *Subject characteristics* - A 75 y.o. male subject with a total knee prosthesis. Height = 1.67
185 m, mass = 65 kg.

186 *Motor task description* - Static acquisition in the upright position was followed by a
187 treadmill gait acquisition at a self-defined comfortable speed (5.8 m/s) over 15 seconds.

188 *STA characteristics* - Skin-marker trajectories in the thigh and shank ACSs are depicted in
189 Fig. 9. A recursive digital filter was used which corresponded to a low-pass filter with a cutoff
190 frequency of 9Hz. Statistical data describing the relevant STAs are shown in Fig. 10.
191 Magnitude of the instantaneous displacement of thigh and shank skin-markers along with the
192 knee joint angular kinematics are depicted in Fig. 11.

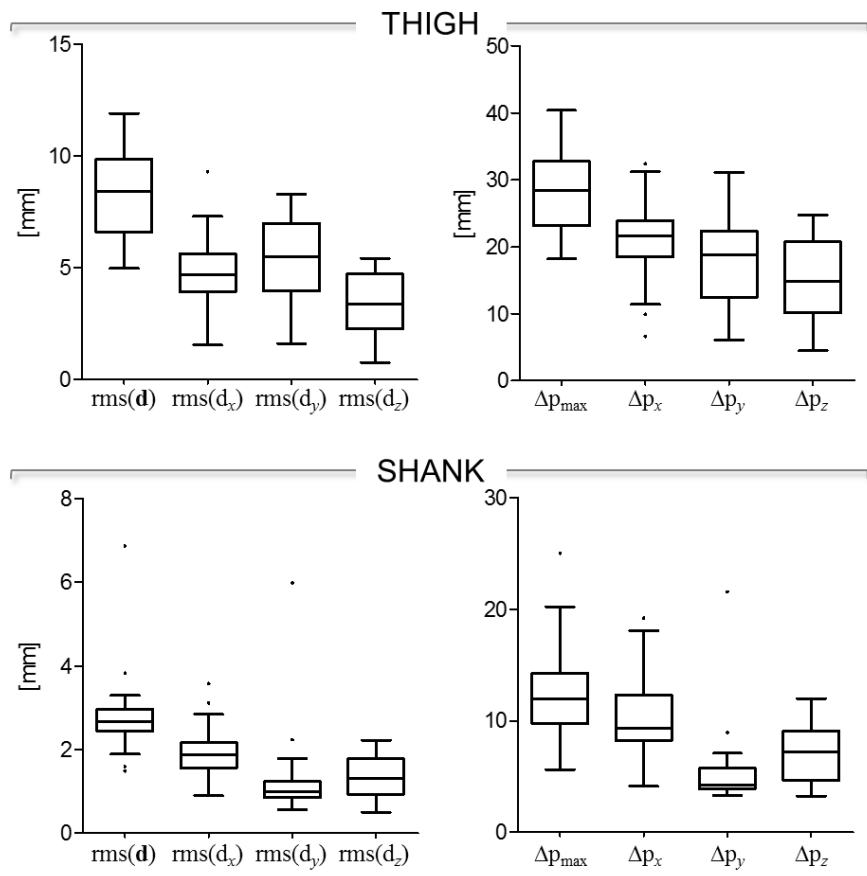
193



194

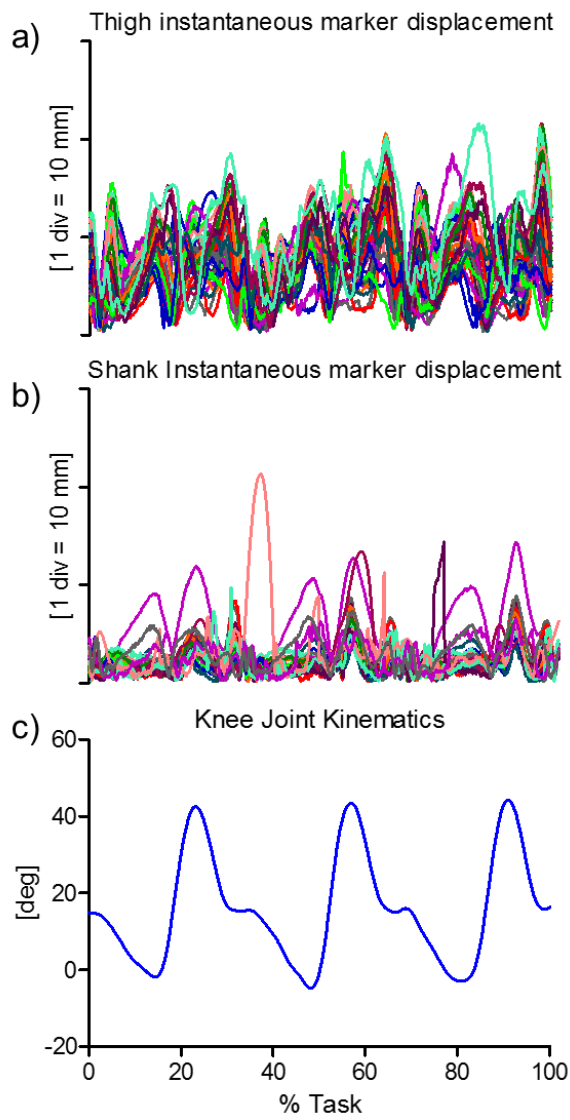
195 **Figure 9 – TREADMILL WAKING** Femur (a) and tibial (b) ACSs, and thigh and shank skin-marker
196 trajectories (represented in blue and red, respectively). The axes of the ACSs are represented in red,
197 green, and blue for the x (antero/posterior, div = 50 mm), y (superior/inferior, div = 50 mm), and z
198 (right/left, div = 20 mm) directions, respectively.

199



200
201
202
203
204
205

Figure 10 – TREADMILL WAKING Box-plots of the eight parameters ($\text{rms}(\mathbf{d})$, $\text{rms}(\mathbf{d}_x)$, $\text{rms}(\mathbf{d}_y)$, and $\text{rms}(\mathbf{d}_z)$, in the left panel; Δp_{\max} , Δp_x , Δp_y , and Δp_z , in the right panel) that describe the STA affecting the thirty-five and twenty-six skin-markers on the thigh and the shank, respectively, during the movement. Outliers are also depicted.



206

207 **Figure 11 – TREADMILL WAKING** Magnitude of the instantaneous displacement of the thirty-five
 208 and twenty-six skin-markers glued on the thigh (a) and shank (b) represented in the relevant ACS. c)
 209 Relevant knee joint kinematics computed according to the convention proposed by Grood and Suntay
 210 (1983) (flexion/extension in blue, with flexion as positive).

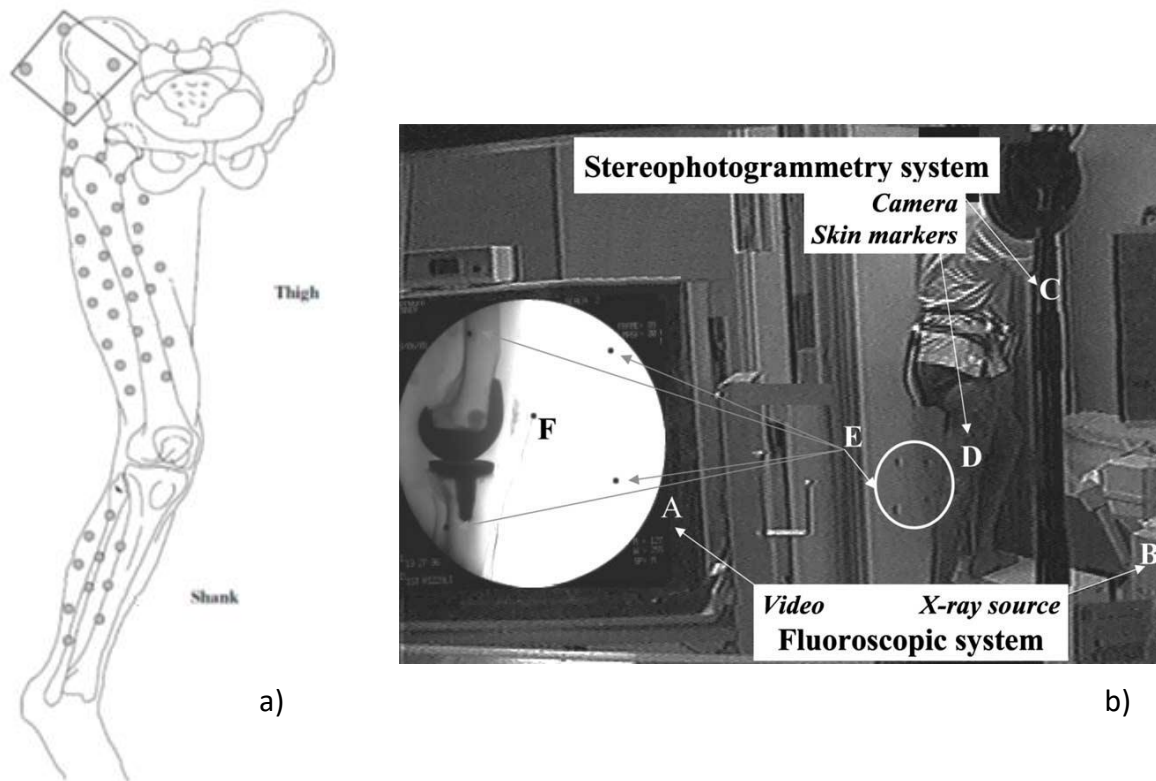
211

212 2.3. ***In-vivo data from UNIBO***

213 *Scientific articles of reference* - A detailed description of the original data set can be found
 214 in Stagni et al. (2005).

215 *Experimental data description* - A cluster of reflecting skin markers was attached to the
 216 lateral aspect of thigh and shank (19 and 10, respectively). The clusters were 4–5 cm spaced
 217 grids of markers with a diameter of 0.6 cm. One rigid plate with four markers was attached to
 218 the pelvis using a modified Milwaukee orthosis (Fig. 12). A static up-right posture was
 219 acquired. The position of 10 anatomical landmarks (right and left anterior iliac spines,
 220 sacrum, greater trochanter, lateral and medial epicondyles, tibial tuberosity, head of fibula,
 221 lateral and medial malleoli) was calibrated with respect to the relevant cluster of markers.
 222 Two repetitions were collected for each of the listed motor tasks.

223 *Anatomical coordinate system definitions* – ACSs were defined according to the CAST
 224 protocol (Benedetti et al., 1998).



225
 226 **Figure 12** a) skin marker distribution on thigh and shank, marker numbers are reported in Figure 13;
 227 b) Experimental set-up: A. real-time visible feed-back of the fluoroscopic images acquired. B. X-rays
 228 sourced of the fluoroscope. C. one of the five cameras of the stereophotogrammetric system. D. skin
 229 markers on the lateral aspect of the thigh and shank. E. the four specialized radiopaque/reflecting
 230 markers for spatial registration. F. the four specialized radiopaque/reflecting marker for temporal
 231 registration

232 *Measurement specifications* - The marker trajectories were collected at 50 frames per
233 second by means of a stereophotogrammetric system with 5 TV cameras (Smart, e-Motion,
234 Padova, Italy). The stereophotogrammetric calibrated field of view was 1.5 x 1.5 x 1 m.

235 *Ground truth* - The subjects performed each motor task with the knee under analysis inside
236 the fluoroscopic 32 cm field of view. Five additional specialized reflecting and radiopaque
237 markers, visible to stereophotogrammetric and fluoroscopic systems, with a diameter of 1.2
238 cm were used. Four of these were placed on a plane parallel to the image plane of the
239 fluoroscope for spatial registration of the two measurement systems. The fifth was attached to
240 the skin over the patella for temporal synchronization. The 3D pose (position and orientation)
241 of the prosthesis components was reconstructed by means of the 2D fluoroscopic projections
242 and CAD models of the prosthesis components. Series of images were acquired at nominal 6
243 samples per second with a standard fluoroscope (DRS, System 1694 D, General Electric
244 CGR, Issy-les-Moulineaux, France). The images were printed out on films and digitised by
245 means of a scanner (Scanmaster DX, Howtek, Hudson, NH, USA). Moreover, images of a 3D
246 cage of plexiglas with 18 tantalum balls in known positions and of a rectangular grid of lead
247 balls 10 mm apart were collected in order to calculate respectively the position of the camera
248 focus and the parameters necessary for image distortion correction. This was obtained using a
249 global spatial warping technique (Gronenschild, 1997). An established technique for 3D
250 kinematics analysis of a known object from a single view was implemented (Banks and
251 Hodge, 1996). Prosthesis component poses in space were obtained from each fluoroscopic
252 image by an iterative procedure using a technique based on CAD-model shape matching. To
253 test for the process accuracy, the femoral and tibial components of the same prosthesis
254 implanted in the subjects of the present study (Optetrak PS-cemented, Exactech Inc.,
255 Gainesville, FL, USA) were fixed in an unknown relative pose using bone-cement.
256 Fluoroscopic images were taken in five different positions within the field of view. The
257 relative pose of the two components in each image was estimated using the method described.
258 These estimates were compared with the ones obtained by a 3D digitizer (MicroScribe,
259 Immersion, San Jose, CA, USA), with nominal accuracy of 0.2 mm. The femoral component
260 was held fixed to a workbench and the coordinates of about 38000 and 23000 points were
261 collected on both the femoral and tibial component surfaces, respectively. The Iterative
262 Closest Point technique (Besl and McKay, 1992) was used for surface rigid registration
263 between the points digitized and the relevant prosthesis component CAD model. Then, the
264 relative pose between the two registered CAD models was calculated. The results showed that
265 the accuracy with which relative orientation and position of the components can be estimated

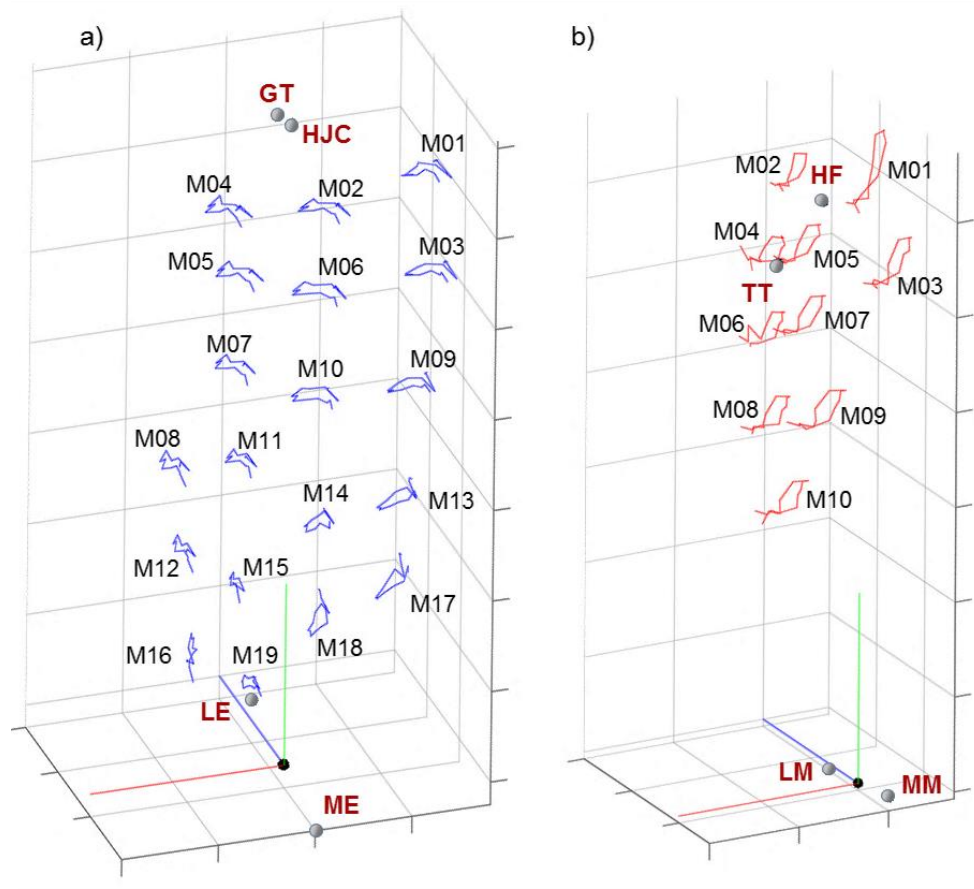
266 is better than 1.5 and 1.5 mm respectively, as good as those previously obtained (Banks and
267 Hodge, 1996). Spatial registration between the stereophotogrammetric and fluoroscopic
268 measurement systems was obtained by defining a common absolute reference coordinate
269 system by means of the four radiopaque and reflecting markers. The temporal synchronization
270 was obtained by matching the fluoroscopic trajectories with the resampled
271 stereophotogrammetric ones of the fifth specialized marker. The matching was obtained by
272 calculating the maximum cross-correlation between the two trajectories, considering the
273 resampling frequency and the starting frame as the parameters to be determined. The possible
274 misalignment of the prosthesis components with respect to the relevant anatomical coordinate
275 system was calculated in the static up-right posture, considered as reference position. This
276 misalignment, if present, is due to surgery. The fluoroscopy-based 3D pose of the anatomical
277 coordinate system was calculated accordingly.

278 *2.3.1. Data samples 6,14,17: knee extension against gravity, sit-to-stand/stand-to-sit,
279 step up/down*

280 *Subject characteristics* - A 67 y.o. female subject with total knee replacement. Height =
281 1.55 m, mass = 58 kg.

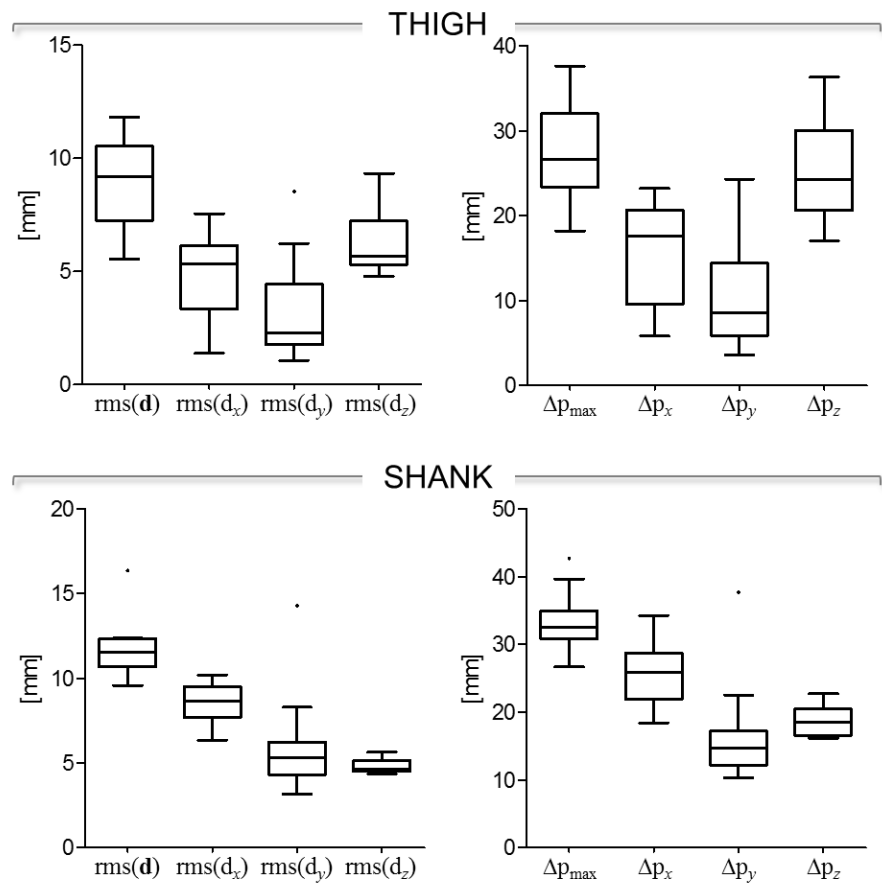
282 *Motor task description* - Knee extension against gravity performed in up-right posture with
283 the hip held flexed at approximately 45 deg, sit-to-stand/stand-to-sit, step up/down.

284 *STA characteristics* - Skin-marker trajectories in the thigh and shank ACSs are depicted in
285 Figs. 13, 16, 19, for knee extension against gravity, sit-to-stand/stand-to-sit and, step
286 up/down, respectively. Stereophotogrammetric data were acquired at 50 Hz and fluoroscopic
287 data at 6Hz, thus synchronized data were all down-sampled at 6 Hz. Statistical data describing
288 the relevant STAs are shown in Figs. 14, 17, 20, for knee extension against gravity, sit-to-
289 stand/stand-to-sit and, step up/down, respectively. For each motor task, the magnitude of the
290 instantaneous displacement of thigh and shank skin-markers along with the knee joint angular
291 kinematics are depicted in Figs. 15, 18, 21, for knee extension against gravity, sit-to-
292 stand/stand-to-sit and, step up/down, respectively.



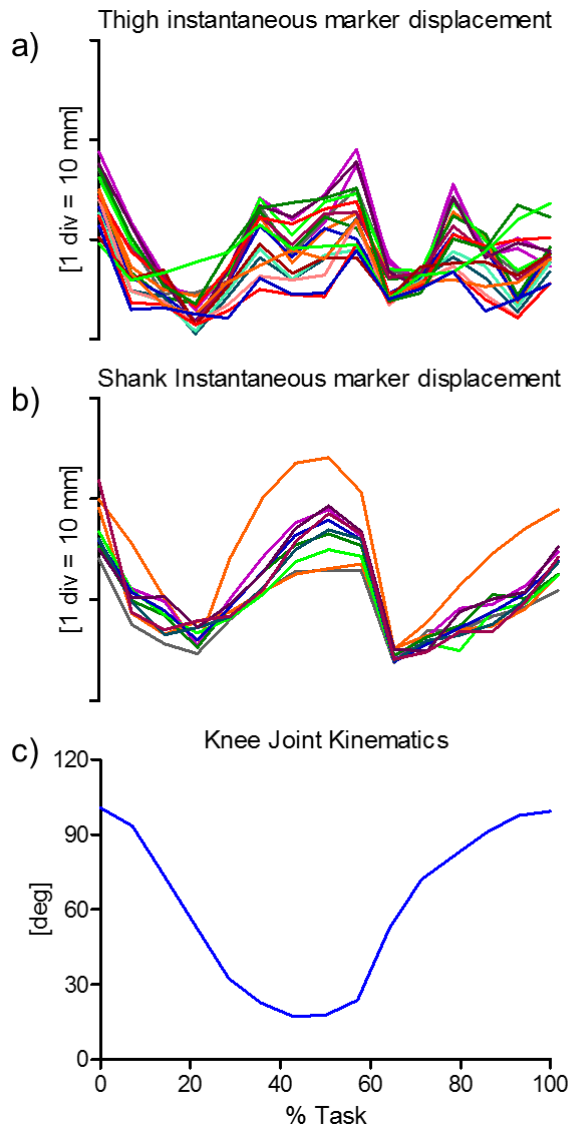
293

294 **Figure 13 – KNEE EXTENSION AGAINST GRAVITY.** Femur (a) and tibial (b) ACSs, relevant
 295 ALs, and thigh and shank skin-marker trajectories (represented in blue and red, respectively). The axes
 296 of the ACSs are represented in red, green, and blue for the x (antero/posterior, div = 50 mm), y
 297 (superior/inferior, div = 50 mm), and z (right/left, div = 50 mm) directions, respectively.
 298



299

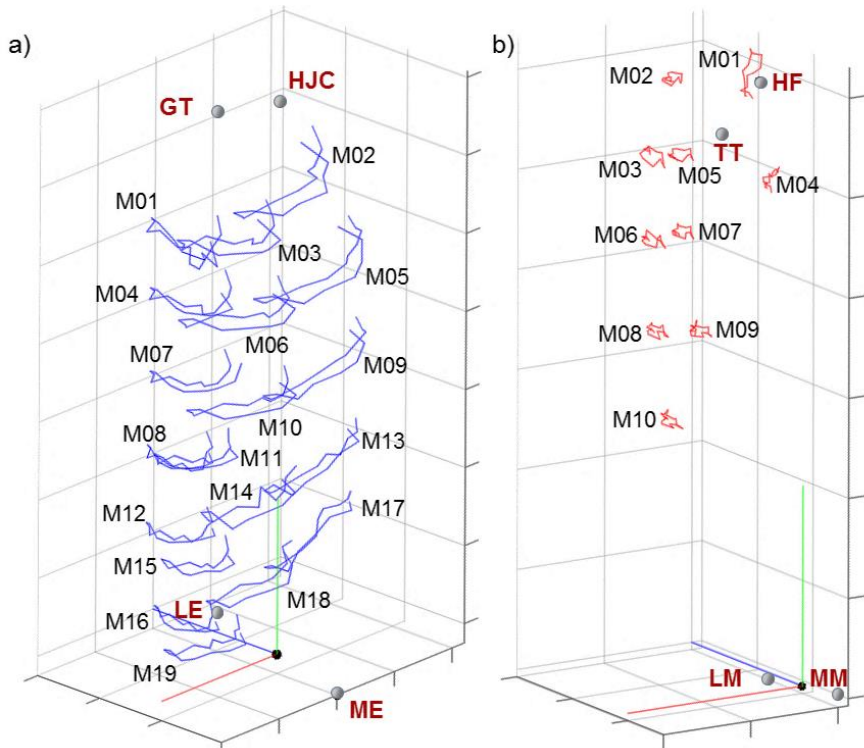
300 **Figure 14 – KNEE EXTENSION AGAINST GRAVITY.** Box-plots of the eight parameters (rms(d),
 301 rms(d_x), rms(d_y), and rms(d_z), in the left panel; Δp_{\max} , Δp_x , Δp_y , and Δp_z , in the right panel)
 302 that
 303 describe the STA affecting the nineteen and ten skin-markers on the thigh and the shank, respectively,
 during the movement. Outliers are also depicted.



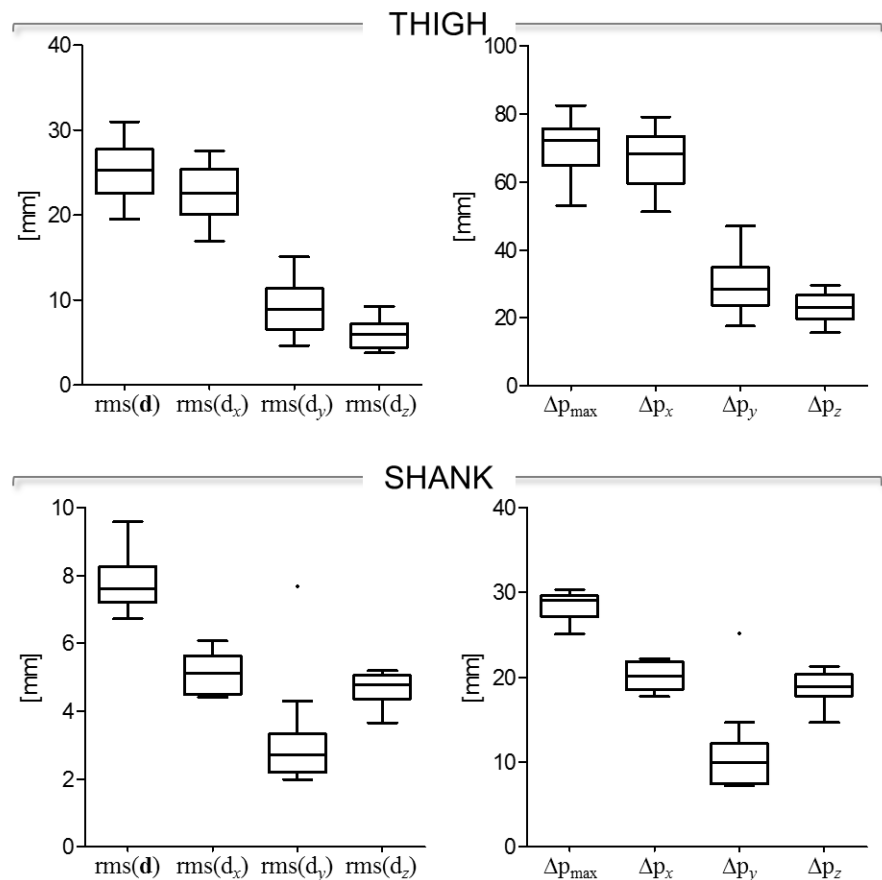
304

305 **Figure 15 – KNEE EXTENSION AGAINST GRAVITY.** Magnitude of the instantaneous
 306 displacement of the nineteen and ten skin-markers glued on the thigh (a) and shank (b) represented in
 307 the relevant ACS. c) Relevant knee joint kinematics computed according to the convention proposed
 308 by Grood and Suntay (1983) (flexion/extension in blue, with flexion as positive).

309

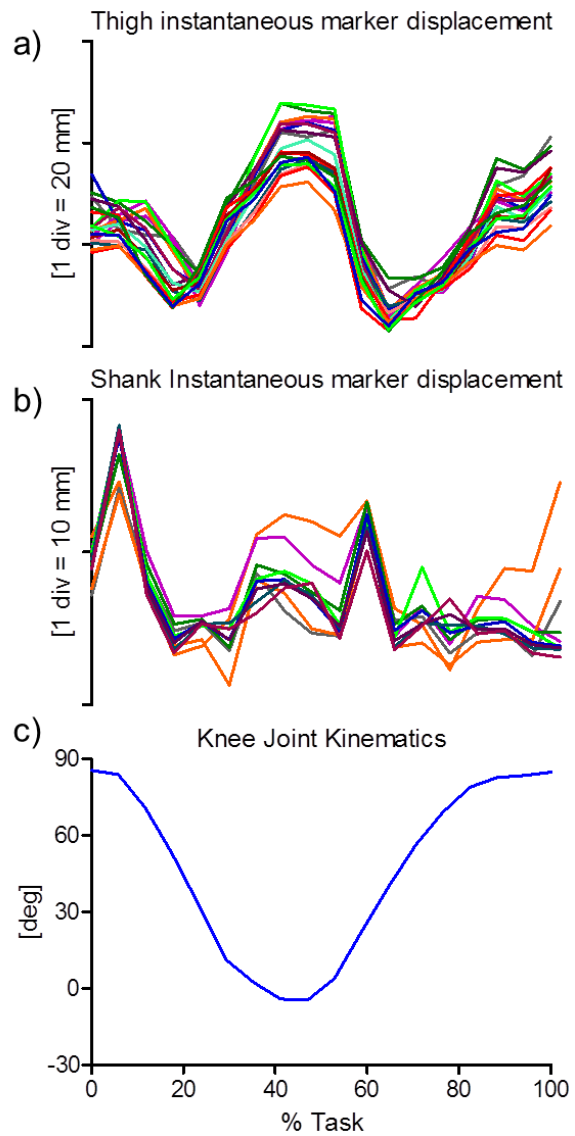


310
 311 **Figure 16 – SIT-TO-STAND/STAND-TO-SIT.** Femur (a) and tibial (b) ACSs, relevant ALs,
 312 and thigh and shank skin-marker trajectories (represented in blue and red, respectively). The axes of the
 313 ACSs are represented in red, green, and blue for the x (antero/posterior, div = 50 mm), y
 314 (superior/inferior, div = 50 mm), and z (right/left, div = 50 mm) directions, respectively.
 315
 316
 317



318
319
320
321
322

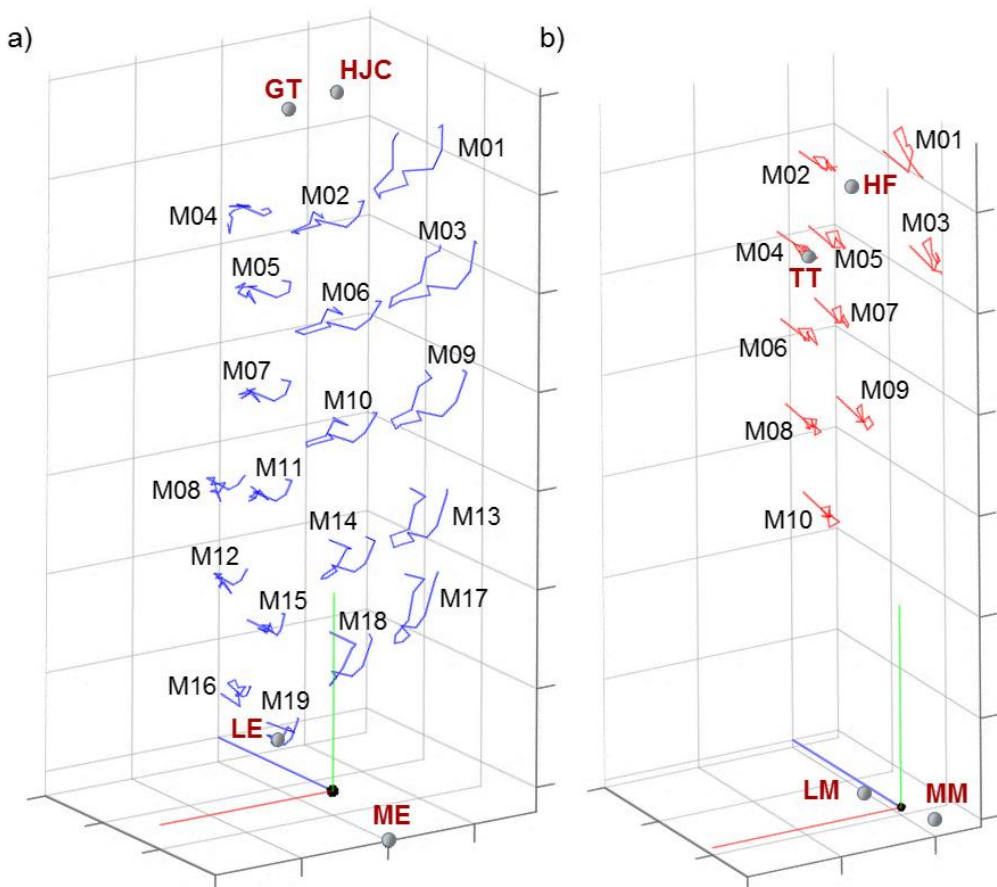
Figure 17 – SIT-TO-STAND/STAND-TO-SIT. Box-plots of the eight parameters ($\text{rms}(\mathbf{d})$, $\text{rms}(\mathbf{d}_x)$, $\text{rms}(\mathbf{d}_y)$, and $\text{rms}(\mathbf{d}_z)$, in the left panel; Δp_{\max} , Δp_x , Δp_y , and Δp_z , in the right panel) that describe the STA affecting the nineteen and ten skin-markers on the thigh and the shank, respectively, during the movement. Outliers are also depicted.



323

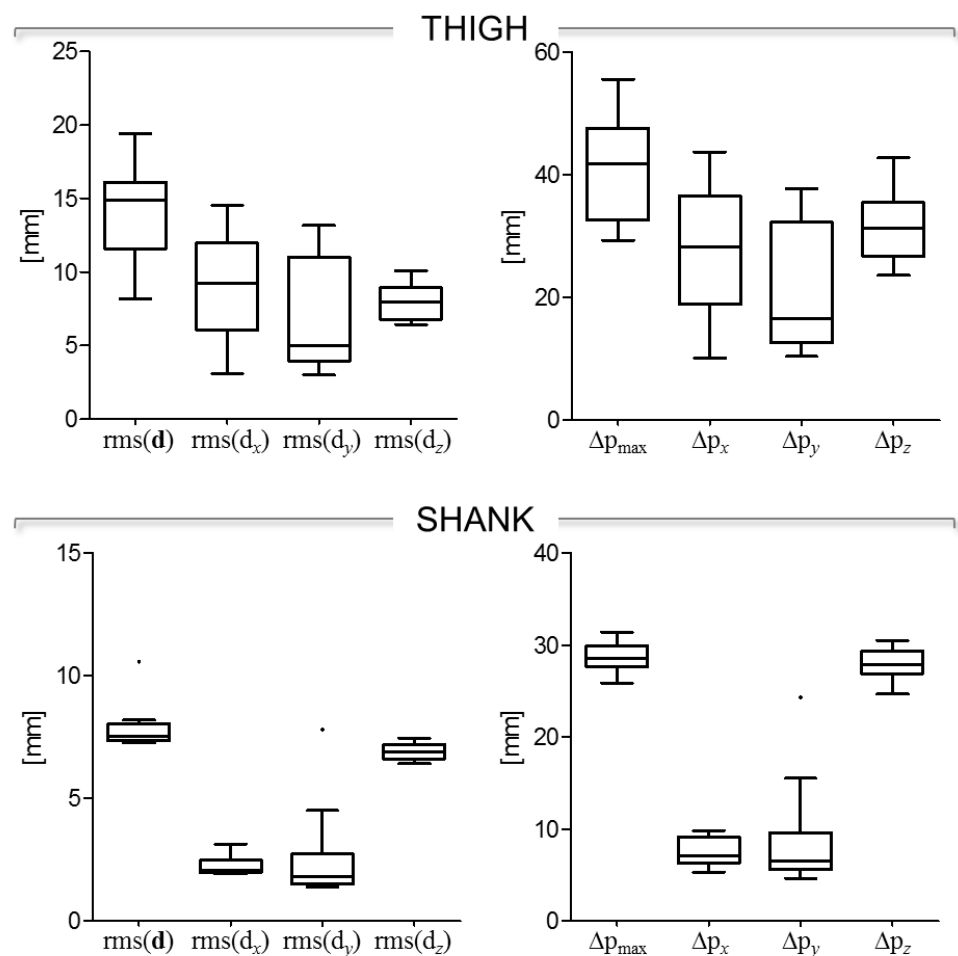
324 **Figure 18 – SIT-TO-STAND/STAND-TO-SIT.** Magnitude of the instantaneous displacement of the
 325 nineteen and ten skin-markers glued on the thigh (a) and shank (b) represented in the relevant ACS. c)
 326 Relevant knee joint kinematics computed according to the convention proposed by Grood and Suntay
 327 (1983) (flexion/extension in blue, with flexion as positive).

328



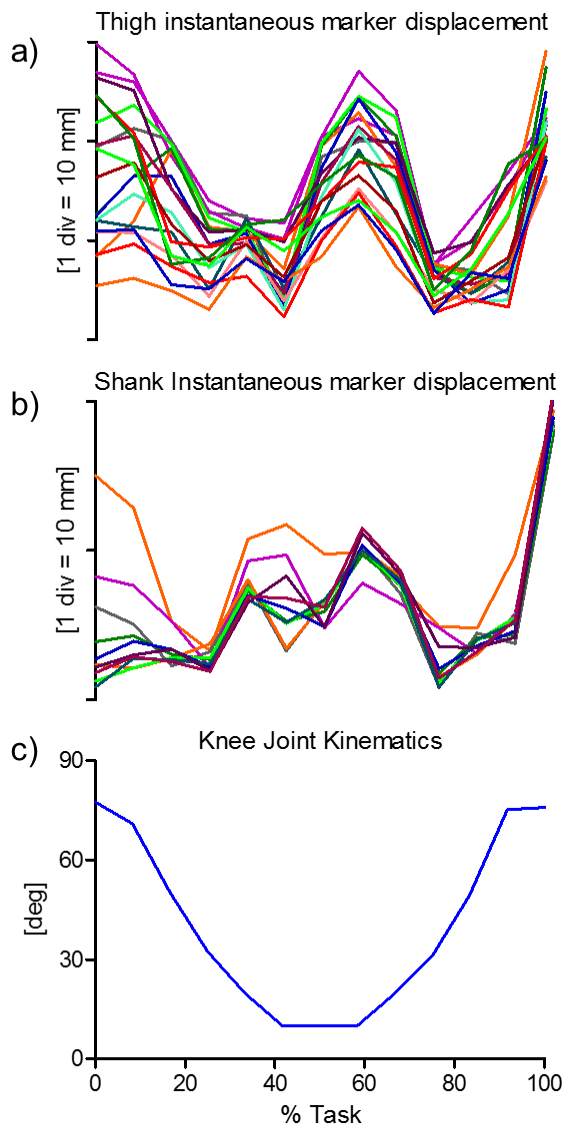
329

330 **Figure 19** – STEP UP/DOWN. Femur (a) and tibial (b) ACSs, relevant ALs,
 331 and thigh and shank skin-marker trajectories (represented in blue and red, respectively). The axes of the ACSs are
 332 represented in red, green, and blue for the x (antero/posterior, div = 50 mm), y (superior/inferior, div =
 333 50 mm), and z (right/left, div = 50 mm) directions, respectively.
 334



335
336
337
338
339

Figure 20 – STEP UP/DOWN. Box-plots of the eight parameters ($\text{rms}(\mathbf{d})$, $\text{rms}(\mathbf{d}_x)$, $\text{rms}(\mathbf{d}_y)$, and $\text{rms}(\mathbf{d}_z)$, in the left panel; Δp_{\max} , Δp_x , Δp_y , and Δp_z , in the right panel) that describe the STA affecting the nineteen and ten skin-markers on the thigh and the shank, respectively, during the movement. Outliers are also depicted.



340

341 **Figure 21 – STEP UP/DOWN.** Magnitude of the instantaneous displacement of the nineteen and ten
 342 skin-markers glued on the thigh (a) and shank (b) represented in the relevant ACS. c) Relevant knee
 343 joint kinematics computed according to the convention proposed by Grood and Suntay (1983)
 344 (flexion/extension in blue, with flexion as positive).

345

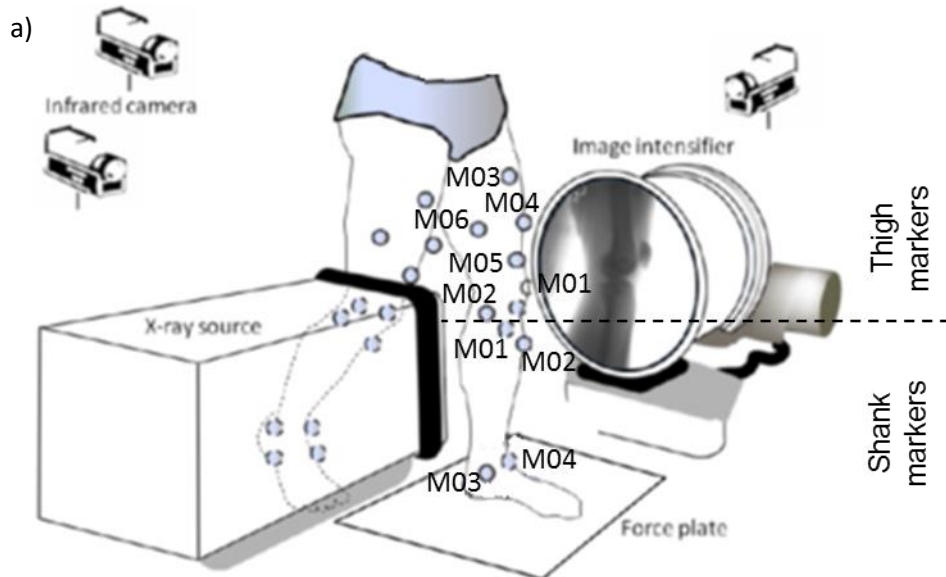
346 **2.4. *In-vivo data from NTU***

347 *Scientific articles of reference* - A detailed description of the original data set can be found
348 in Tsai et al. (2009, 2011) and in Kuo et al. (2011).

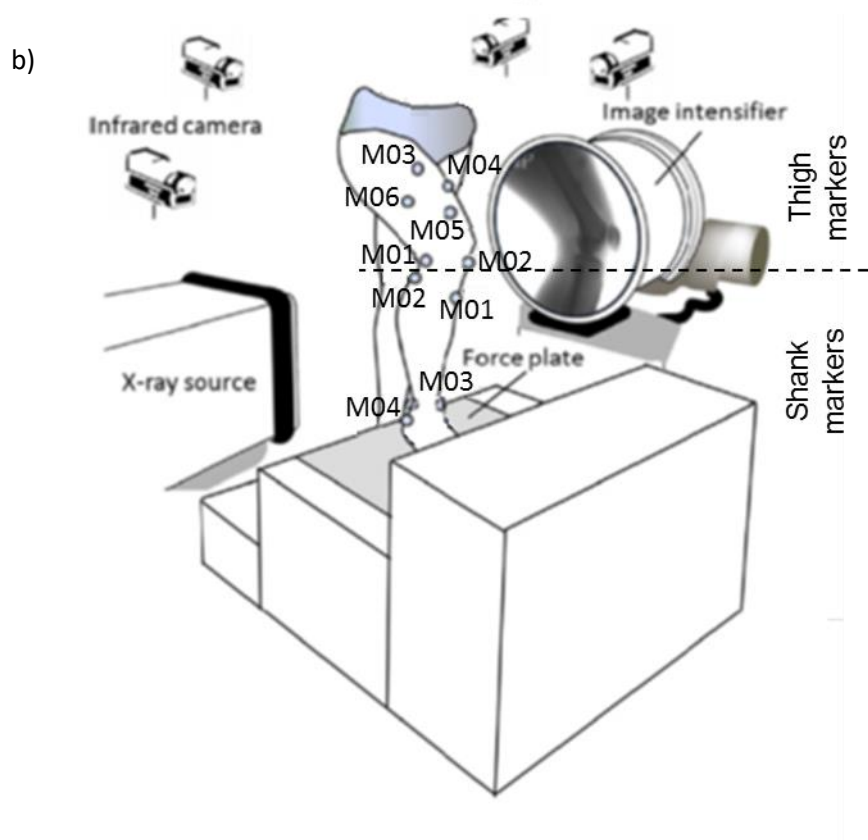
349 *Experimental data description* - Ten markers were used to track the motion of the thigh
350 (MFC and LFC were renamed as ME and LE in the available data for coherence with the
351 adopted lexicon; thigh markers: T1, T2, T3, and T4) and shank (TT, FH, MMA, and LMA;
352 the latter two were renamed as MM and LM in the available data for coherence with the
353 adopted lexicon); markers are depicted in Fig. 22 for the different motor tasks. Data for the
354 subjects standing at the anatomical position were also collected.

355 *Anatomical coordinate system definitions* – ACSs for the bones were defined based on the
356 anatomical features of the bones following the literature (Miranda et al., 2010).

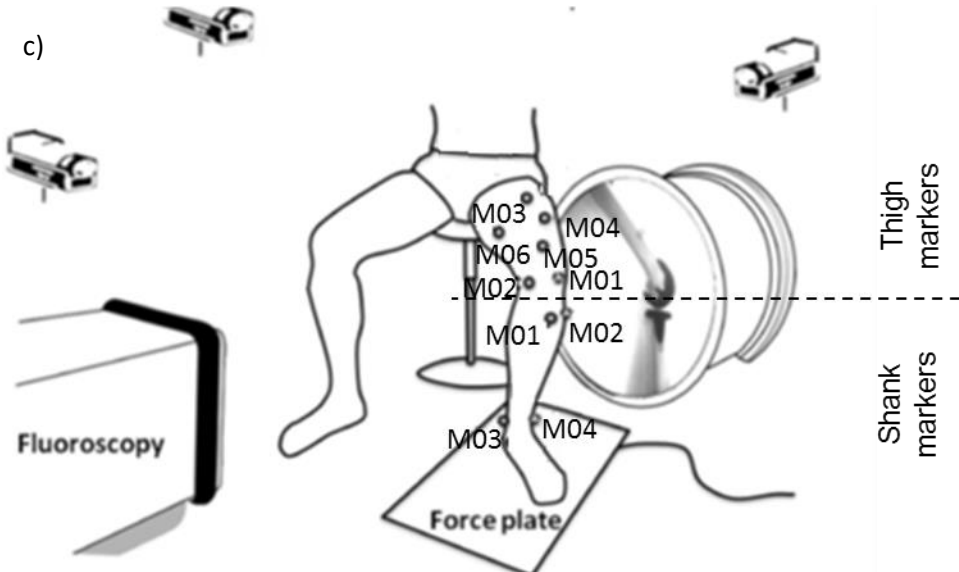
357



358



359



360

361

362

363 **Figure 22** A subject performing (a) overground walking (b) stair ascending and (c) sit-to-stand tasks
 364 while kinematic data were measured using a 7-camera stereophotogrammetry system and a
 365 fluoroscopy system and kinetic data using a force plate. The cameras shown are schematic
 366 representation whereas in the real life situations, the cameras were placed around the subjects without
 367 interfering with the activities. The following ALs were manually identified and equipped with
 368 markers: RASIS, LASIS, RPSIS, LPSIS, ME, LE, HF, TT, LM, MM (see definitions in Table 3.3).
 369 Some markers were affixed onto anatomical landmarks (thigh: M01-LE, M02-ME; shank: TT-M01,
 370 HF-M02, LM-M03, MM-M04).

371 *Measurement specifications* - The sampling rate of the two 7-camera Vicon systems
 372 (VICON 370, VICON 512, Oxford Metrics, UK) was set at 60 sample/s.

373 *Ground truth* - Each subject received a computed tomography scan of the knee joint (CT,
 374 PQ-5000, Picker International, USA), from 15 cm superior to the joint line to 15 cm inferior,
 375 with a slice thickness of 1 mm and a pixel size of 0.625×0.625 mm. The CT data were
 376 segmented using a threshold filter to obtain volumetric models of the individual bones,
 377 namely the femur, tibia, fibula and patella. These subject-specific volumetric bone models,
 378 including their external surfaces and internal structures, were then used for subsequent
 379 registration with fluoroscopic images. The fluoroscopy system was calibrated using a 30×30
 380 cm transparent calibration box, two parallel sides of which were marked with lead markers at
 381 given positions. The box was placed with one of the marked sides on the image intensifier of
 382 the fluoroscopy and its image obtained. The image was used to correct image distortions via a
 383 modified polynomial method (Baltzopoulos, 1995) and to estimate the position of the point
 384 Xray source. For the spatial registration between the fluoroscopy and Vicon systems, five
 385 infrared retro-reflective markers were attached at known positions on the calibration box.

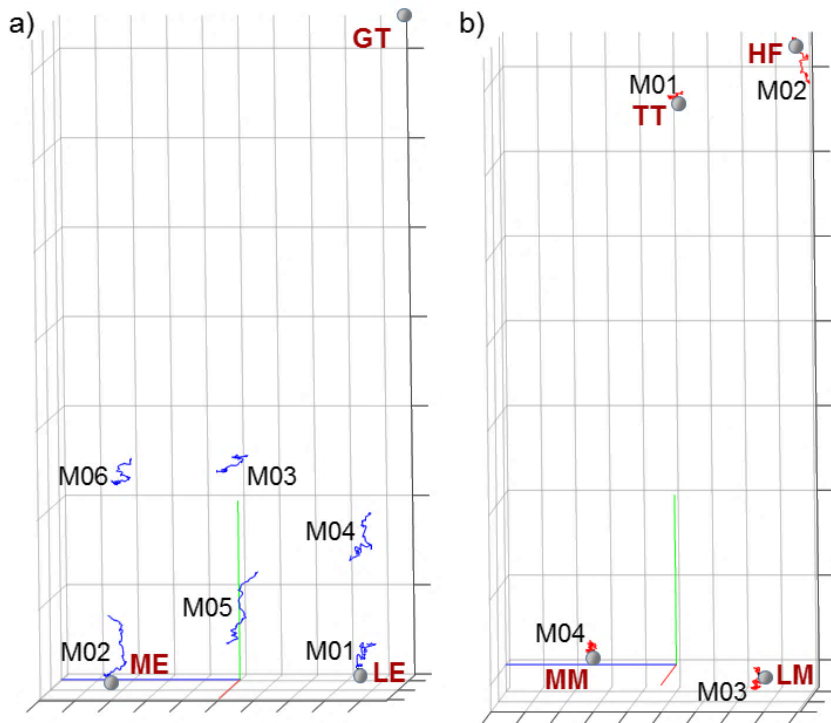
386 During tests, the fluoroscopic images were obtained at a sampling rate of 30 sample/s using
387 an image grabber card (PCI bus frame grabber, Foresight, USA). During STS, the projection
388 beam of the fluoroscopy system was adjusted so that the image plane was slightly oblique
389 with respect to the sagittal plane of the tested knee to avoid overlapping of the bilateral knee
390 joints on the fluoroscopic image, Fig. 22c. Temporal synchronization of the two systems was
391 achieved using an electrical trigger. The registration of the CT-derived volumetric bone
392 models and fluoroscopy images was performed by comparing systematically the fluoroscopic
393 image with the digitally reconstructed radiograph (DRR) of the volumetric bone model (Lu et
394 al., 2008). A DRR was generated by casting X-rays through the volumetric CT data of a bone
395 model and projecting onto the image plane to form an image resembling a radiograph with
396 detailed internal information of the bony structures (Penney et al., 1998). The 3D pose of the
397 bone at each image frame was obtained by searching for the pose of the bone model using an
398 optimization procedure to produce the DRR which best matched the fluoroscopic image. A
399 computer graphics user interface (GUI) was developed to assist with the visualization of the
400 registration and reconstruction of the 3D bone poses. The registration method has previously
401 been evaluated for its accuracy using a cadaveric knee, giving means and standard deviations
402 of the knee pose errors of 0.24 ± 0.77 mm, 0.41 ± 3.06 mm and 0.59 ± 1.13 deg for in-plane
403 translation, out-of-plane translation, and all rotations, respectively (Lu et al., 2008).

404 *2.4.1. Data sample 5: knee flexion/extension*

405 *Subject characteristics* - An adult male subject free from musculoskeletal diseases. Height
406 = 1.76 m, mass = 74 kg.

407 *Motor task description* – The subject sat on an armless, height-adjustable chair to perform
408 a complete cycle of active knee flexion/extension at an average speed of about 30 deg/s with
409 the assistance of a metronome.

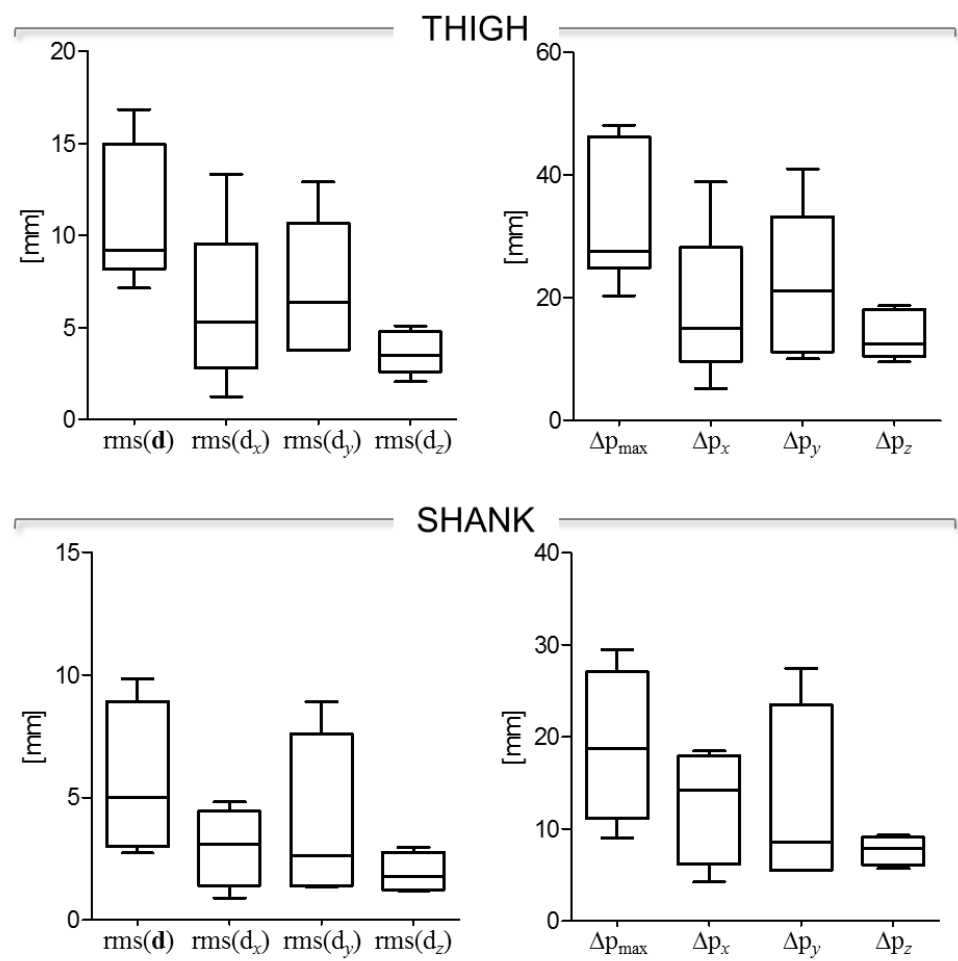
410 *STA characteristics* - Skin-marker trajectories in the thigh and shank ACSs are depicted in
411 Fig. 23. Stereophotogrammetric data were acquired at 60 Hz and then down-sampled to 30
412 Hz. Statistical data describing the relevant STAs are shown in Fig. 24 for knee
413 flexion/extension. Magnitude of the instantaneous displacement of thigh and shank skin-
414 markers along with the knee joint angular kinematics is depicted in Fig. 25 for knee
415 flexion/extension.



416

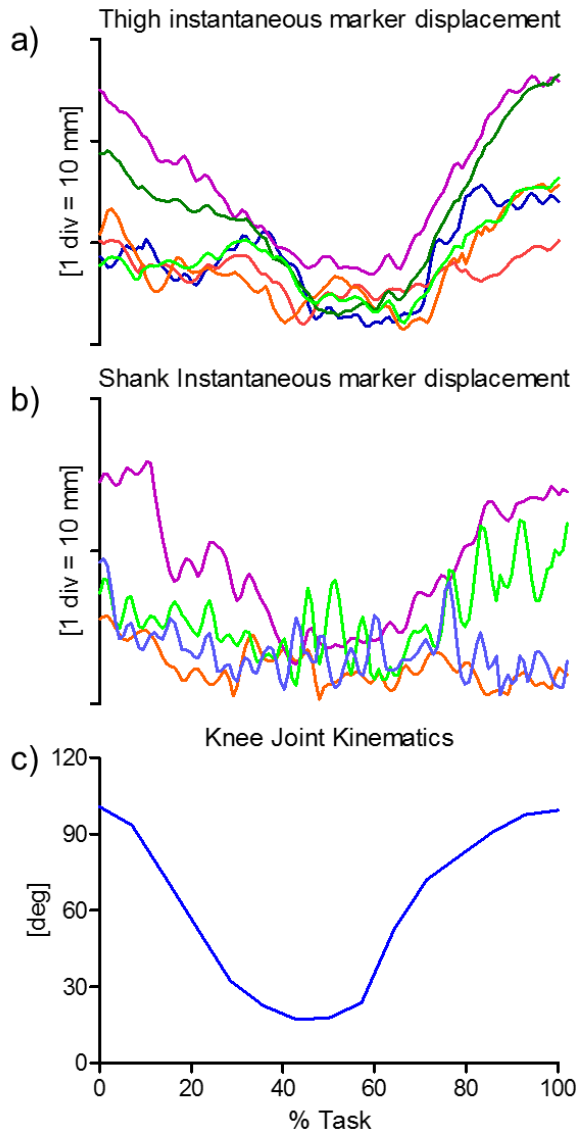
417 **Figure 23** – Femur (a) and tibial (b) ACSs, relevant ALs, and thigh and shank skin-marker trajectories
 418 (represented in blue and red, respectively). The axes of the ACSs are represented in red, green, and
 419 blue for the x (antero/posterior, div = 50 mm), y (superior/inferior, div = 50 mm), and z (right/left, div
 420 = 20 mm) directions, respectively.

421



422

423 **Figure 24** – Box-plots of the eight parameters ($\text{rms}(\mathbf{d})$, $\text{rms}(\mathbf{d}_x)$, $\text{rms}(\mathbf{d}_y)$, and $\text{rms}(\mathbf{d}_z)$, in the left panel;
424 Δp_{\max} , Δp_x , Δp_y , and Δp_z , in the right panel) that describe the STA affecting the six and four skin-
425 markers on the thigh and the shank, respectively, during the movement. Outliers are also depicted.



426

427 **Figure 25** –Magnitude of the instantaneous displacement of the six and four skin-markers glued on the
 428 thigh (a) and shank (b) represented in the relevant ACS. c) Relevant knee joint kinematics computed
 429 according to the convention proposed by Grood and Suntay (1983) (flexion/extension in blue, with
 430 flexion as positive).

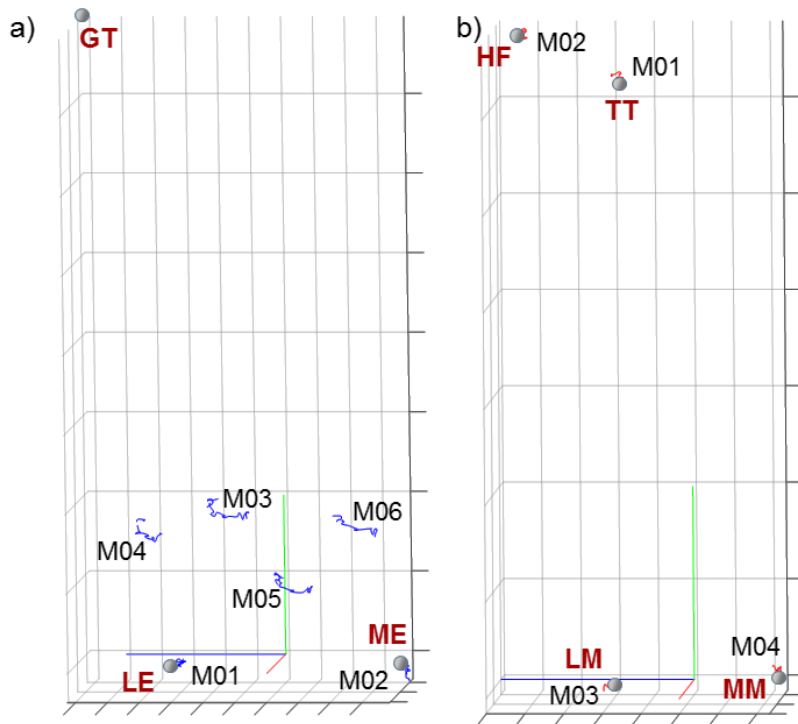
431

432 2.4.2. Data samples 9, 12, 16: overground walking, sit to stand, step-up

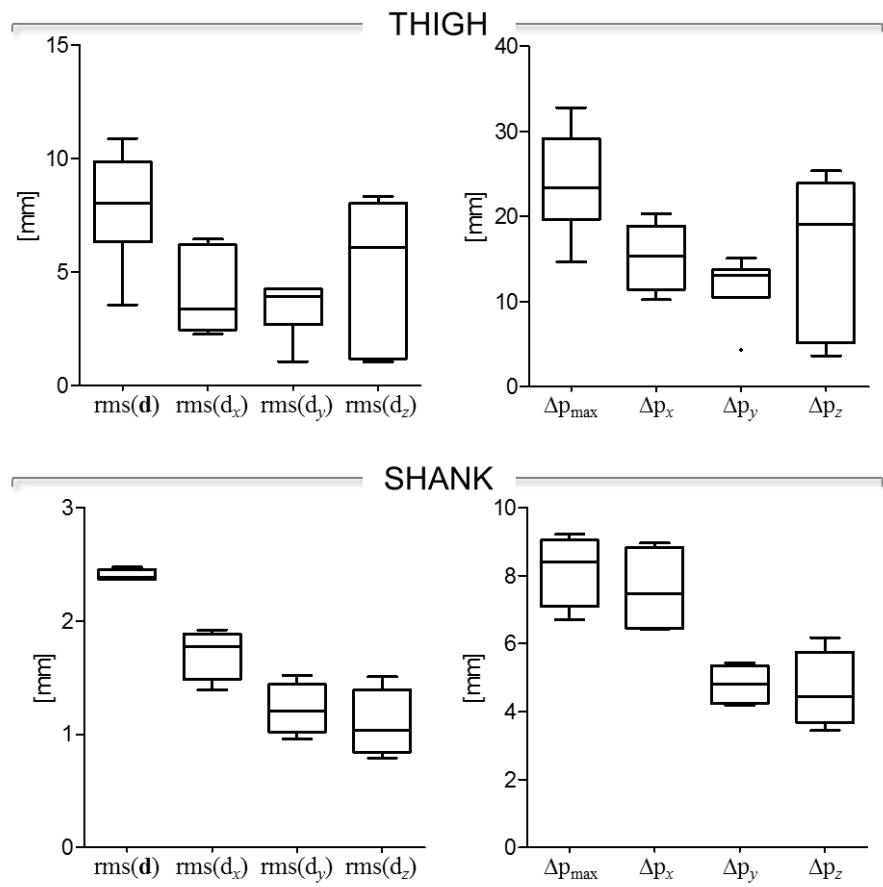
433 *Subject characteristics* - An adult male subject free from musculoskeletal diseases. Height
 434 = 1.74 m, mass = 83 kg.

435 *Motor task description* - Overground walking at the subject's self-selected speed was
 436 measured only during the stance phase, as depicted in Fig. 22a. For the sit-to-stand task, each
 437 subject was asked to sit with the hips abducted at about 30 deg on an armless, height-
 438 adjustable chair and stand up at a self-selected speed (Fig. 22b). The height of the chair was
 439 set at 115% of the knee-heel distance for each subject. Step-up was performed on a three-step
 440 stair (height: 18 cm; depth: 46 cm) at a self-selected speed (Fig. 22c).

441 STA characteristics - Skin-marker trajectories in the thigh and shank ACSs are depicted in
 442 Figs. 26, 29, 32, for stance phase overground walking, sit to stand, and step-up, respectively.
 443 Stereophotogrammetric data were acquired at 60Hz and then down-sampled to 30Hz.
 444 Statistical data describing the STAs are shown in Figs. 27, 30, 33, for overground walking, sit
 445 to stand, and step-up, respectively. For each motor task, the magnitude of the instantaneous
 446 displacement of thigh and shank skin-markers along with the knee joint angular kinematics is
 447 depicted in Figs. 28, 31, 34, for stance phase overground walking, sit to stand, and step-up,
 448 respectively.

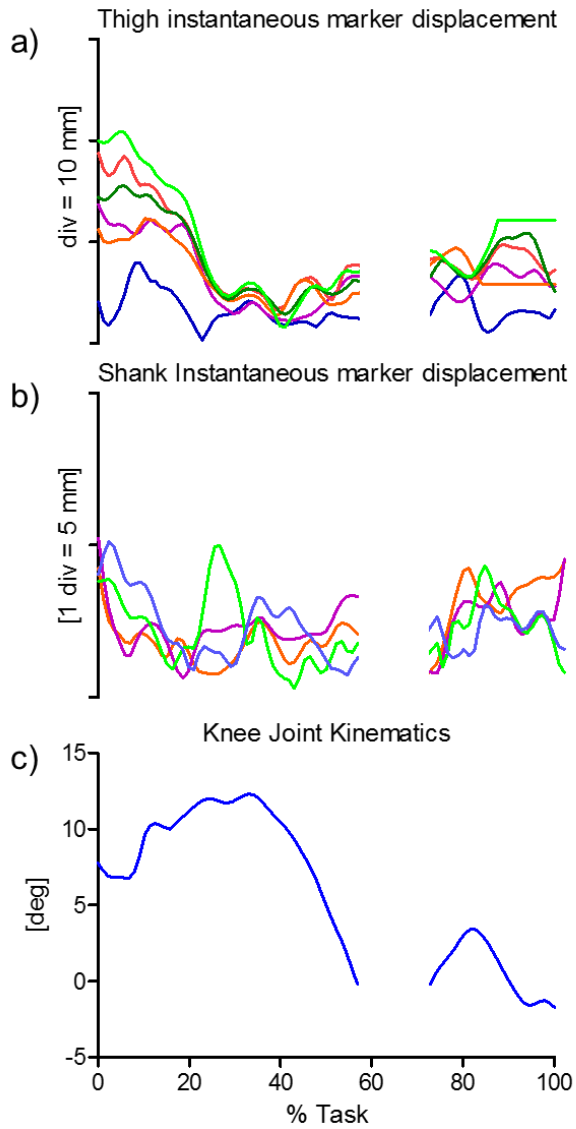


449
 450 **Figure 26 – STANCE PHASE OVERGROUND WALKING.** Femur (a) and tibial (b) ACSs, relevant
 451 ALs, and thigh and shank skin-marker trajectories (represented in blue and red, respectively). The axes
 452 of the ACSs are represented in red, green, and blue for the x (antero/posterior, div = 50 mm), y
 453 (superior/inferior, div = 50 mm), and z (right/left, div = 20 mm) directions, respectively.
 454



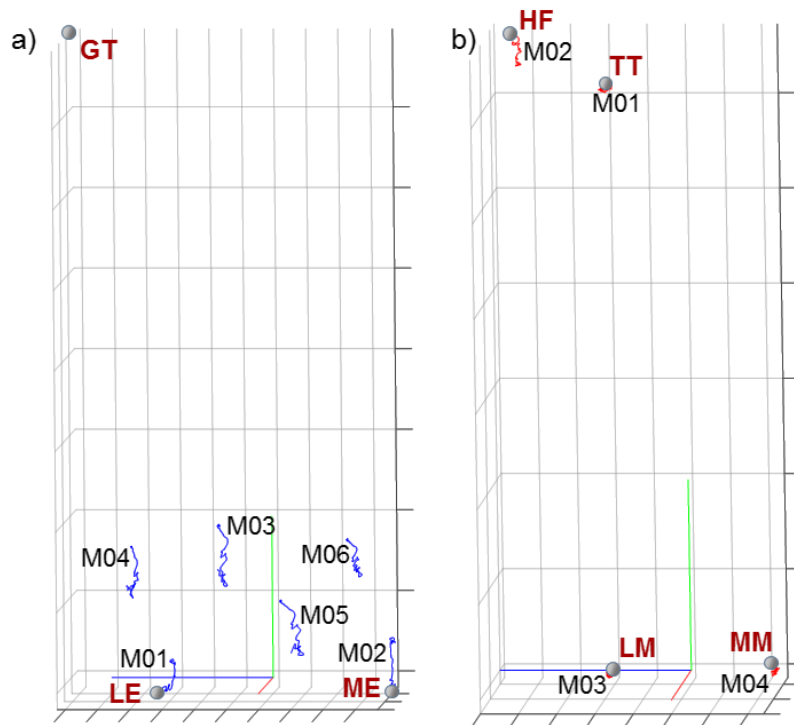
455

456 **Figure 27 – STANCE PHASE OVERGROUND WALKING.** Box-plots of the eight parameters
 457 (rms(d), rms(d_x), rms(d_y), and rms(d_z), in the left panel; Δp_{max}, Δp_x, Δp_y, and Δp_z, in the right panel)
 458 that describe the STA affecting the six and four skin-markers on the thigh and the shank, respectively,
 459 during the movement. Outliers are also depicted.



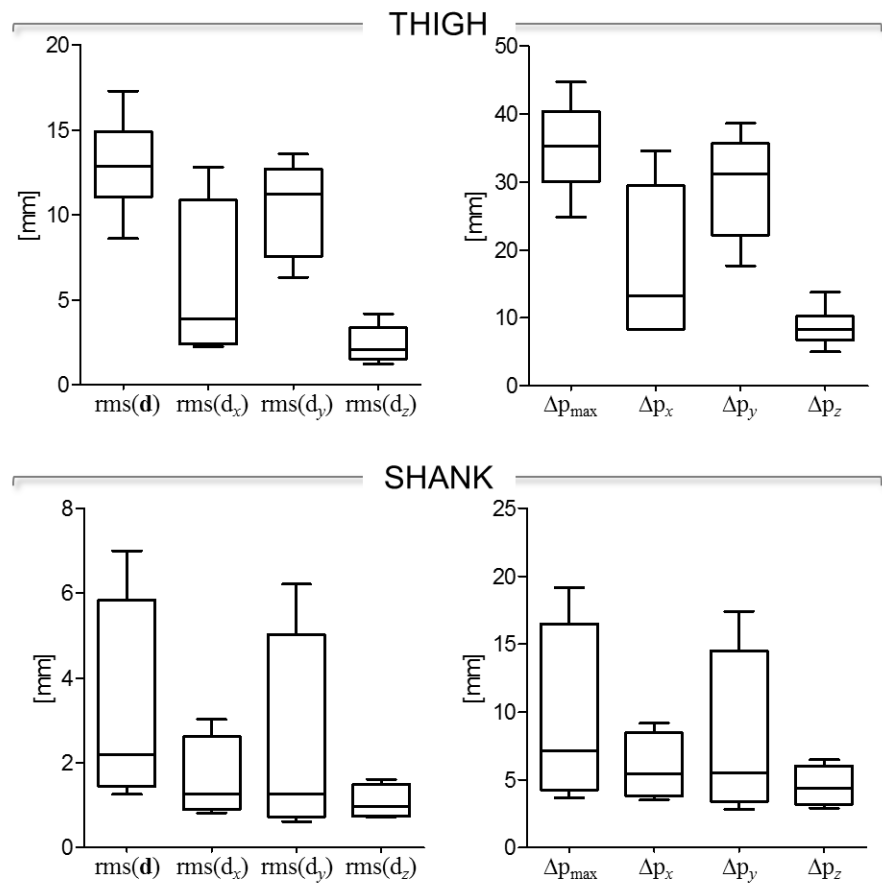
460

461 **Figure 28 – STANCE PHASE OVERGROUND WALKING.** Magnitude of the instantaneous
 462 displacement of the six and four skin-markers glued on the thigh (a) and shank (b) represented in the
 463 relevant ACS. c) Relevant knee joint kinematics computed according to the convention proposed by
 464 Grood and Suntay (1983) (flexion/extension in blue, with flexion as positive). The data between 60%-
 465 70% were not shown because the knee joints were overlapped on the fluoroscopic images.



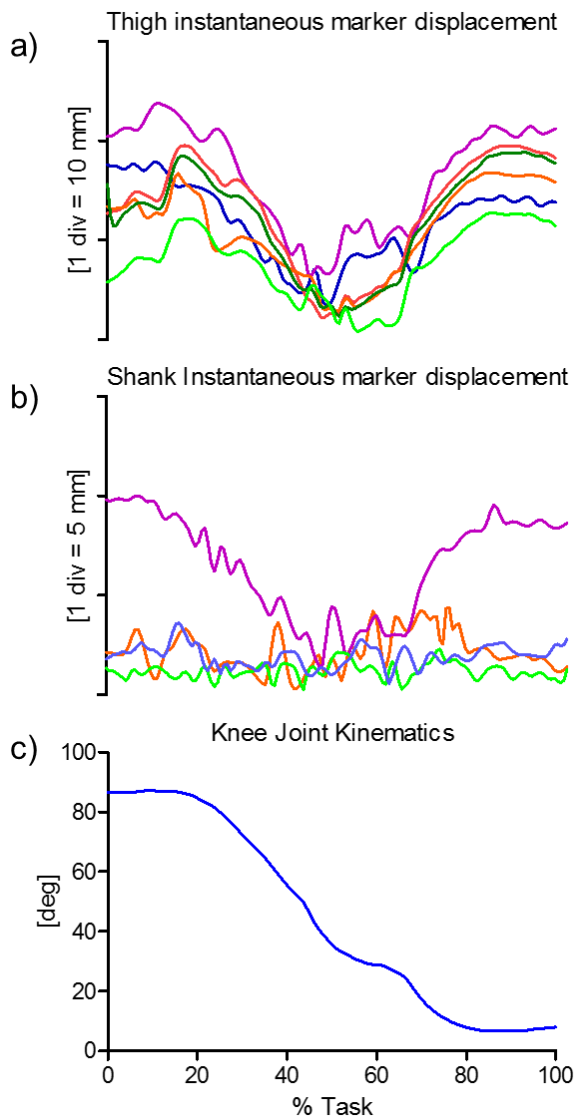
466

467 **Figure 29 – SIT TO STAND.** Femur (a) and tibial (b) ACSs, relevant ALs,
 468 and thigh and shank skin-
 469 marker trajectories (represented in blue and red, respectively). The axes of the ACSs are represented in
 470 red, green, and blue for the x (antero/posterior, div = 50 mm), y (superior/inferior, div = 50 mm), and z
 471 (right/left, div = 20 mm) directions, respectively.



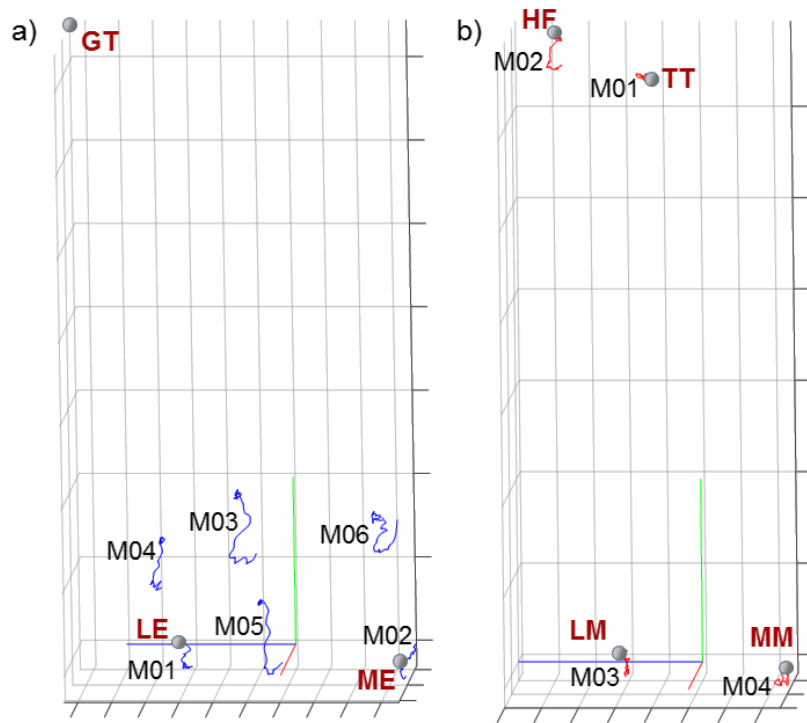
472

473 **Figure 30 – SIT TO STAND.** Box-plots of the eight parameters (rms(d), rms(d_x), rms(d_y), and
474 rms(d_z), in the left panel; Δp_{\max} , Δp_x , Δp_y , and Δp_z , in the right panel) that describe the STA affecting
475 the six and four skin-markers on the thigh and the shank, respectively, during the movement. Outliers
476 are also depicted.



477

478 **Figure 31 – SIT TO STAND.** Magnitude of the instantaneous displacement of the six and four skin-
 479 markers glued on the thigh (a) and shank (b) represented in the relevant ACS. c) Relevant knee joint
 480 kinematics computed according to the convention proposed by Grood and Suntay (1983)
 481 (flexion/extension in blue, with flexion as positive).

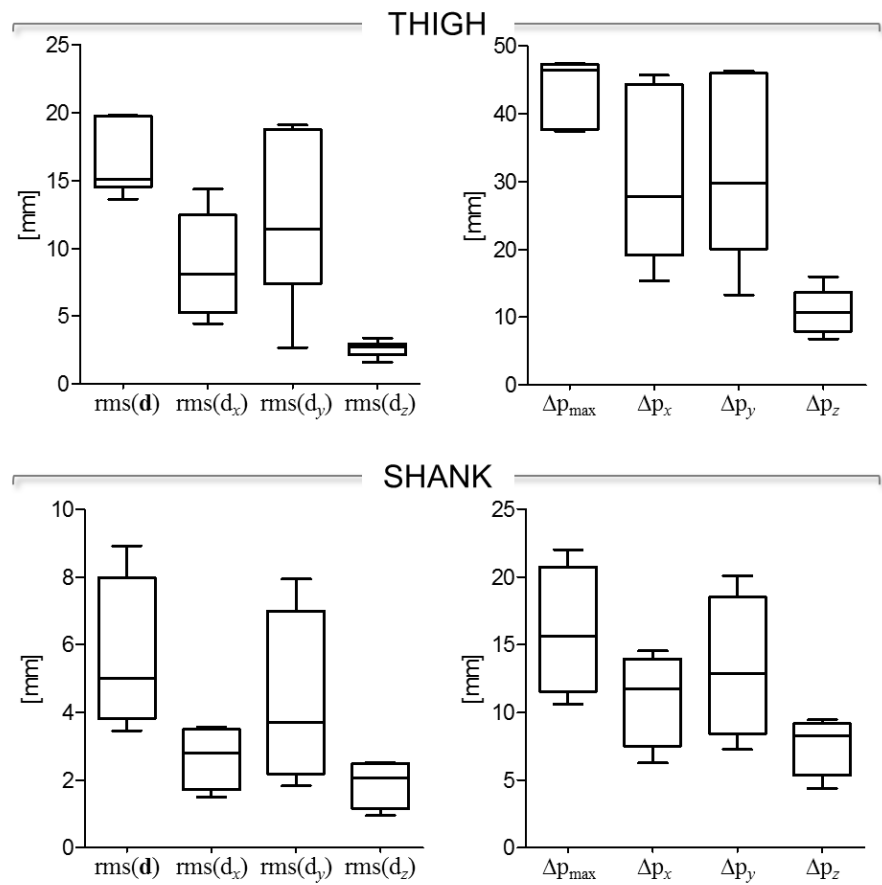


482

483 **Figure 32 – STEP-UP.** Femur (a) and tibial (b) ACSs, relevant ALs,
 484 and thigh and shank skin-marker
 485 trajectories (represented in blue and red, respectively). The axes of the ACSs are represented in red,
 486 green, and blue for the x (antero/posterior, div = 50 mm), y (superior/inferior, div = 50 mm), and z
 487 (right/left, div = 20 mm) directions, respectively.

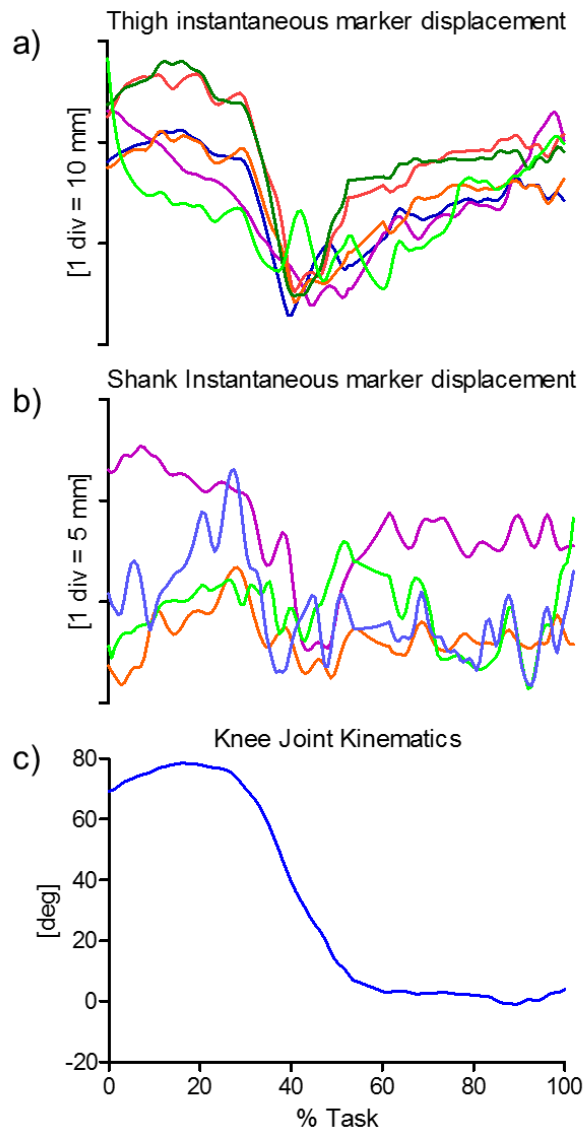
487

488



489

490 **Figure 33 – STEP-UP.** Box-plots of the eight parameters ($\text{rms}(\mathbf{d})$, $\text{rms}(\mathbf{d}_x)$, $\text{rms}(\mathbf{d}_y)$, and $\text{rms}(\mathbf{d}_z)$, in the
491 left panel; Δp_{\max} , Δp_x , Δp_y , and Δp_z , in the right panel) that describe the STA affecting the six and four
492 skin-markers on the thigh and the shank, respectively, during the movement. Outliers are also
493 depicted.



494

495 **Figure 34 – STEP-UP.** Magnitude of the instantaneous displacement of the six and four skin-markers
 496 glued on the thigh (a) and shank (b) represented in the relevant ACS. c) Relevant knee joint kinematics
 497 computed according to the convention proposed by Grood and Suntay (1983) (flexion/extension in
 498 blue, with flexion as positive).

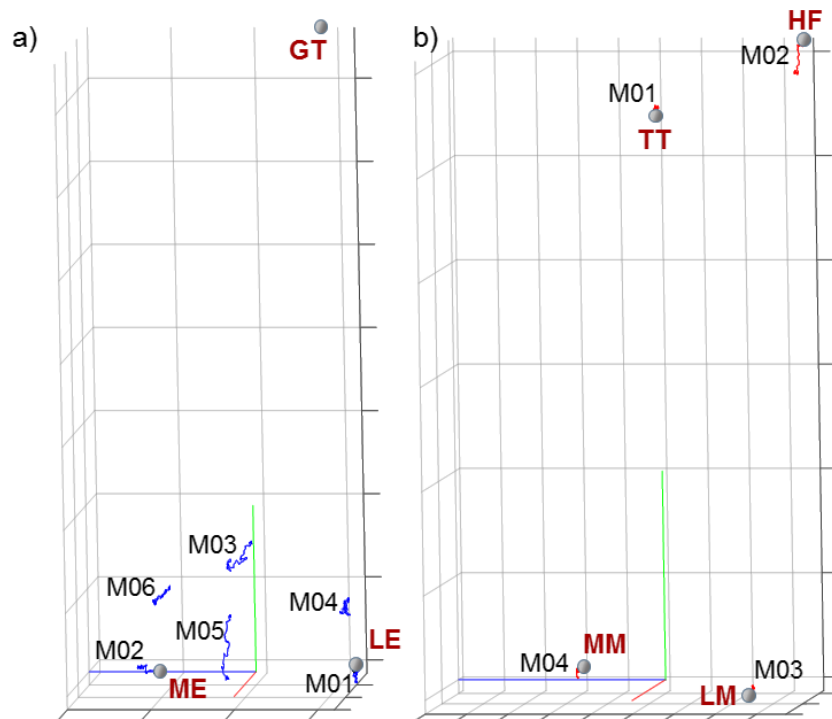
499

500 2.4.3. Data sample 13: sit to stand

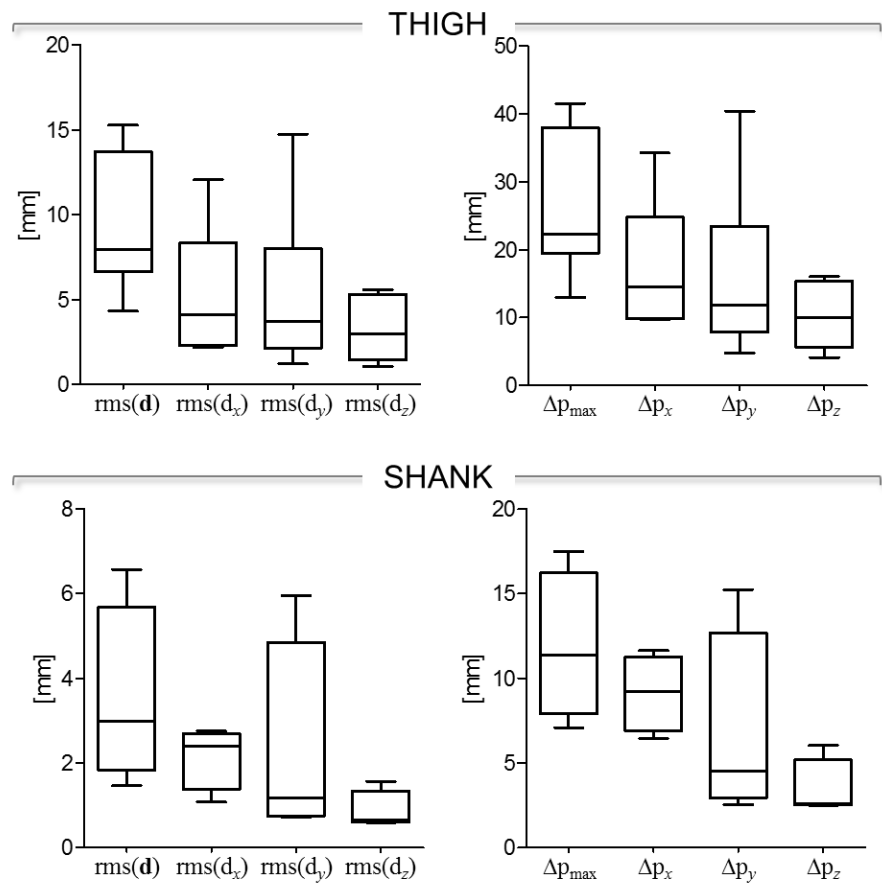
501 *Subject characteristics* - An adult female subject with posterior cruciate ligament retaining
 502 mobile bearing total knee replacement. Height = 1.61 m, mass = 87 kg.

503 *Motor task description* - Each subject sat with the hips abducted at about 30 degrees on an
 504 armless, height-adjustable chair and stood up at a self-selected speed. The projection beam of
 505 the fluoroscopy system was adjusted so that the image plane was slightly oblique with respect
 506 to the sagittal plane of the tested knee to avoid overlapping of the bilateral knee joints on the
 507 fluoroscopic image.

508 *STA characteristics* - Skin-marker trajectories in the thigh and shank ACSs are depicted in
509 Fig. 35. Stereophotogrammetric data were acquired at 60 Hz and then down-sampled to 30
510 Hz. Statistical data describing the relevant STAs are shown in Fig. 36. Magnitude of the
511 instantaneous displacement of thigh and shank skin-markers along with the knee joint angular
512 kinematics is depicted in Fig. 37.

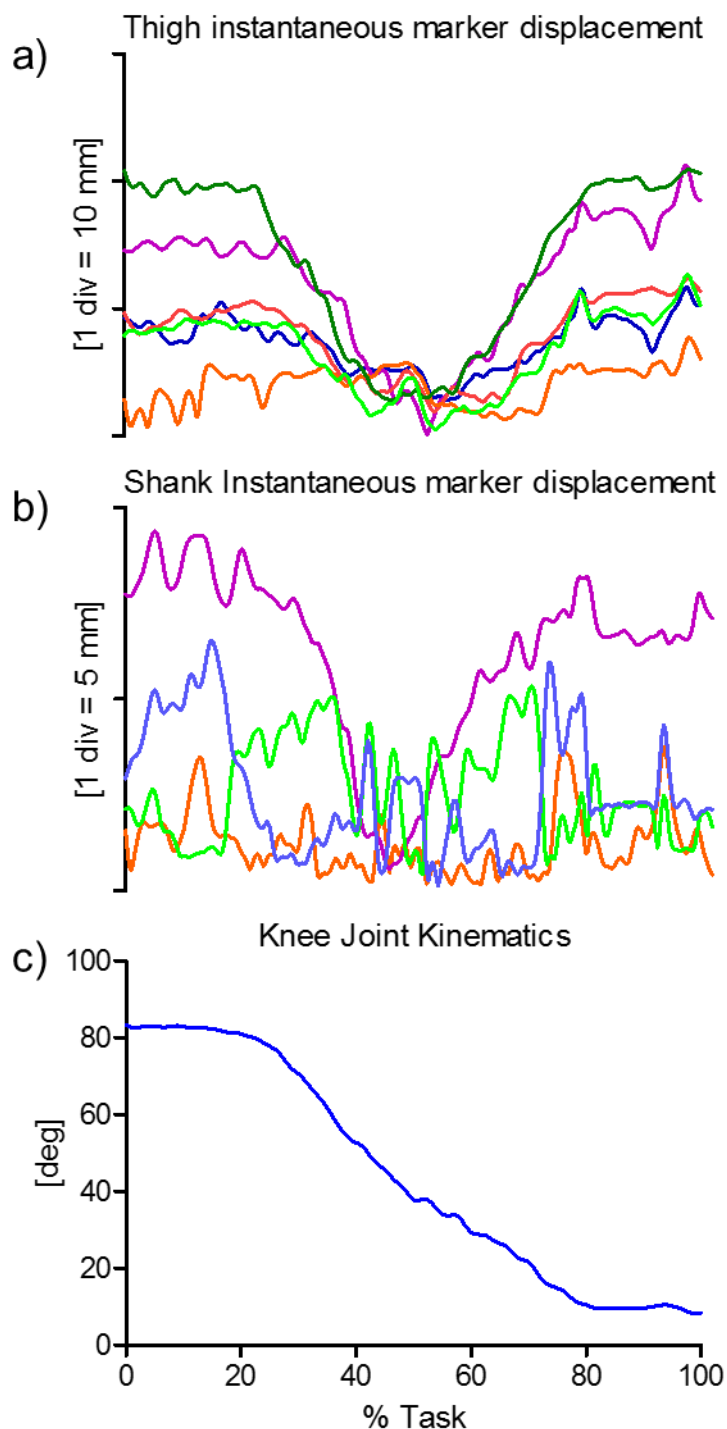


513
514 **Figure 35** – Femur (a) and tibial (b) ACSs, relevant ALs, and thigh and shank skin-marker trajectories
515 (represented in blue and red, respectively). The axes of the ACSs are represented in red, green, and
516 blue for the x (antero/posterior, div = 50 mm), y (superior/inferior, div = 50 mm), and z (right/left, a)
517 div = 50 mm; b) div = 20 mm) directions, respectively.
518
519



520

521 **Figure 36** – Box-plots of the eight parameters ($\text{rms}(\mathbf{d})$, $\text{rms}(\mathbf{d}_x)$, $\text{rms}(\mathbf{d}_y)$, and $\text{rms}(\mathbf{d}_z)$, in the left panel;
522 Δp_{\max} , Δp_x , Δp_y , and Δp_z , in the right panel) that describe the STA affecting the six and four skin-
523 markers on the thigh and the shank, respectively, during the movement. Outliers are also depicted.



524

525 **Figure 37** –Magnitude of the instantaneous displacement of the six and four skin-markers glued on the
 526 thigh (a) and shank (b) represented in the relevant ACS. c) Relevant knee joint kinematics computed
 527 according to the convention proposed by Grood and Suntay (1983) (flexion/extension in blue, with
 528 flexion as positive).

529

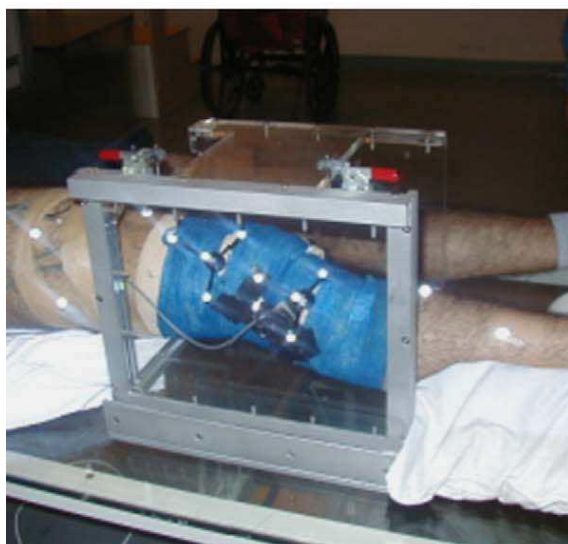
530 **2.5. *In-vivo data from OTTAWA***

531 *Scientific articles of reference* - A detailed description of the original data set can be found
532 in Benoit et al., 2006 and in Andersen et al., 2012 for hopping.

533 *Experimental data description* - Triads of three non-collinear 7 mm reflective markers
534 (pin-markers) were affixed to the pins. Additional clusters of four 10 mm surface markers
535 (skin-markers) were affixed onto the lateral and frontal aspects of both the right thigh and
536 shank (Fig. 38a and 38b). Skin-markers were spaced 10–15 cm from adjacent markers within
537 their respective cluster and their arrangement was chosen to ensure they remained non-
538 coplanar in at least two camera views throughout the range of motion. Reflective markers
539 were also placed on the right heel, 5th metatarsal and lateral malleolus.



(a)



(b)

540

541 **Figure 38** a) Picture of the bone-pin and surface markers configurations for a representative subject.
542 The pins are inserted in the tibia and femur, respectively. Each pin is equipped with a 4 marker-cluster.
543 The skin is equipped with 4 retroreflective markers for the thigh and 4 for the shank. Skin-marker
544 names as shown in Figures 39, 42, 45. b) RSA procedure and calibration box. The right leg is
545 extended.

546 *Measurement specifications* - Bone-pin and skin-marker trajectories were tracked within
547 0.8 m³ measurement volume (1.1 m x 0.8 m x 0.9 m) using four infrared cameras (ProReflex,
548 Qualisys AB, Sweden), sampling at 120 sample/s. Marker coordinates were transformed using
549 the direct linear transform (DLT) and the raw 3D coordinates exported and saved to a local
550 computer for analysis.

551 *Anatomical coordinate system definitions* – To define femur and tibia ACSs, the following
552 19 anatomical landmarks were identified on RSA radiographs (described below):

- 553 1–4. Tibial pin-markers.
- 554 5. Proximal medial tibial eminence (tibial reference point).
- 555 6. The most distal point along a line through point 5 and parallel to the long axis of the tibia.
- 556 7–8. Medial and lateral edges of proximal tibia respectively.
- 557 9. A distal point along a line drawn perpendicular to the long axis of the tibia and running
558 originating at the tibial reference point.
- 559 10–14. Femoral pin-markers.
- 560 15. Proximal (deepest) point of the condylar groove (notch)
561 (femoral reference point).
- 562 16. The most distal point along a line through point
563 15 and parallel to the long axis of the femur.
- 564 17–18. Medial and lateral edges of the distal femur, respectively.
- 565 19. A distal point along a line drawn perpendicular to the long axis of the femur and
566 originating at the femoral reference point.

567 The origin of the femoral coordinate system was located at the deepest point of the
568 intercondylar groove (point 15). The origin of the tibial coordinate system was located at the
569 highest point of the medial intercondylar eminence (point 5). Local coordinate systems of the
570 femur and tibia were defined as follows:

- 571 X_f cross product of vectors Z_f and Y_f; from the femoral origin, directed laterally.
- 572 Y_f cross product of Z_f and vector joining points 17 and 18; from the femoral origin,
573 directed anteriorly.
- 574 Z_f vector joining points 15 and 16; from the femoral origin directed longitudinally along
575 the femoral axis in the frontal plane.
- 576 X_t cross product of vectors Z_t and Y_t; from the tibial origin, directed laterally.
- 577 Y_t cross product of Z_t and vector joining points 7 and 8; from the tibial origin, directed
578 anteriorly.

579 Zt vector joining points 5 and 6; from the tibial origin directed longitudinally along the
580 tibial axis in the frontal plane.

581 *Ground truth* – Stainless steel Apex self-drilling/self-tapping pins (Stryker Howmedica AB
582 Sweden, 3.0 mm diameter, #5038-2-110) were inserted under local anaesthetic into the distal
583 femur and proximal tibia of the right leg (Ramsey et al., 2003) at the Karolinska University
584 Hospital (Stockholm, Sweden). The femoral pin was inserted between the iliotibial band and
585 the quadriceps tendon superior of the vastus lateralis to minimise impingement problems.
586 Following surgery subjects performed active flexion and extension movements while standing
587 to identify whether movement restrictions were evident. Subjects were then transported by
588 wheelchair to the motion analysis laboratory for data collection. To test for eventual pin
589 bending, standing reference trial were performed before and after each block of movement
590 trials and the orientation of the target clusters from the first reference trial was matched
591 against the second to verify the pins did not bend and the triad did not rotate during testing.
592 Following the motion analysis recordings, the leg was extended through a biplanar calibration
593 box (Cage 10, RSA Biomedical Innovations, Umea°, Sweden) and biplanar radiographs
594 (RSA) were recorded (Fig. 38b). All radiographs were taken with the subject supine and the
595 knee flexed between 0 deg and 10 deg. From these radiographs, two local anatomical
596 reference points were identified and digitized with the aid of an experienced RSA technician
597 (Sahlgrenska University Hospital Gothenburg, Sweden). In total, the 19 points described in
598 the ACS section were digitised to derive the anatomical coordinate system using UMRSA
599 software (version 5, Biomedical Innovations-AB, Umea, Sweden).

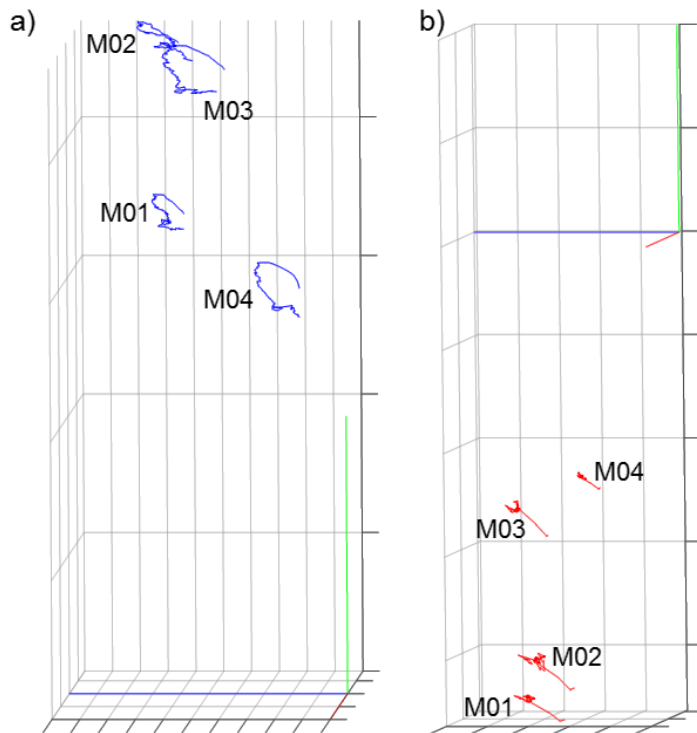
600

601 *2.5.1. Data samples 10,11,19: Overground walking, lateral cutting manoeuvres,
602 hopping*

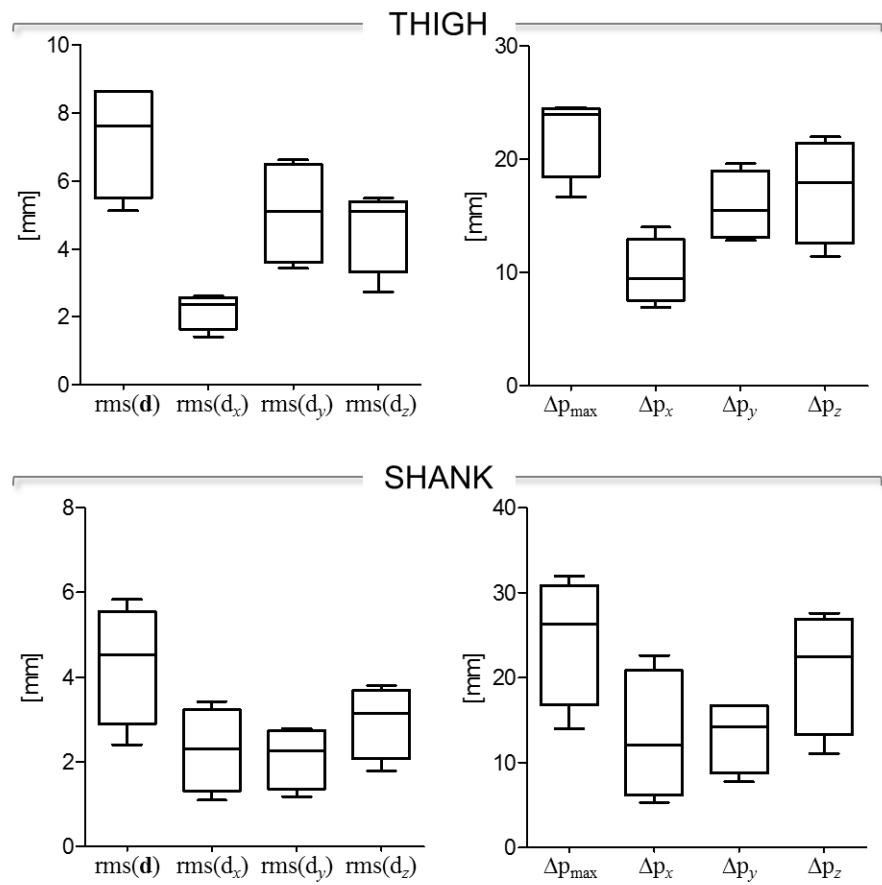
603 *Subject characteristics* - A 22 y.o. subject. Height = 1.75 m, mass = 63 kg.

604 *Motor task description* - The participant perform a series of overground walking trials and
605 lateral cutting manoeuvres, after a several practice trials. For gait testing, subjects walked
606 along a 12 m walkway at a self-selected pace, and the stance phase was analysed. Before
607 performing the lateral cutting manoeuvre, subjects jumped for maximal horizontal distance.
608 Their longest measurement was recorded and marked on the floor to determine the proper
609 takeoff distance to the force platform. From an initial standing position the subject pushed off
610 using the left leg and, upon landing onto their right foot, immediately pushed off the platform,
611 cutting to the left at an angle of approximately 45 deg.

612 *STA characteristics* - Skin-marker trajectories in the thigh and shank ACSs are depicted in
 613 Figs. 39, 42, 45, for stance phase overground walking, lateral cutting manoeuvres, hopping,
 614 respectively. Unfiltered data were used. Statistical data describing the STAs are shown in
 615 Figs. 40, 43, 46, for stance phase overground walking, lateral cutting manoeuvres, hopping,
 616 respectively. Magnitude of the instantaneous displacement of thigh and shank skin-markers
 617 along with the knee joint angular kinematics is depicted in Figs. 41, 44, 47, for stance phase
 618 overground walking, lateral cutting manoeuvres, hopping, respectively.

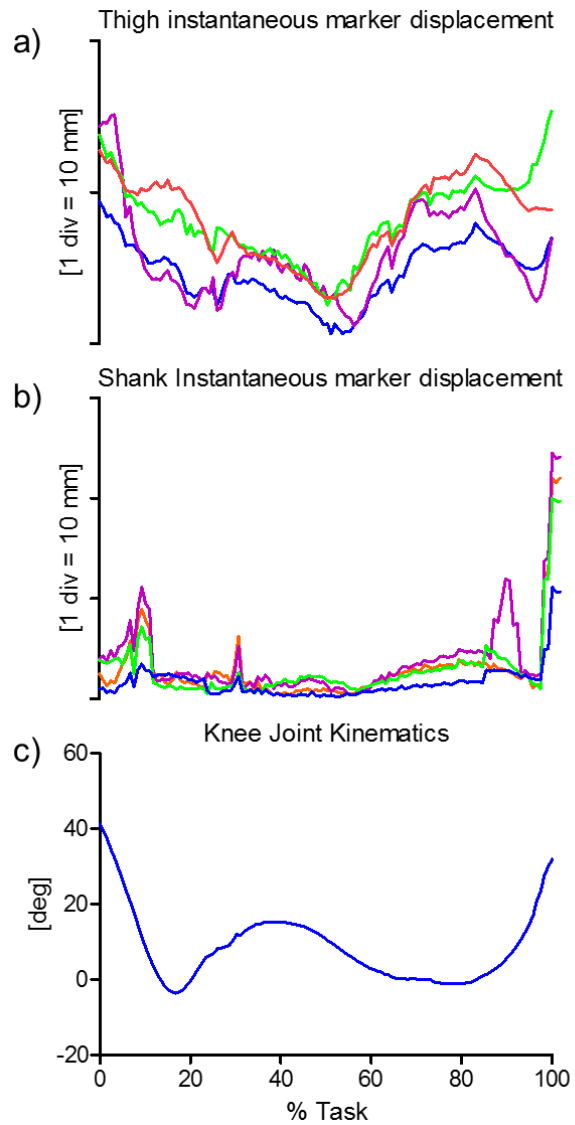


619
 620 **Figure 39 – STANCE PHASE OVERGROUND WALKING.** Femur (a) and tibial (b) ACSs, and
 621 thigh and shank skin-marker trajectories (represented in blue and red, respectively). The axes of the
 622 ACSSs are represented in red, green, and blue for the x (antero/posterior, div = 50 mm), y
 623 (superior/inferior, div = 50 mm), and z (right/left, div = 20 mm) directions, respectively.
 624



625

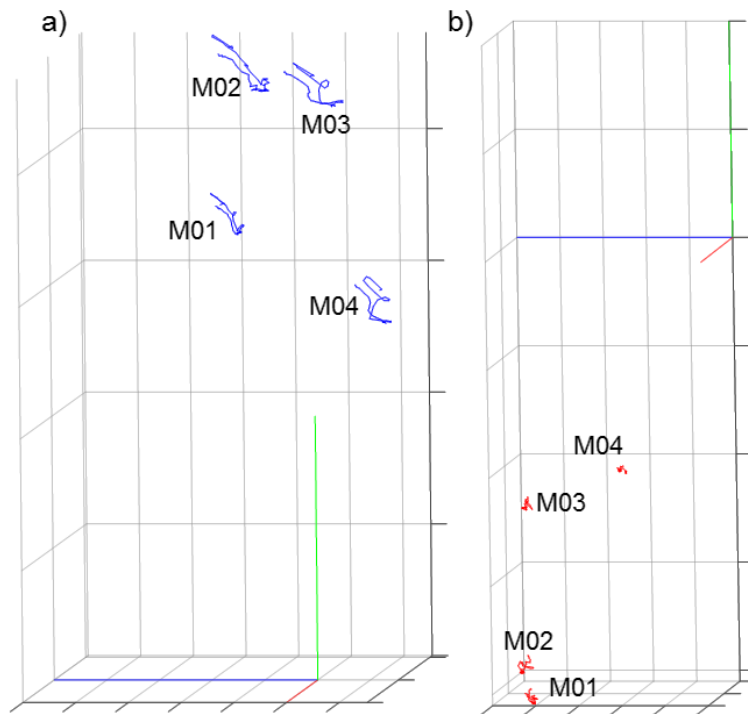
626 **Figure 40 – STANCE PHASE OVERGROUND WALKING.** Box-plots of the eight parameters
 627 (rms(d), rms(d_x), rms(d_y), and rms(d_z), in the left panel; Δp_{max}, Δp_x, Δp_y, and Δp_z, in the right panel)
 628 that describe the STA affecting the four skin-markers on the thigh and shank, respectively, during the
 629 movement. Outliers are also depicted.



630

631 **Figure 41 – STANCE PHASE OVERGROUND WALKING.** Magnitude of the instantaneous
 632 displacement of the four skin-markers glued on the thigh (a) and shank (b) represented in the relevant
 633 ACS. c) Relevant knee joint kinematics computed according to the convention proposed by Grood and
 634 Suntay (1983) (flexion/extension in blue, with flexion as positive).

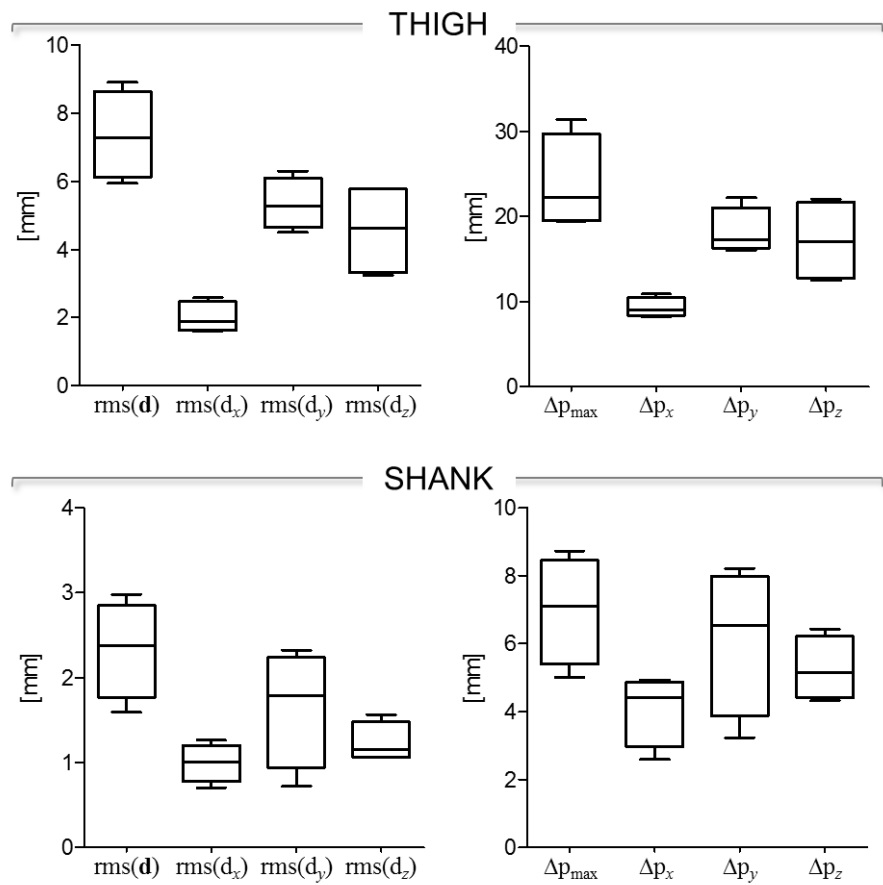
635



636

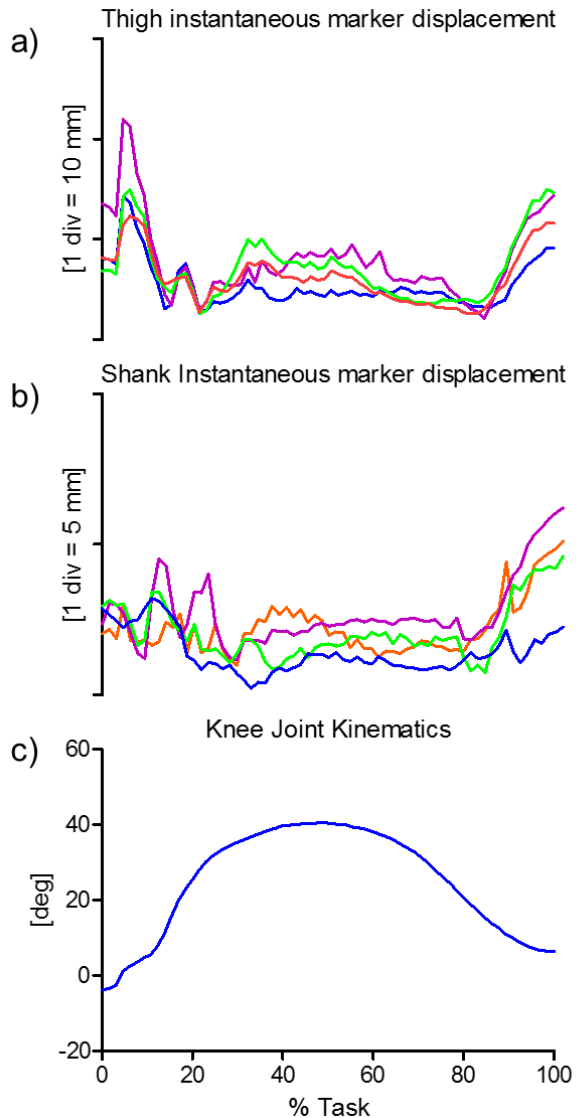
637 **Figure 42 – LATERAL CUTTING MANOEUVRES.** Femur (a) and tibial (b) ACSs, and thigh and
 638 shank skin-marker trajectories (represented in blue and red, respectively). The axes of the ACSs are
 639 represented in red, green, and blue for the x (antero/posterior, div = 50 mm), y (superior/inferior, div =
 640 50 mm), and z (right/left, div = 20 mm) directions, respectively.

641



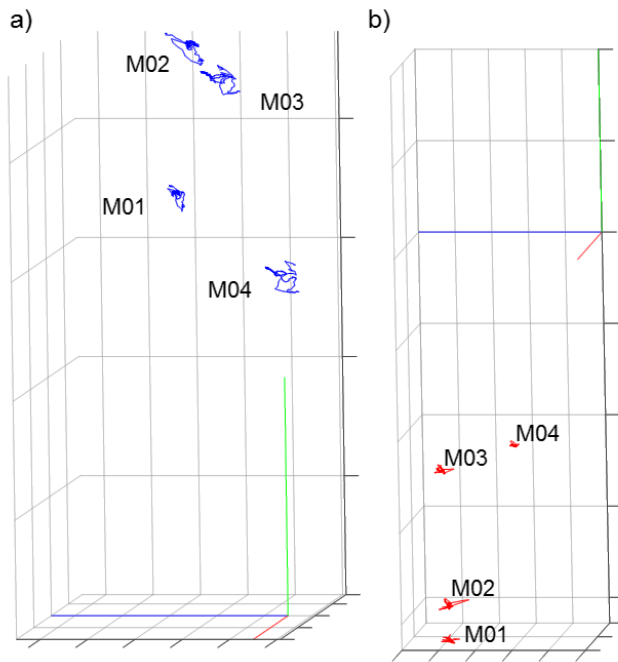
642

643 **Figure 43 – LATERAL CUTTING MANOEUVRES.** Box-plots of the eight parameters (rms(d),
644 rms(d_x), rms(d_y), and rms(d_z), in the left panel; Δp_{max}, Δp_x, Δp_y, and Δp_z, in the right panel)
645 that describe the STA affecting the four skin-markers on the thigh and shank, respectively, during the
646 movement. Outliers are also depicted.



647

648 **Figure 44 – LATERAL CUTTING MANOEUVRES.** Magnitude of the instantaneous displacement of
 649 the four skin-markers glued on the thigh (a) and shank (b) represented in the relevant ACS. c)
 650 Relevant knee joint kinematics computed according to the convention proposed by Grood and Suntay
 651 (1983) (flexion/extension in blue, with flexion as positive).



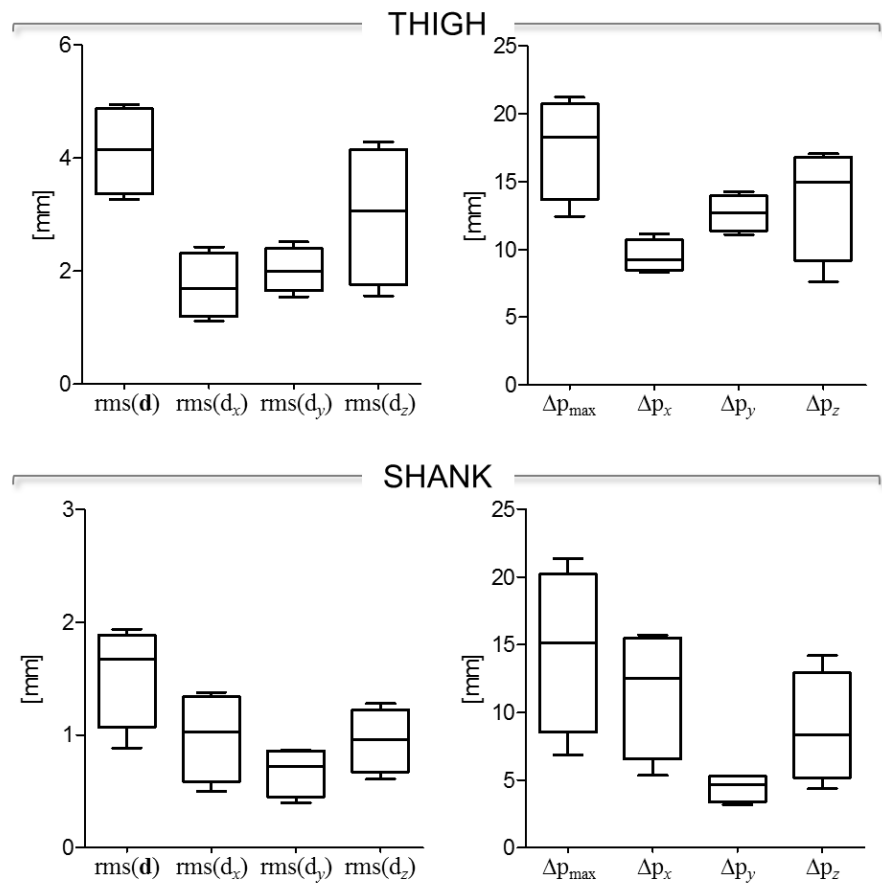
652

653 **Figure 45 – HOPPING.** Femur (a) and tibial (b) ACSs, and thigh and shank skin-marker trajectories
 654 (represented in blue and red, respectively). The axes of the ACSs are represented in red, green, and
 655 blue for the x (antero/posterior, div = 50 mm), y (superior/inferior, div = 50 mm), and z (right/left, a)
 656 div = 50 mm; b) div = 20 mm) directions, respectively.

657

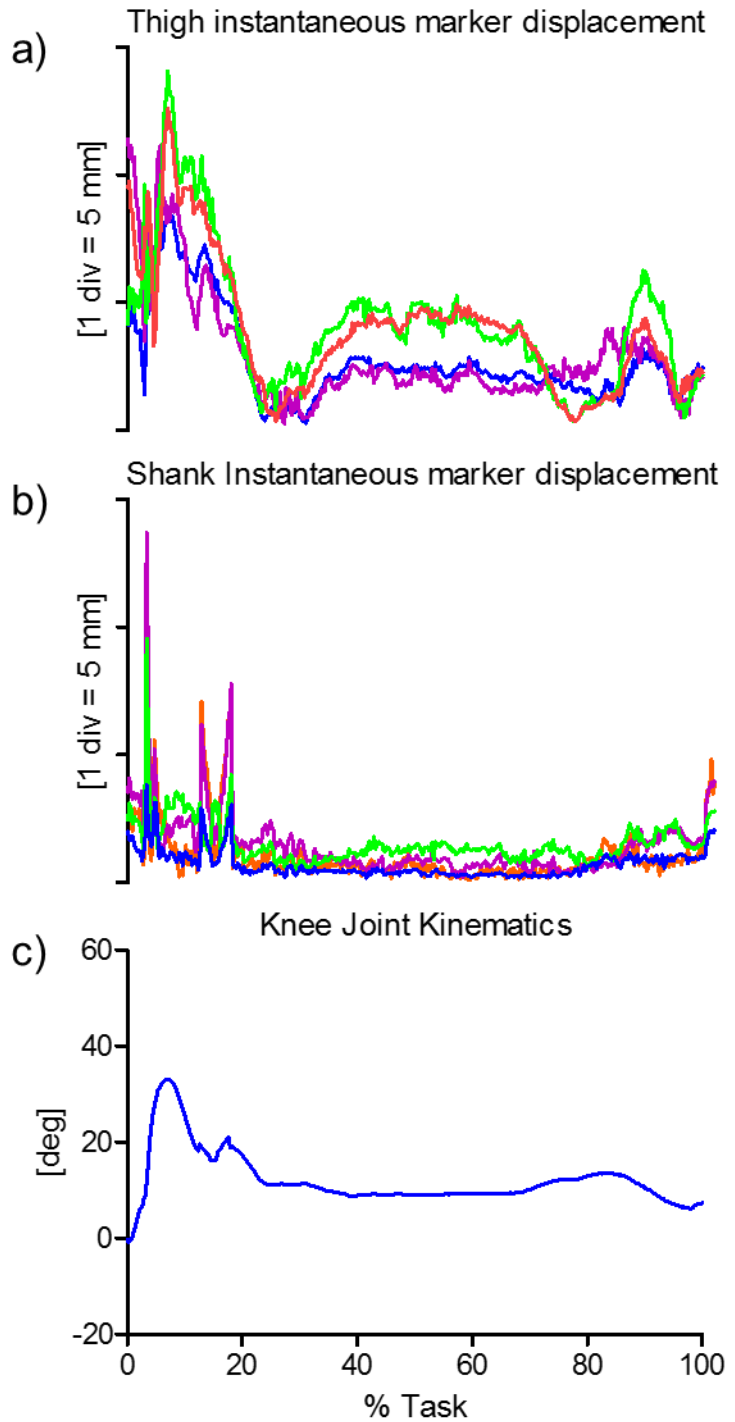
658

659



660
661
662
663
664

Figure 46 – HOPPING. Box-plots of the eight parameters ($\text{rms}(\mathbf{d})$, $\text{rms}(\mathbf{d}_x)$, $\text{rms}(\mathbf{d}_y)$, and $\text{rms}(\mathbf{d}_z)$, in the left panel; Δp_{\max} , Δp_x , Δp_y , and Δp_z , in the right panel) that describe the STA affecting the four skin-markers on the thigh and shank, respectively, during the movement. Outliers are also depicted.



665

666 **Figure 47** – HOPPING. Magnitude of the instantaneous displacement of the four skin-markers glued
 667 on the thigh (a) and shank (b) represented in the relevant ACS. c) Relevant knee joint kinematics
 668 computed according to the convention proposed by Grood and Suntay (1983) (flexion/extension in
 669 blue, with flexion as positive).

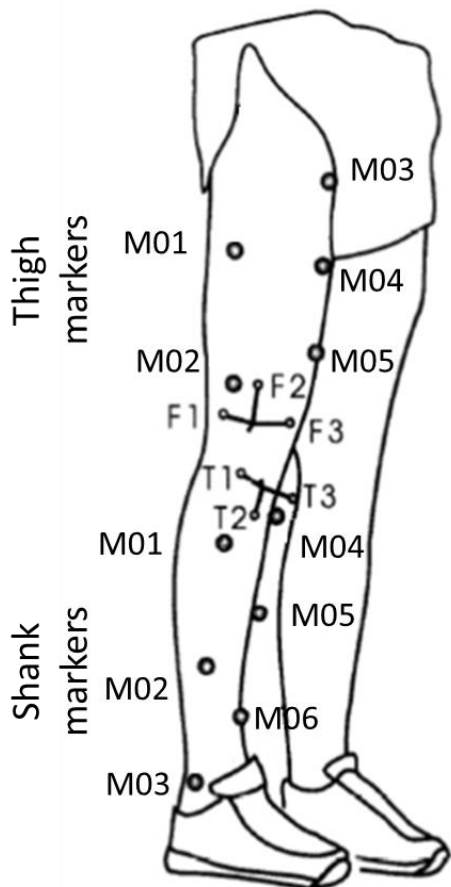
670

671 2.6. ***In-vivo data from CSUOHIO***

672 *Scientific articles of reference* - A detailed description of the original data set can be found
673 in Reinschmidt et al.,1997.

674 *Experimental data description* - Six skin markers were attached to each shank and thigh at
675 standardized locations determined by anatomical landmarks (thigh: M01-M05 placed at 0, 40,
676 and 80% of the distance between greater trochanter and distal end of the lateral femoral
677 condyle; M03-M05 placed along 45, 70, and 95% of the distance between the anterior
678 superior iliac spine and proximal patella. Shank: M01-M03 positioned at 20, 60, and 100% of
679 the distance between the proximal end of the lateral tibial condyle and lateral malleolus;
680 M04-M06 were attached at 0, 40, and 80% of the distance between the mid-tibial plateau and
681 the distal end of the tibia. Three bone markers were also attached (femur: F1-F3; tibia: T1-T3),
682 Fig. 48.

683 *Anatomical coordinate system definitions* – The tibial and femoral ACS were defined
684 based on a standing trial where the subject stood in a neutral hip-wide fully extended knee
685 position with the segments aligned with the force plate representing the laboratory coordinate
686 system (LCS). During this standing trial, the ACS were assumed to be identical to the LCS, to
687 allow for a consistent definition for both the skin and skeletal marker based ACS. A singular-
688 value decomposition method (Soderkvist and Wedin, 1993) was used to calculate the
689 transformation matrices (for each instant in time) between the femur and the tibia ACSs.



690

691 **Figure 48** Bone marker (femur: F1-F3; tibia: T1-T3) and skin markers (thigh: M01-M05; shank: M01-
 692 M06) placement. M01-M05 were placed at 0,40, and 80% of the distance between greater trochanter
 693 and distal end of the lateral femoral condyle. M03-M05 were placed along 45, 70, and 95% of the
 694 distance between greater trochanter and distal end of the lateral femoral condyle. M01-M03 were
 695 positioned at 20, 60, and 100% of the distance between the proximal end of the lateral tibial condyle
 696 and lateral malleolus. M04-M06 were attached at 0, 40, and 80% of the distance between the mid-
 697 tibial plateau and the distal end of the tibia.

698 *Measurement specifications* - Right leg was filmed with three high-speed tine cameras
 699 (200 sample/s). The cameras were synchronized using LEDs triggered by a threshold detector
 700 connected to the force plate. Fluctuations in camera speed were corrected with timing
 701 information from internal LEDs. Each frame was manually digitized, and camera coordinates
 702 were filtered with a bi-directional fourth order low-pass Butterworth filter with a 10 Hz cut-
 703 off frequency determined from a residual analysis (Winter, 1990). Marker coordinates were
 704 time normalized with respect to stance phase and the spatial marker positions were calculated
 705 using DLT (Abdel-Aziz and Karara, 1971). The calibration frame available was not optimal
 706 due to the small number of calibration points (Hatze, 1988) and due to the small size of the
 707 frame (Wood and Marshall, 1986). This was of particular concern for the proximal thigh
 708 markers which were typically outside the calibrated volume. To assess the appropriateness of

709 the DLT model for each marker and to estimate the accuracy in determining the knee
710 rotations, lens distortion errors were estimated from residuals of the three-dimensional
711 reconstruction. Errors (residuals) for the markers were typically 2.5 mm. In the worst case, a
712 2.5 mm lens distortion could lead to about a 2 deg error in orientation of the skeletal
713 segments, and a 1 deg error for the external segments. However, lens distortion tends to be in
714 the same direction on the same segment, and therefore has a considerably smaller effect on
715 joint rotations. Additionally, the 2.5 mm residuals also include errors due to the imperfect
716 synchronization of the cameras affecting similarly the skin and skeletal marker based
717 segments. Differences between skin and skeletal knee rotations well in excess of 2 deg cannot
718 be attributed to inaccuracies of the motion analysis system. Random digitization errors were,
719 after filtering, negligible.

720 *Ground truth* - Intracortical Hofmann bone pins (2.5 mm diameter) with triads of reflective
721 markers were inserted under local anesthesia into the lateral tibia1 and femoral condyles of
722 the subject's right leg. For one subject, skin marker based knee kinematics were also recorded
723 prior to surgery to identify possible changes in running style due to the pin insertion. Knee
724 kinematics showed a small (< 3 deg) shift from pre- to post-surgery condition for all rotations,
725 attributed to slightly different standing trials used to define the anatomical coordinate
726 systems. None of the subjects stated that his ability to run was affected by the pins.

727 *2.6.1. Data sample 18: running*

728 *Subject characteristics* - A male subject whose specific characteristics are not known was
729 randomly selected out of three male subjects (age = 25.7 ± 2.1 y.o., height = 1.87 ± 0.10 m,
730 mass = 85.5 ± 9.6 kg).

731 *Motor task description* - Stance phase of five heel-toe running trials (2.9 ± 0.2 m/s). The
732 subjects wore slightly altered running shoes (Adidas Equipment Cushioning, 1994).

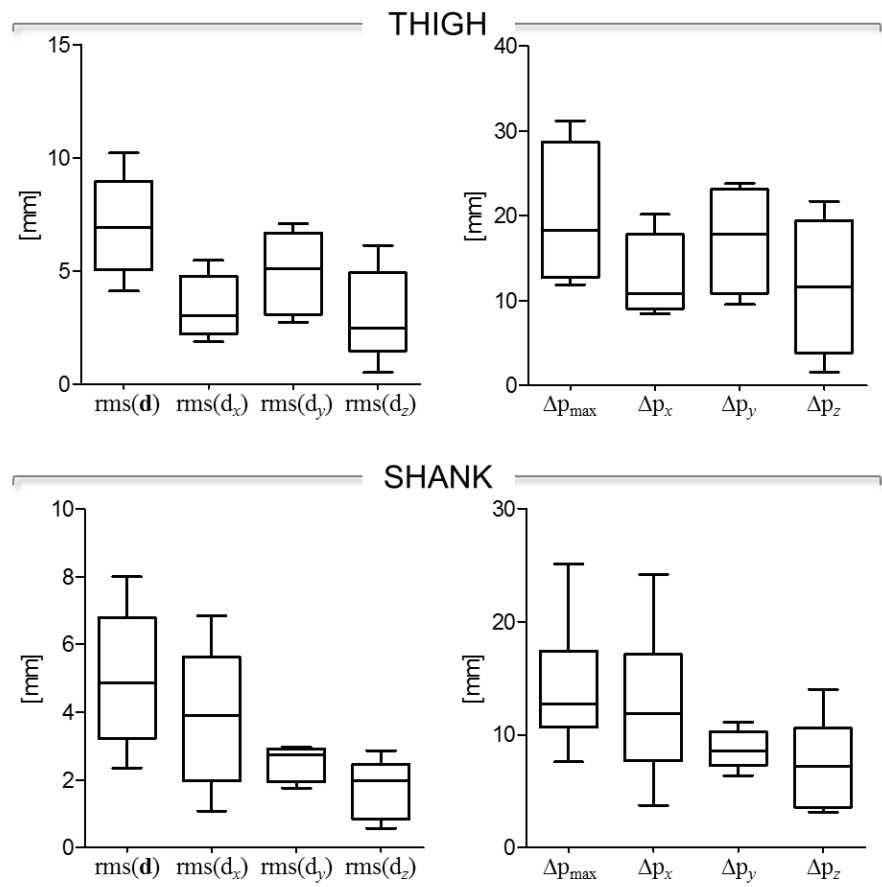
733 *STA characteristics* - Skin-marker trajectories in the thigh and shank ACSs are depicted in
734 Fig. 49. Trajectories were filtered with a bi-directional fourth order low-pass Butterworth
735 filter with a 10 Hz cutoff frequency. Statistical data describing the relevant STAs are shown
736 in Fig. 50. Magnitude of the instantaneous displacement of thigh and shank skin-markers
737 along with the knee joint angular kinematics is depicted in Fig.51.

738

739 **Figure 49** – Femur (a) and tibial (b) ACSs, and thigh and shank skin-marker trajectories (represented
740 in blue and red, respectively). The axes of the ACSs are represented in red, green, and blue for the x
741 (antero/posterior, div = 50 mm), y (superior/inferior, div = 50 mm), and z (right/left, div = 20 mm)
742 directions, respectively.

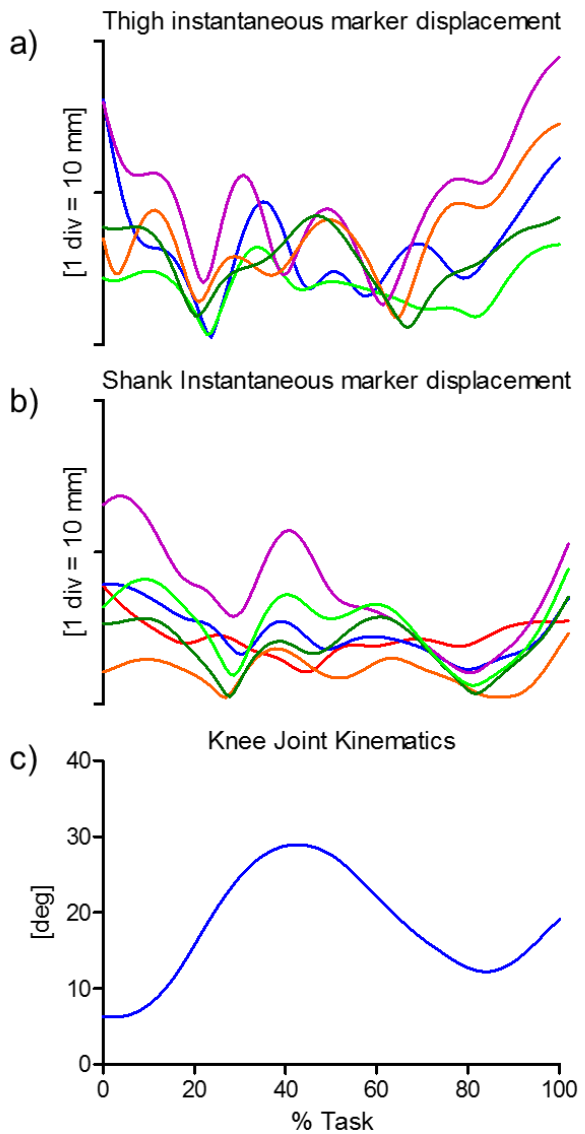
743





744

745 **Figure 50** –Box-plots of the eight parameters ($\text{rms}(\mathbf{d})$, $\text{rms}(\mathbf{d}_x)$, $\text{rms}(\mathbf{d}_y)$, and $\text{rms}(\mathbf{d}_z)$, in the left panel;
 746 Δp_{\max} , Δp_x , Δp_y , and Δp_z , in the right panel) that describe the STA affecting the five and six skin-
 747 markers on the thigh and shank, respectively, during the movement. Outliers are also depicted.



748

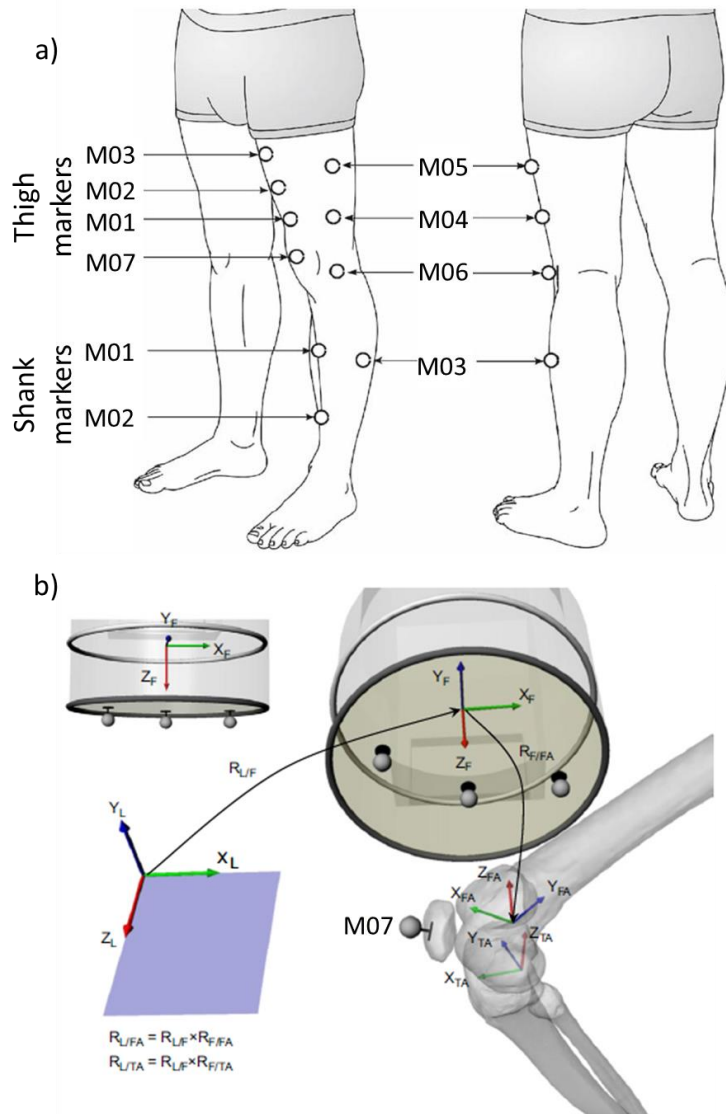
749 **Figure 51** –Magnitude of the instantaneous displacement of the five and six skin-markers glued on the
 750 thigh (a) and shank (b) represented in the relevant ACS. c) Relevant knee joint kinematics computed
 751 according to the convention proposed by Grood and Suntay (1983) (flexion/extension in blue, with
 752 flexion as positive).

753

754 **2.7. In-vivo data from UNIMELB**

755 *Scientific articles of reference* - A detailed description of the original data set can be found
 756 in Akbarshahi et al. (2010).

757 *Experimental data description* - Ten reflective markers were placed on each subject's left
 758 leg (Fig. 52). Markers were positioned on the anterior and lateral aspects of the mid and distal
 759 third of the thigh (M02–M06), the mid anterior and lateral aspects of the shank (M01–M03),
 760 the lateral femoral epicondyle (M01) and the patella (M07).



761

762 **Figure 52** a) Schematic diagram showing the location of the skin-markers. Marker numbers are given
 763 as in the data samples 2, 4, 7, 15. B) three retro-reflective/radio-opaque markers were used to derive
 764 the transformation matrix ($R_{L/F}$) between the laboratory coordinate system (X_L , Y_L , Z_L) and the
 765 fluoroscopy coordinate system (X_F , Y_F , Z_F). Following the registration of the 3D bone models to the
 766 2D X-ray images, the transformation matrices ($R_{F/FA}$ and $R_{F/TA}$) between the anatomical coordinate
 767 systems of the femur and tibia and the fluoroscopy coordinate system were calculated. (L: laboratory
 768 coordinate system; F: fluoroscopy coordinate system; TA: lower leg (tibia/fibula) anatomical
 769 coordinate system, M07: patellar marker used for synchronization).

770 *Anatomical coordinate system definitions* - ACSs were defined using the 3D MRI-based
771 femur and tibia models. Bone-embedded as described in Fernandez et al. (2008) and Eckhoff
772 et al. (2005).

773 *Measurement specifications* - The instantaneous markers position was reconstructed using
774 a 9-camera stereophotogrammetric system (VICON 512 with M1 cameras) acquiring at 120
775 sample/s. The measurement volume was smaller than a 2-m-sided cube.

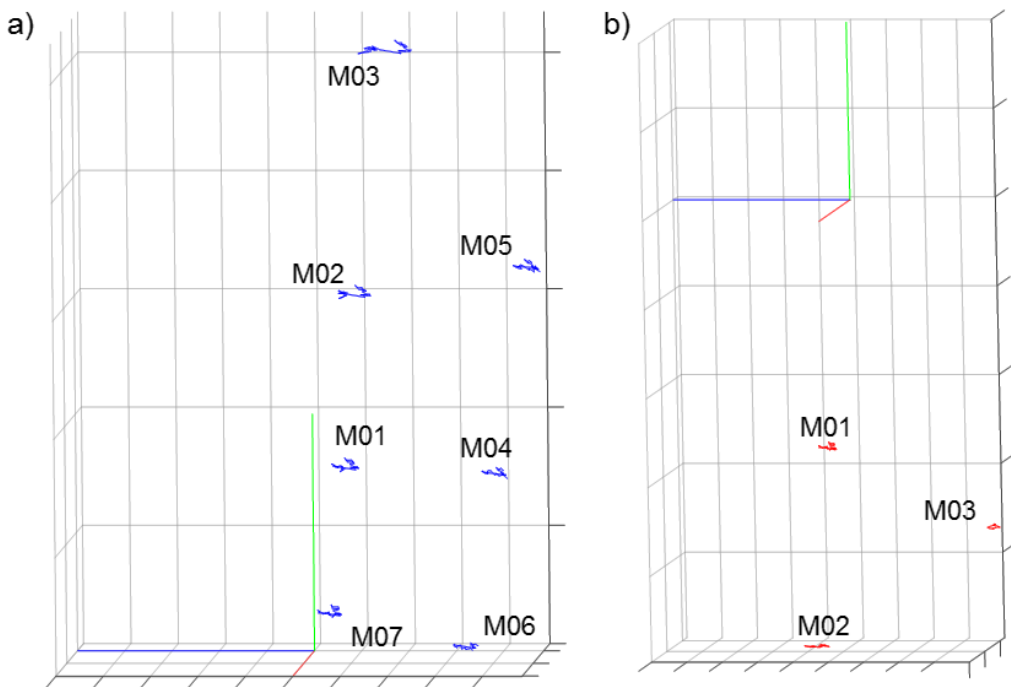
776 *Ground truth* - An X-ray fluoroscopy unit (Pulsera, Philips) operating in pulsed mode at 30
777 sample/s was used. were configured to acquire X-ray images at a maximal frame rate of 30
778 sample/s. Three radio-opaque reflective markers, visible in both stereophotogrammetric and
779 fluoroscopy systems, were placed on a plane parallel to the image plane of the X-ray unit.
780 These markers were used to synchronize data between the two systems using the distance
781 between these and the marker on the patella and to perform relevant coordinate systems
782 transformations. The X-ray images were corrected for image distortion, and the projective
783 parameters of the X-ray system were determined using a calibration routine (Banks and
784 Hodge, 1996). The 3D MRI-based model of the femur and of the tibia were acquired from a
785 3T Siemens MRI device and they were registered to the two dimensional X-ray images using
786 custom software that iteratively matched the model pose to the X-ray images. Maximum
787 errors obtained for the fluoroscopy measurements were 1.5mm for in-plane translations, 3mm
788 for translations normal to the image plane, and 0.61 for rotations in all planes.

789 *2.7.1. Data samples 2,4,7,15: hip axial rotation, open-chain knee flexion, treadmill
790 walking, and step-up*

791 *Subject characteristics* - A 34 y.o. male healthy subject. Height = 1.76 m, mass = 74 kg.

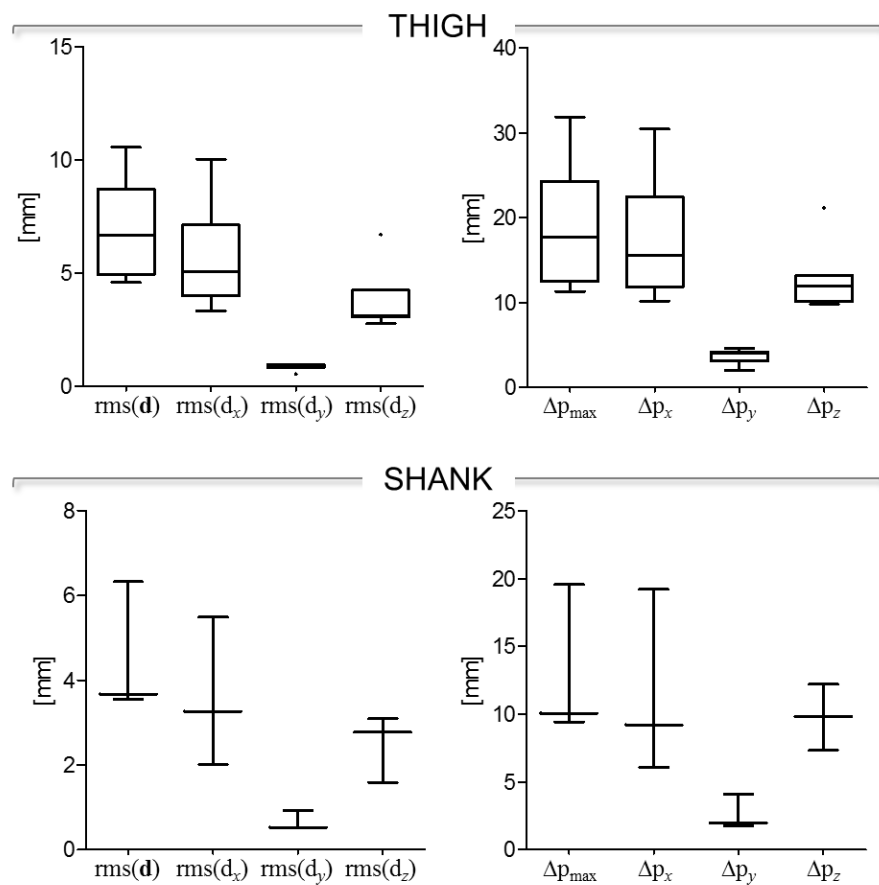
792 *Motor task description* - hip axial rotation with the knee extended and the foot resting in
793 the centre of a swivel disc; open-chain knee flexion; walking on a treadmill (data were visible
794 only from mid-swing to mid-stance due to the limited imaging field of view and occlusion
795 from the contralateral leg); and a step-up.

796 *STA characteristics* - Skin-marker trajectories in the thigh and shank ACSs are depicted in
797 Figs. 53, 56, 59, 62, for hip axial rotation, open-chain knee flexion, treadmill walking, and
798 step-up, respectively. Stereophotogrammetric data were acquired at 120 Hz and then down-
799 sampled to 30 Hz. Statistical data describing the STAs are shown in Figs. 54, 57, 60, 63, for
800 hip axial rotation, open-chain knee flexion, treadmill walking, and step-up, respectively. For
801 each motor task, the magnitude of the instantaneous displacement of thigh and shank skin-
802 markers along with the knee joint angular kinematics are depicted in Figs. 55, 58, 61, 64, for
803 hip axial rotation, open-chain knee flexion, treadmill walking, and step-up, respectively.



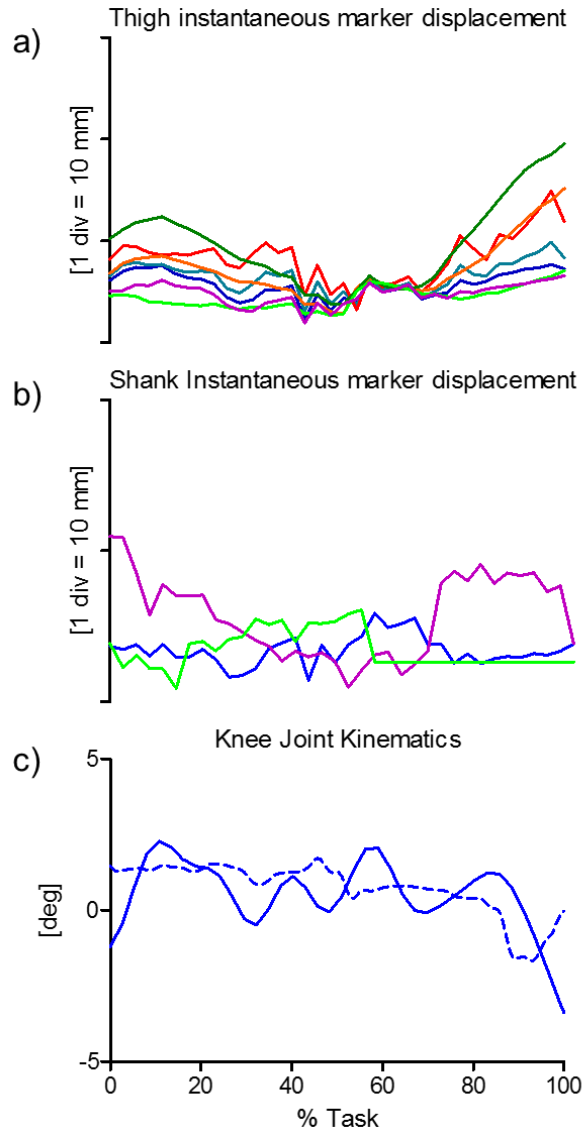
804

805 **Figure 53 – HIP AXIAL ROTATION.** Femur (a) and tibial (b) ACSs, and thigh and shank skin-
 806 marker trajectories (represented in blue and red, respectively). The axes of the ACSs are represented in
 807 red, green, and blue for the x (antero/posterior, div = 50 mm), y (superior/inferior, div = 50 mm), and z
 808 (right/left, div = 20 mm) directions, respectively.
 809

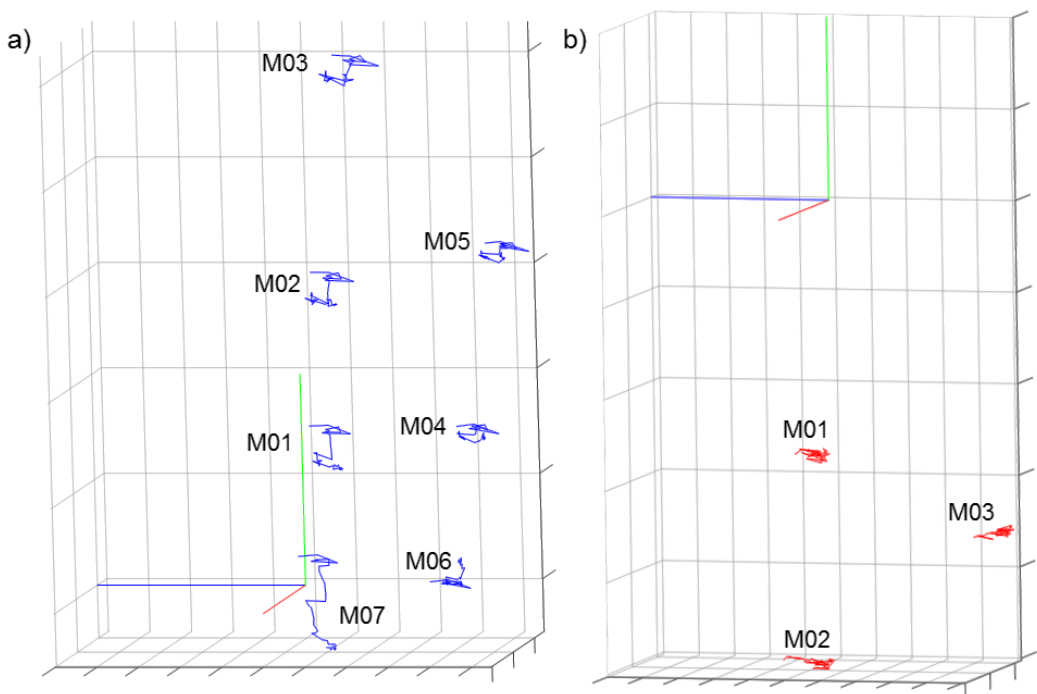


810

811 **Figure 54** – HIP AXIAL ROTATION. Box-plots of the eight parameters (rms(**d**), rms(d_x), rms(d_y),
 812 and rms(d_z), in the left panel; Δp_{\max} , Δp_x , Δp_y , and Δp_z , in the right panel) that describe the STA
 813 affecting the six and three skin-markers on the thigh and shank, respectively, during the movement.
 814 Outliers are also depicted.

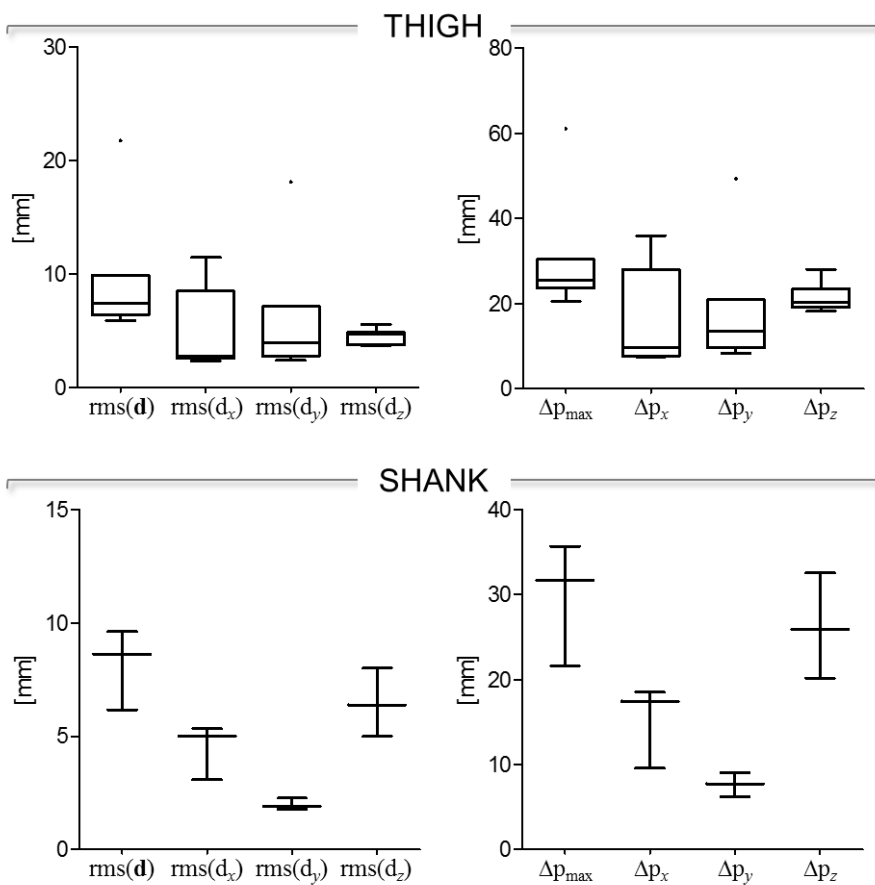


815
 816 **Figure 55** – HIP AXIAL ROTATION. Magnitude of the instantaneous displacement of the six and
 817 three skin-markers glued on the thigh (a) and shank (b) represented in the relevant ACS. c) Relevant
 818 knee joint kinematics computed according to the convention proposed by Grood and Suntay (1983)
 819 (flexion/extension in blue, with flexion as positive – fluoro kinematics in continuous line and the best
 820 performing marker-based kinematic in dotted line).



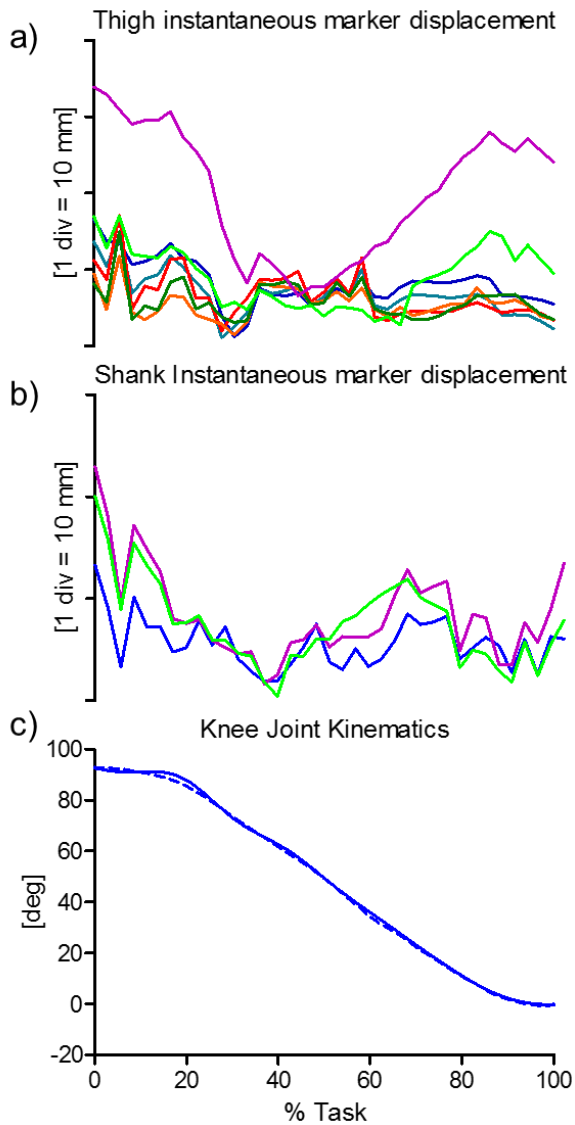
821

822 **Figure 56 – OPEN-CHAIN KNEE FLEXION.** Femur (a) and tibial (b) ACSs, and thigh and shank
 823 skin-marker trajectories (represented in blue and red, respectively). The axes of the ACSs are
 824 represented in red, green, and blue for the x (antero/posterior, div = 50 mm), y (superior/inferior, div =
 825 50 mm), and z (right/left, div = 20 mm) directions, respectively.
 826

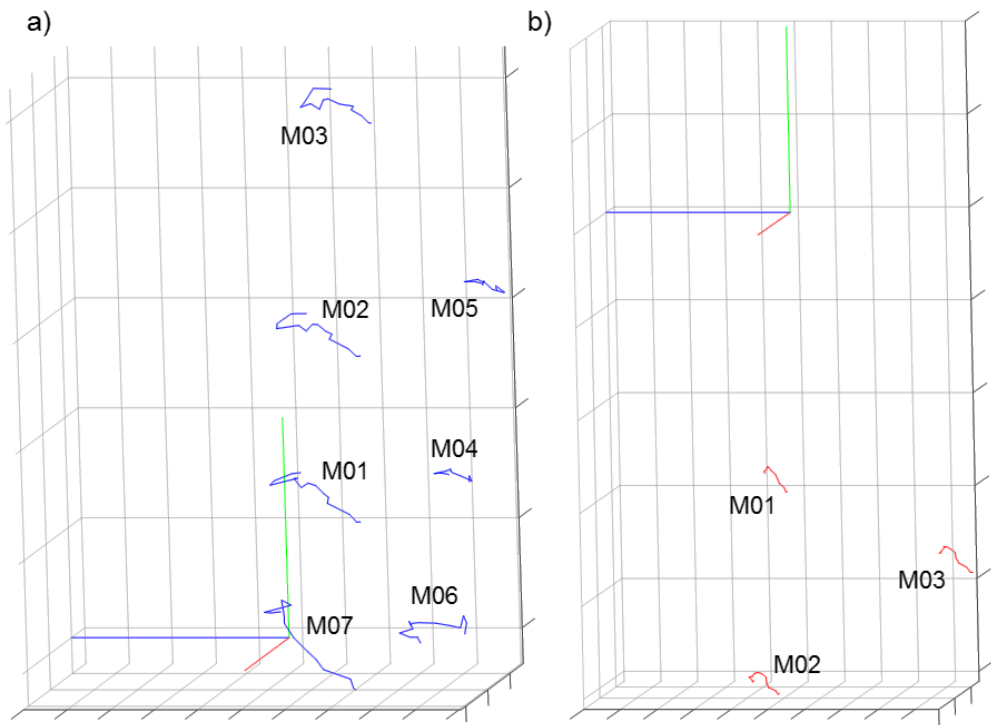


827

828 **Figure 57** – OPEN-CHAIN KNEE FLEXION. Box-plots of the eight parameters (rms(**d**), rms(d_x),
 829 rms(d_y), and rms(d_z), in the left panel; Δp_{\max} , Δp_x , Δp_y , and Δp_z , in the right panel) that describe the
 830 STA affecting the six and three skin-markers on the thigh and shank, respectively, during the
 831 movement. Outliers are also depicted.



832
 833 **Figure 58** – OPEN-CHAIN KNEE FLEXION. Magnitude of the instantaneous displacement of the six
 834 and three skin-markers glued on the thigh (a) and shank (b) represented in the relevant ACS. c)
 835 Relevant knee joint kinematics computed according to the convention proposed by Grood and Suntay
 836 (flexion/extension in blue, with flexion as positive – fluoro kinematics in continuous line and
 837 the best performing marker-based kinematic in dotted line).

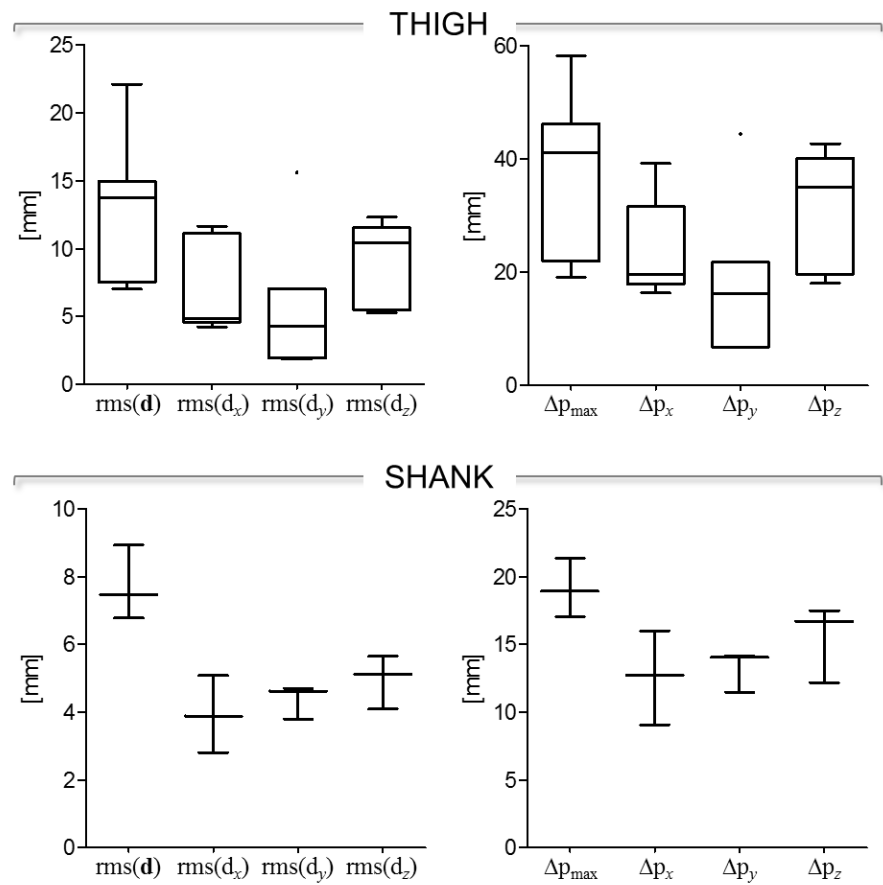


838

839 **Figure 59 – WALKING ON A TREADMILL.** Femur (a) and tibial (b) ACSs, and thigh and shank
 840 skin-marker trajectories (represented in blue and red, respectively). The axes of the ACSs are
 841 represented in red, green, and blue for the x (antero/posterior, div = 50 mm), y (superior/inferior, div =
 842 50 mm), and z (right/left, div = 20 mm) directions, respectively.

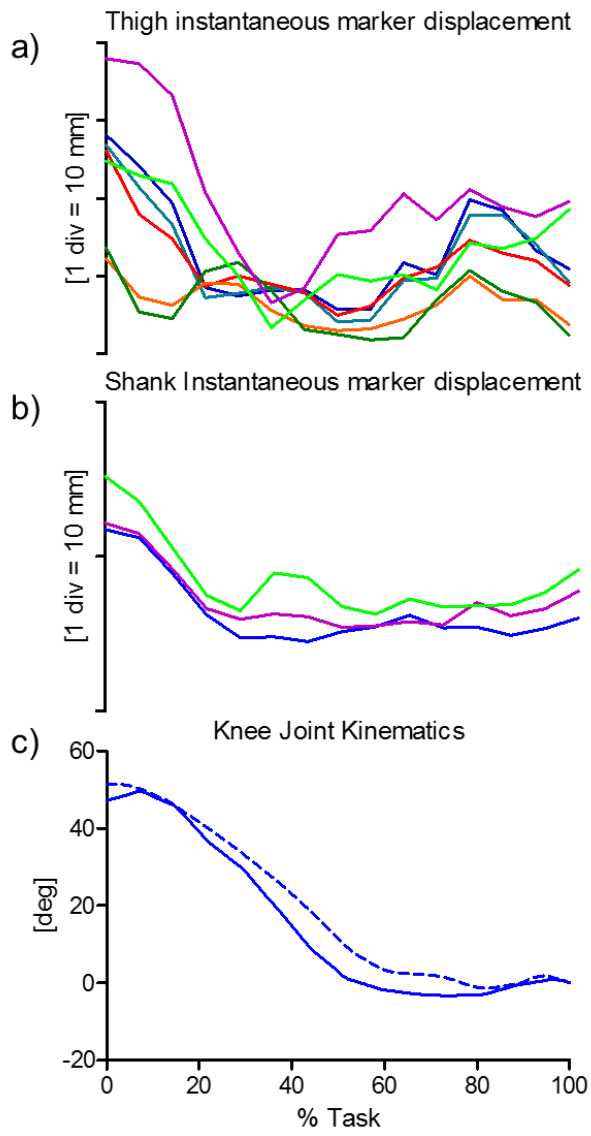
843

844



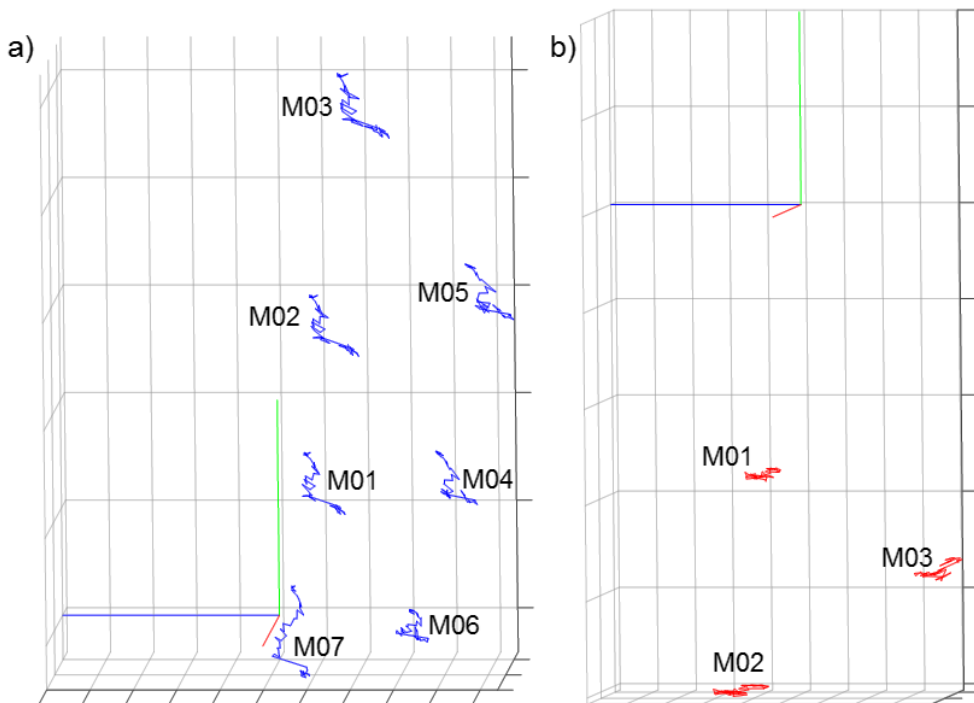
845

846 **Figure 60 – WALKING ON A TREADMILL.** Box-plots of the eight parameters (rms(d), rms(d_x),
 847 rms(d_y), and rms(d_z), in the left panel; Δp_{max}, Δp_x, Δp_y, and Δp_z, in the right panel) that describe the
 848 STA affecting the six and three skin-markers on the thigh and shank, respectively, during the
 849 movement. Outliers are also depicted.



850

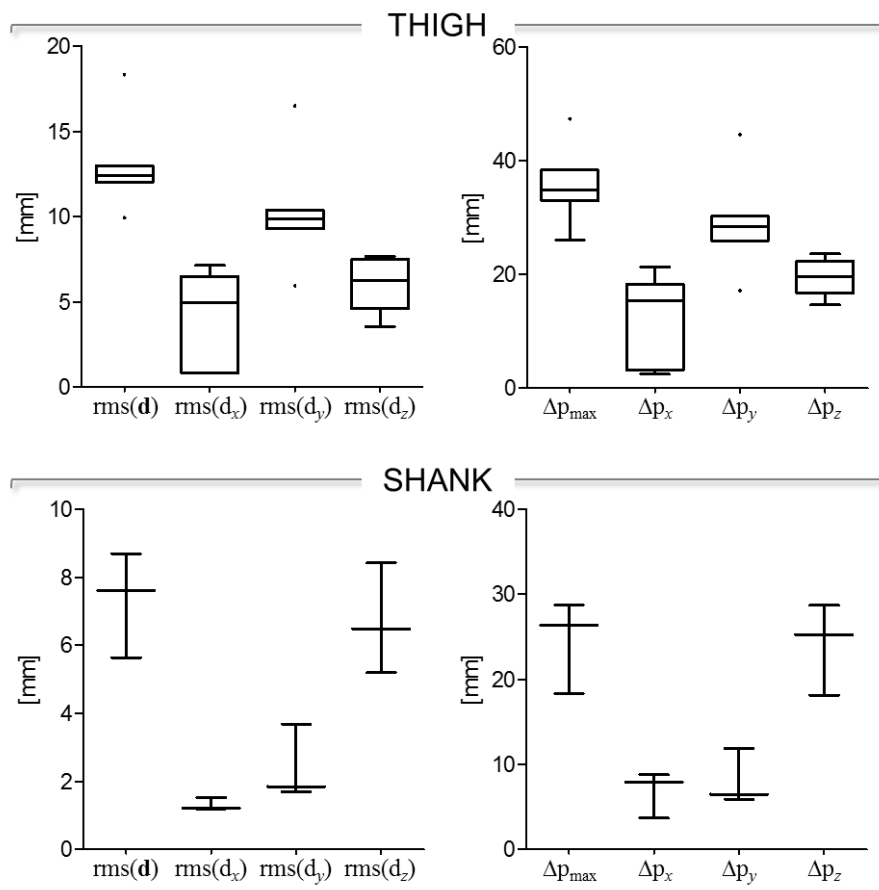
851 **Figure 61 – WALKING ON A TREADMILL.** Data were visible only from mid-swing to mid-stance.
 852 Magnitude of the instantaneous displacement of the six and three skin-markers glued on the thigh (a)
 853 and shank (b) represented in the relevant ACS. c) Relevant knee joint kinematics computed according
 854 to the convention proposed by Grood and Suntay (1983) (flexion/extension in blue, with flexion as
 855 positive – fluoro kinematics in continuous line and the best performing marker-based kinematic in
 856 dotted line).



857

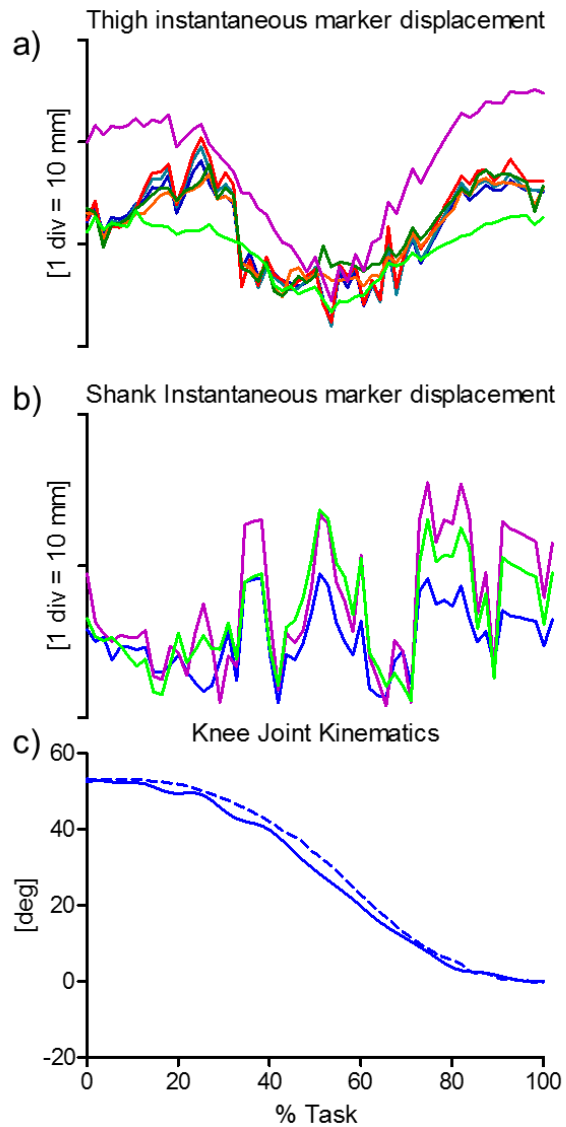
858 **Figure 62 – STEP-UP.** Femur (a) and tibial (b) ACSs, and thigh and shank skin-marker trajectories
 859 (represented in blue and red, respectively). The axes of the ACSs are represented in red, green, and
 860 blue for the x (antero/posterior, div = 50 mm), y (superior/inferior, div = 50 mm), and z (right/left, div
 861 = 20 mm) directions, respectively.

862



863

864 **Figure 63** – STEP-UP. Box-plots of the eight parameters ($\text{rms}(\mathbf{d})$, $\text{rms}(d_x)$, $\text{rms}(d_y)$, and $\text{rms}(d_z)$, in the
 865 left panel; Δp_{\max} , Δp_x , Δp_y , and Δp_z , in the right panel) that describe the STA affecting the six and three
 866 skin-markers on the thigh and shank, respectively, during the movement. Outliers are also depicted.



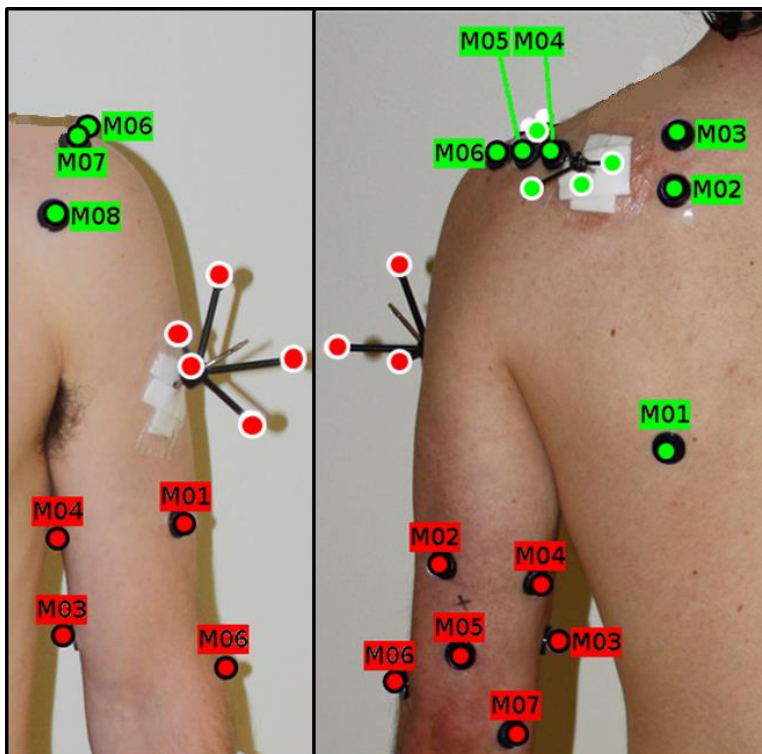
867
 868 **Figure 64** – STEP-UP. Magnitude of the instantaneous displacement of the six and three skin-markers
 869 glued on the thigh (a) and shank (b) represented in the relevant ACS. c) Relevant knee joint kinematics
 870 computed according to the convention proposed by Grood and Suntay (1983) (flexion/extension in
 871 blue, with flexion as positive – fluoro kinematics in continuous line and the best performing marker-
 872 based kinematic in dotted line).

873

874 2.8. *In-vivo data from S2M*

875 *Scientific articles of reference* - A detailed description of the original data set can be found
876 in Dal Maso et al., (2014) and Dal Maso et al., (2015).

877 *Experimental data description* - Seven and eight markers were attached on the humeral and
878 scapular regions, respectively. This included two markers on the humerus ALs (EL, EM, the
879 third “AL marker” was the gleno-humeral joint centre optimally located via a functional
880 approach (Begon et al., 2007)), three markers on the scapular ALs (AI, TS, AA), and seven
881 and eight technical markers on the arm and over the region of the scapula, respectively. (Fig.
882 65).



883
884 **Figure 65** – Marker placement including both pin- and skin-marker clusters (over anatomical
885 landmarks and in technical positions). Only the markers included in the data samples 20,21,23-31 are
886 shown, for the scapula (in green, M02 = TS, M06 = AA, M01 = AI) and for the arm (in red, M06=EL,
887 M07=EM).

888 *Anatomical coordinate system definitions* - Both humeral and scapular ACSs were
889 determined according to the definitions proposed in Wu et al. (2005).

890 *Measurement specifications* - The instantaneous markers position was reconstructed using
891 an 18-camera stereophotogrammetric system (VICON; Oxford Metrics Ltd., Oxford, UK; 5
892 cameras T20S and 13 cameras T40S) acquiring at 300 sample/s. The measurement volume
893 was a 2.5-m-sided square, 1.6-m-height. A rigid stick was used to perform a spot-check of the
894 stereophotogrammetric system accuracy and revealed an accuracy of 0.5 mm (min-max
895 range).

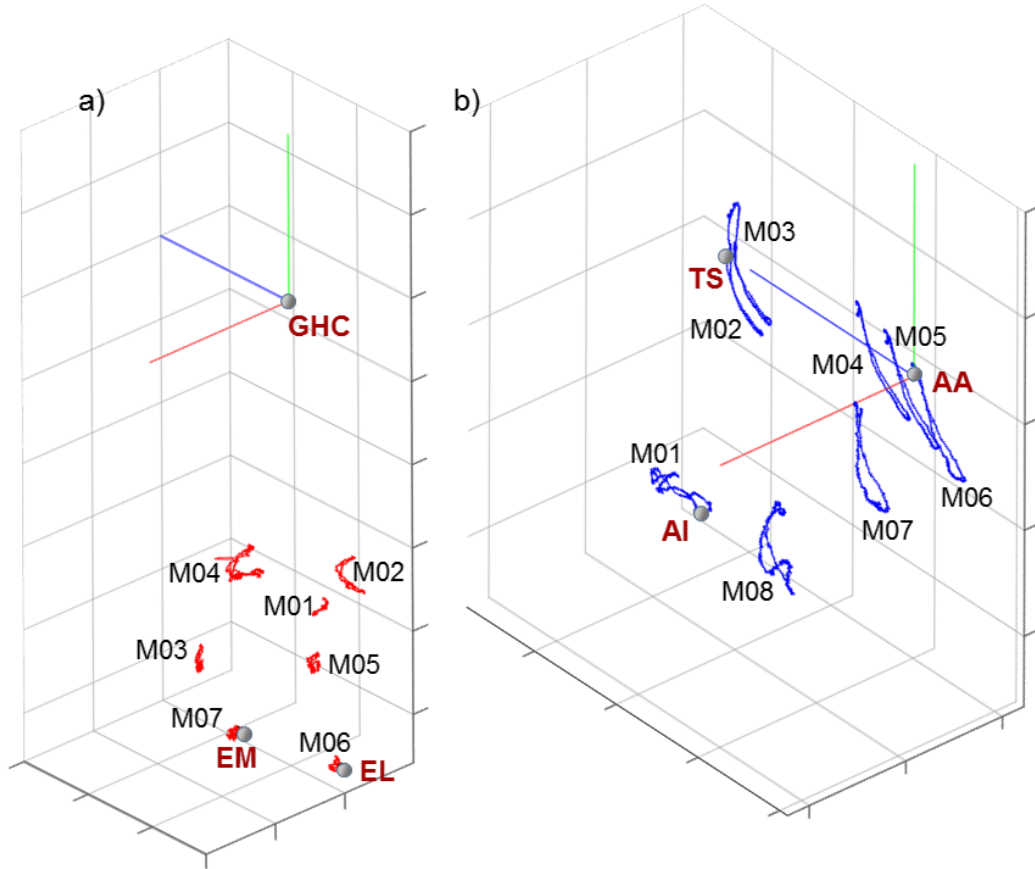
896 *Ground truth* - Intracortical pins were inserted into the first third of the scapular spine and
897 on the lateral aspect of the humerus just below the attachment of the middle deltoid of the
898 participants' left side. Clusters of four and five reflective markers were secured on scapular
899 and humeral pins, respectively. Pin locations were chosen to avoid muscles and the rigidity of
900 the montage was manually checked.

901 *2.8.1. Data samples 20,21,23,25: Arm elevations*

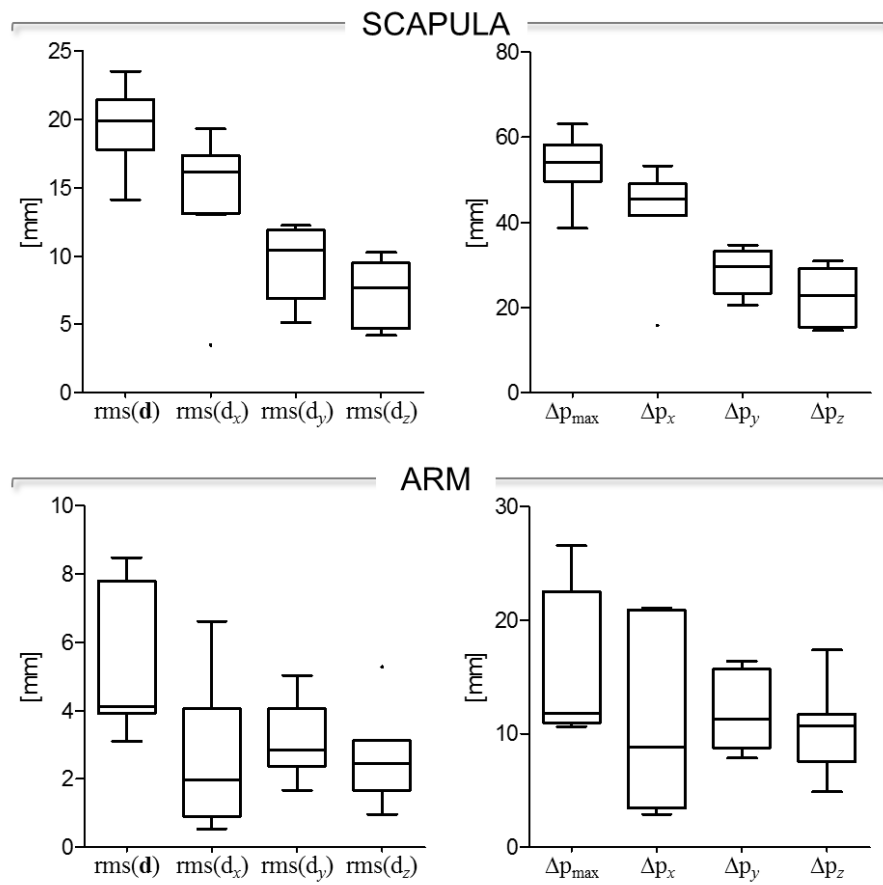
902 *Subject characteristics* - A healthy male subject 27 y.o. Height = 1.65 m, mass = 57 kg.

903 *Motor task description* - The trial started with the arm relaxed at the side with thumb
904 pointing forward referred to as neutral axial rotation. The following shoulder motions were
905 analyzed: one arm elevation at their maximum range of motion in four planes of elevation
906 adduction, abduction, flexion, and extension. The subject was asked to elevate his arm at his
907 own pace without changing its axial rotation from the relaxed position. The elbow was kept
908 extended throughout the elevations.

909 *STA characteristics* - Skin-marker trajectories in the scapula and arm ACSs are depicted in
910 Figs. 66, 69, 72, 75, for arm elevations during adduction, abduction, flexion, and extension,
911 respectively. Unfiltered data were used. Statistical data describing the STAs are shown in
912 Figs. 67, 70, 73, 76, for arm elevations during adduction, abduction, flexion, and extension,
913 respectively. For each motor task, the magnitude of the instantaneous displacement of scapula
914 and arm skin-markers along with the shoulder joint angular kinematics are depicted in Figs.
915 68, 71, 74, 77, for arm elevations during adduction, abduction, flexion, and extension,
916 respectively.

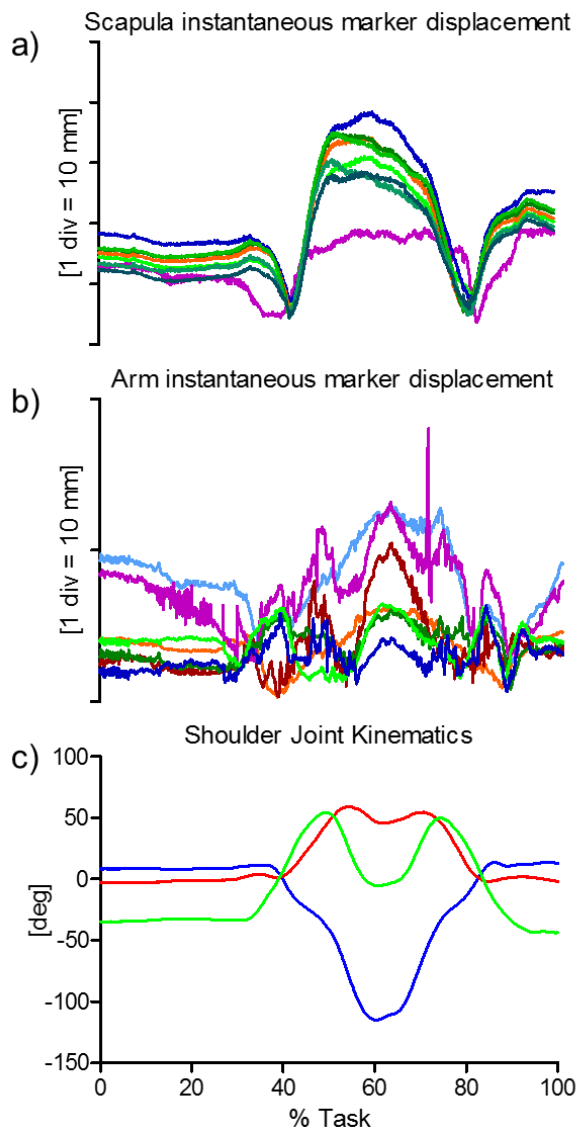


917
 918 **Figure 66 – ADDUCTION.** Humeral (a) and scapular (b)
 919 ACSs, relevant ALs,
 920 and arm and scapula
 921 skin-marker trajectories
 922 (represented in red and blue,
 923 respectively). The axes of the ACSs are
 represented in red, green, and blue for the x
 (antero/posterior, div = 50 mm), y
 (superior/inferior, div =
 50 mm), and z (right/left, div = 50 mm) directions, respectively.



924

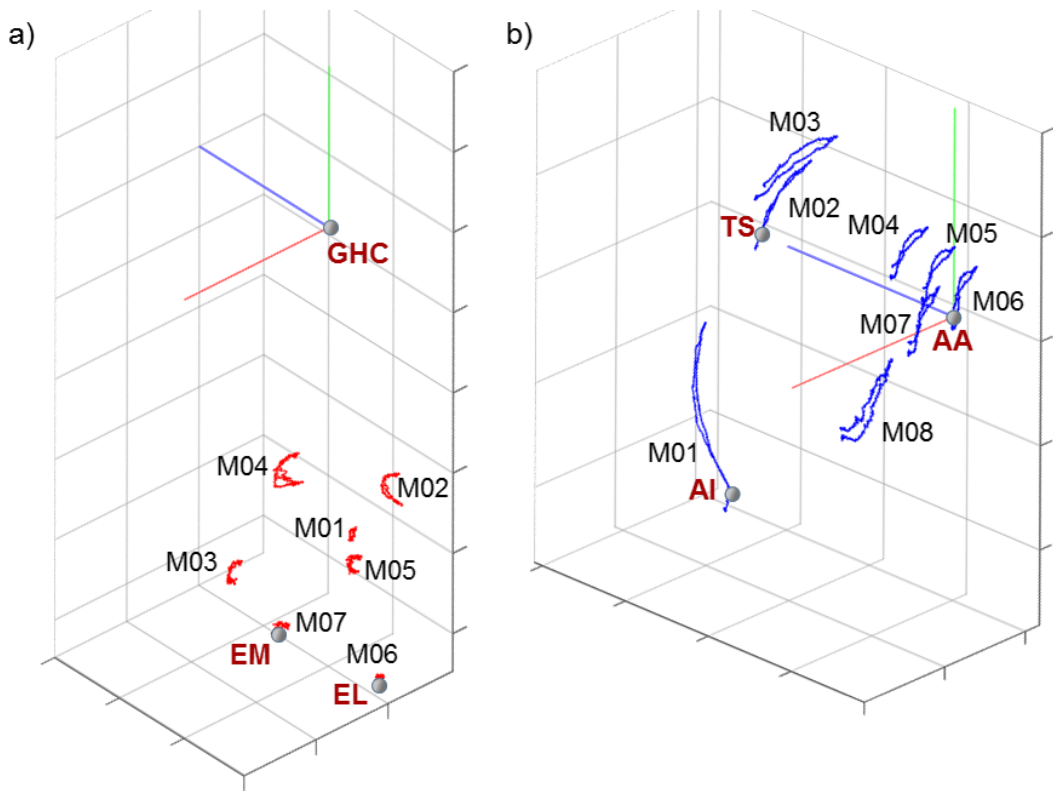
925 **Figure 67 – ADDUCTION.** Box-plots of the eight parameters (rms(d), rms(d_x), rms(d_y), and rms(d_z),
 926 in the left panel; Δp_{\max} , Δp_x , Δp_y , and Δp_z , in the right panel) that describe the STA affecting the eight
 927 and seven skin-markers on the scapula and arm, respectively, during the movement. Outliers are also
 928 depicted.



929
930
931
932
933
934
935
936

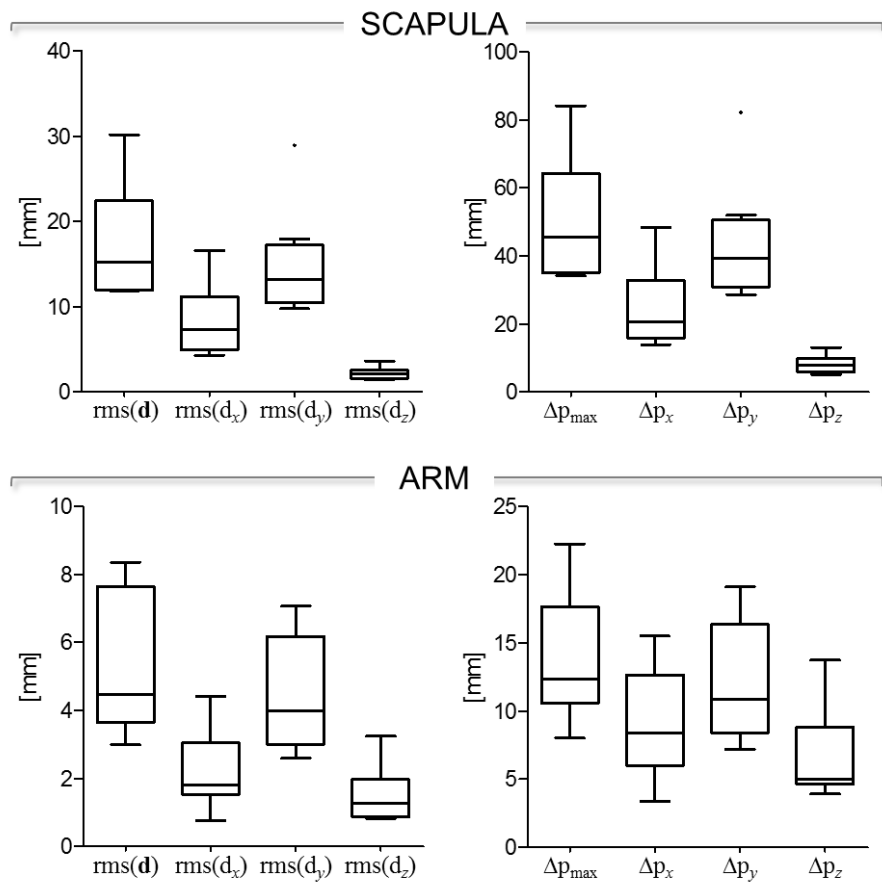
Figure 68 – ADDUCTION. Magnitude of the instantaneous displacement of the eight and seven skin-markers glued on the scapula (a) and arm (b) represented in the relevant ACS. c) Relevant shoulder kinematics calculated using the $X_t Z_f' Y_h''$ sequence (Bonnefoy-Mazure et al., 2012): rotation around the X_t axis of the thorax corresponding to the shoulder elevation (blue); rotation around the floating Z_f' axis corresponding to the shoulder flexion/extension (red); rotation around the Y_h'' axis of the humerus corresponding to the shoulder axial rotation (green). Superior elevation, flexion and internal rotations are positive.

937



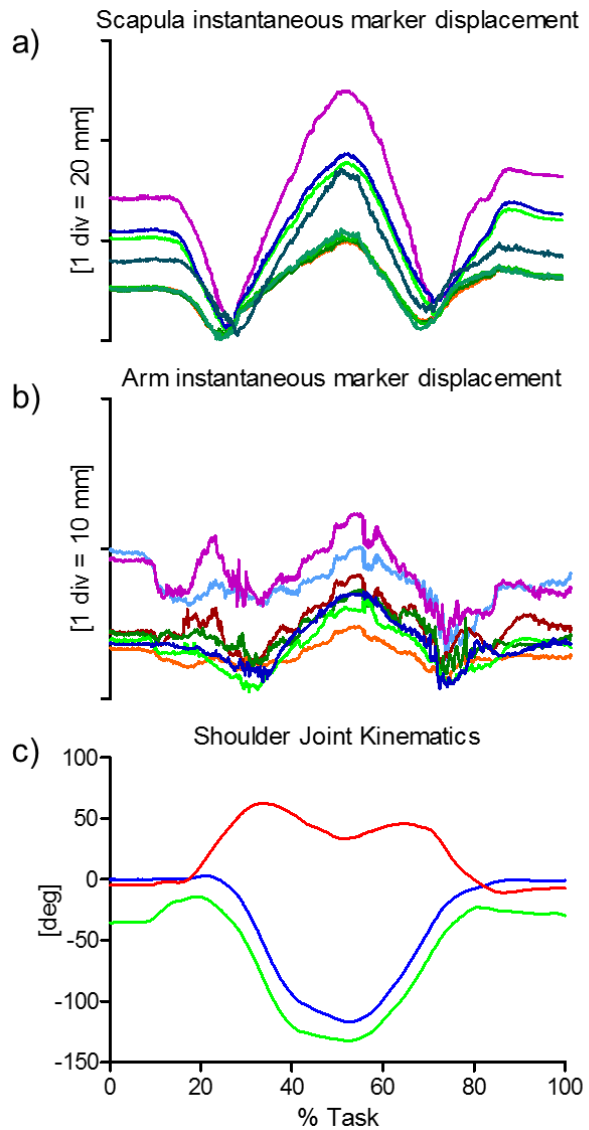
938
 939
 940
 941
 942
 943

Figure 69 – ABDUCTION. Humeral (a) and scapular (b) ACSs, relevant ALs, and arm and scapula skin-marker trajectories (represented in red and blue, respectively). The axes of the ACSs are represented in red, green, and blue for the x (antero/posterior, div = 50 mm), y (superior/inferior, div = 50 mm), and z (right/left, div = 50 mm) directions, respectively.



944
945
946
947
948

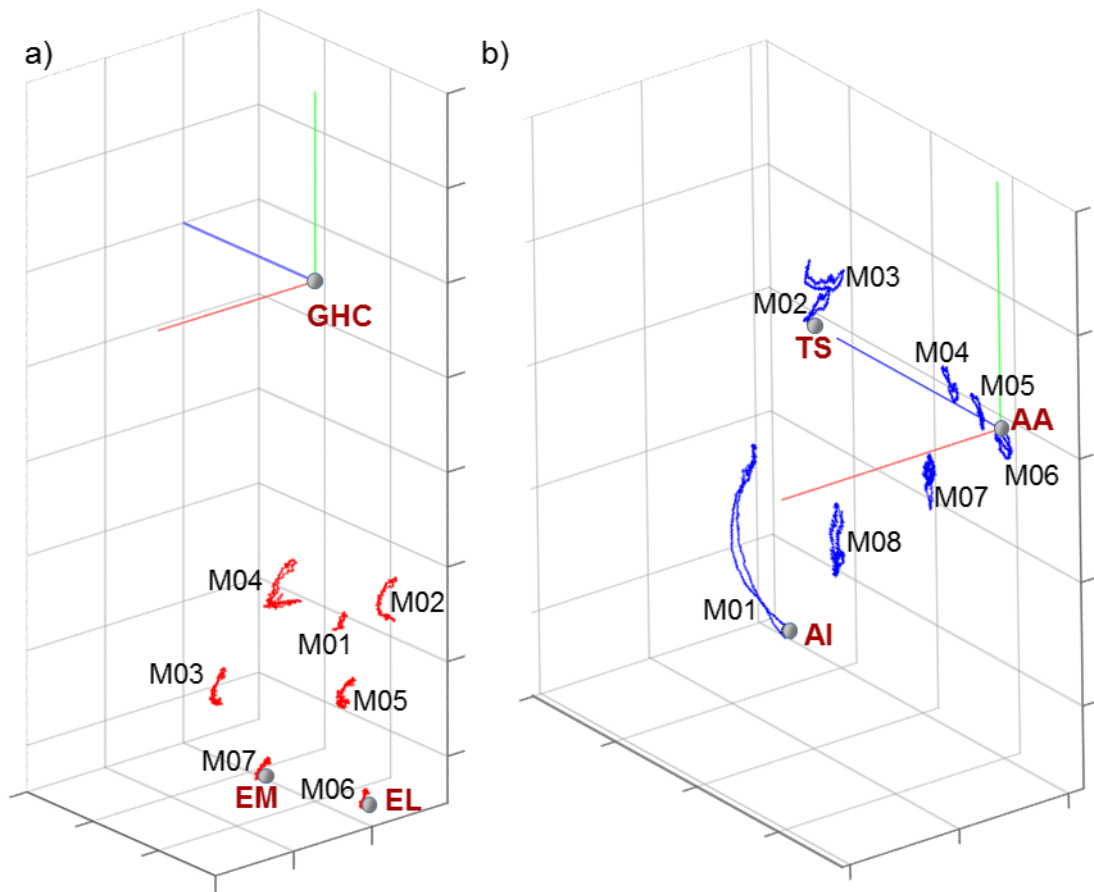
Figure 70 – ABDUCTION. Box-plots of the eight parameters ($\text{rms}(\mathbf{d})$, $\text{rms}(\mathbf{d}_x)$, $\text{rms}(\mathbf{d}_y)$, and $\text{rms}(\mathbf{d}_z)$, in the left panel; Δp_{\max} , Δp_x , Δp_y , and Δp_z , in the right panel) that describe the STA affecting the eight and seven skin-markers on the scapula and arm, respectively, during the movement. Outliers are also depicted.



949
950
951
952
953
954
955
956

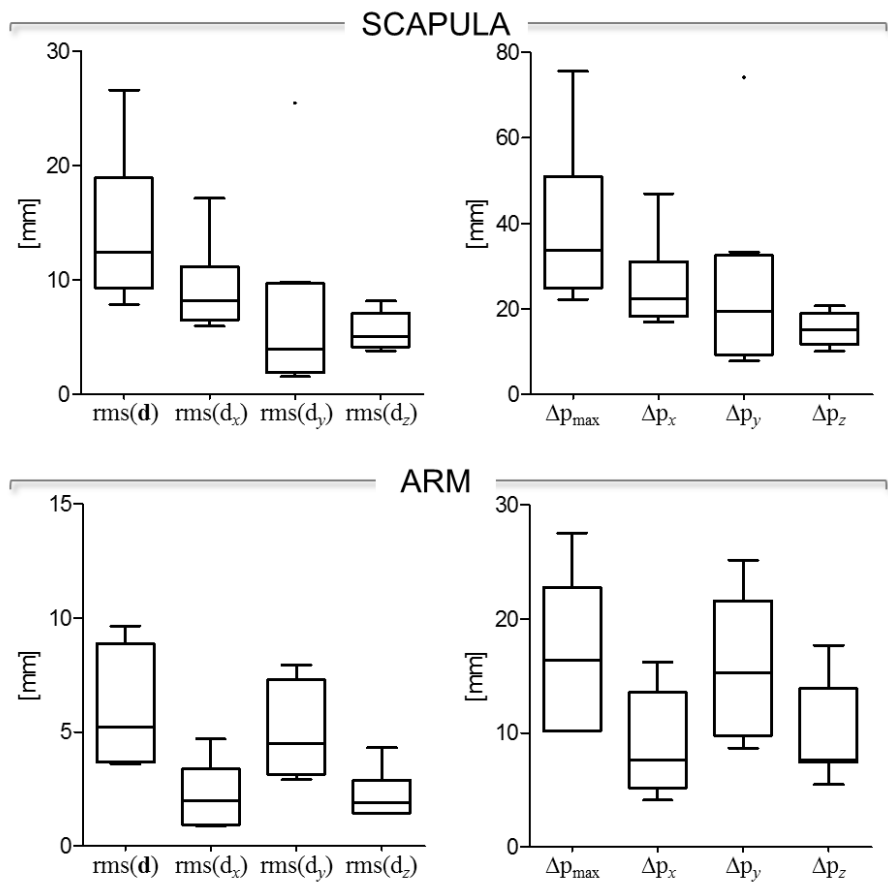
Figure 71 – ABDUCTION. Magnitude of the instantaneous displacement of the eight and seven skin-markers glued on the scapula (a) and arm (b) represented in the relevant ACS. c) Relevant shoulder kinematics calculated using the X_t Z_f' Y_h'' sequence (Bonnefoy-Mazure et al., 2012): rotation around the X_t axis of the thorax corresponding to the shoulder elevation (blue); rotation around the floating Z_f' axis corresponding to the shoulder flexion/extension (red); rotation around the Y_h'' axis of the humerus corresponding to the shoulder axial rotation (green). Superior elevation, flexion and internal rotations are positive.

957



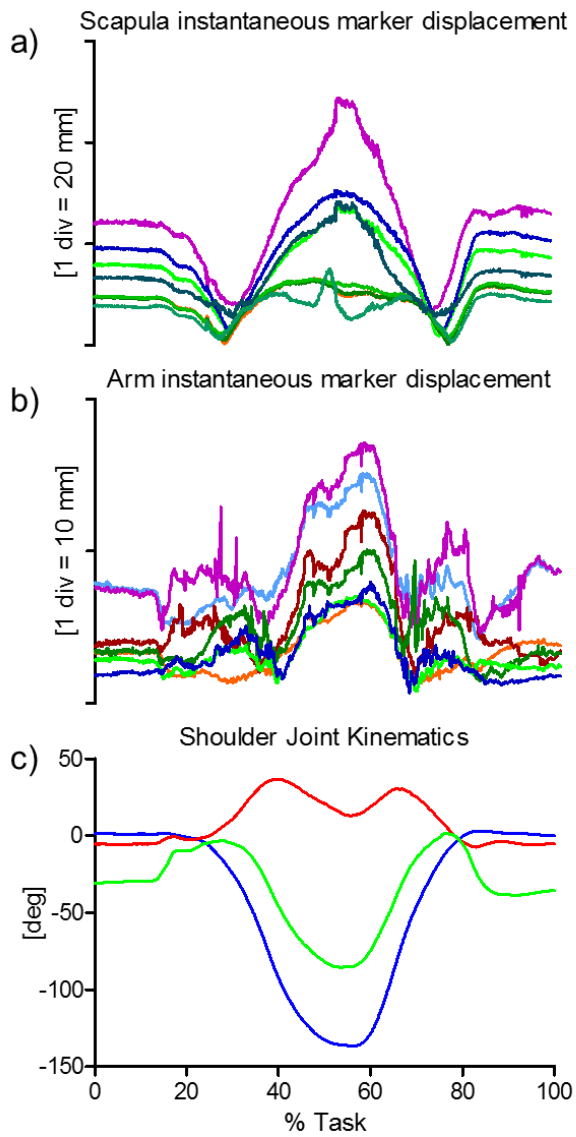
958
 959
 960
 961
 962
 963
 964

Figure 72 – FLEXION. Humeral (a) and scapular (b) ACSs, relevant ALs, and arm and scapula skin-marker trajectories (represented in red and blue, respectively). The axes of the ACSs are represented in red, green, and blue for the x (antero/posterior, div = 50 mm), y (superior/inferior, div = 50 mm), and z (right/left, div = 50 mm) directions, respectively.



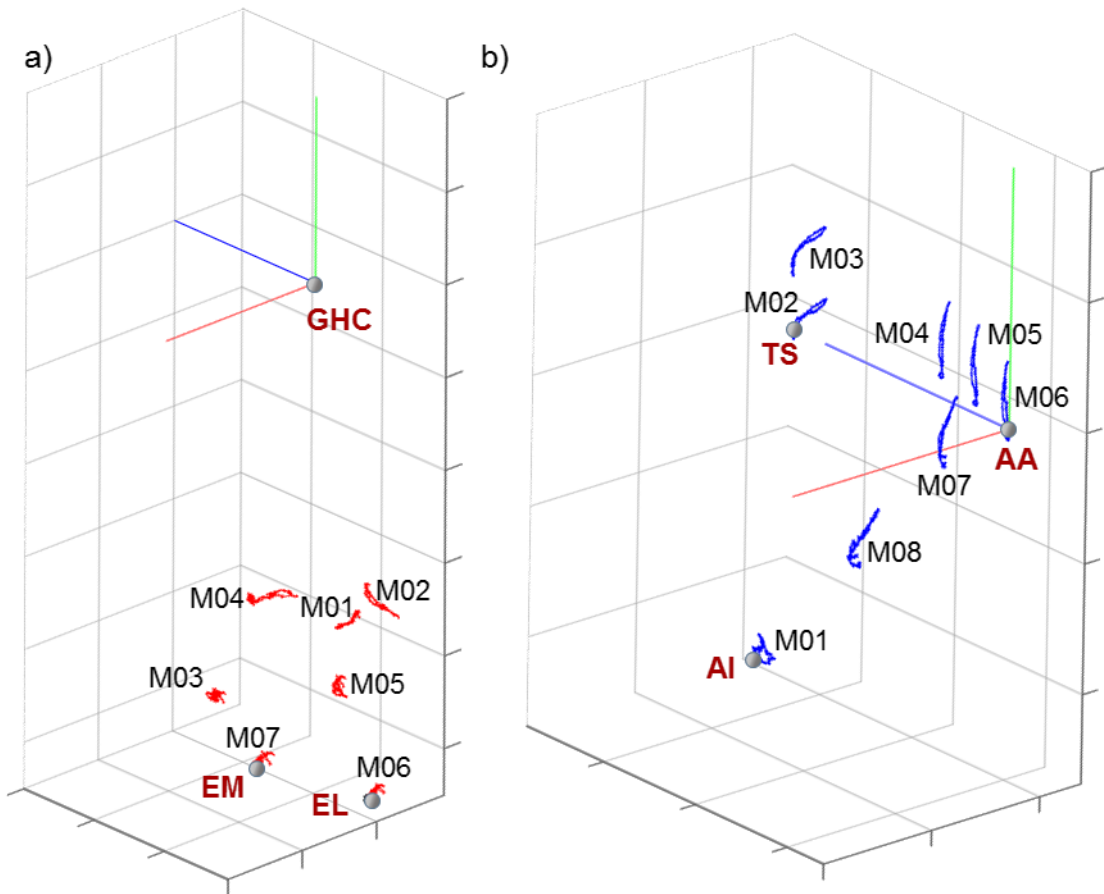
965
966
967
968
969

Figure 73 – FLEXION. Box-plots of the eight parameters ($\text{rms}(\mathbf{d})$, $\text{rms}(\mathbf{d}_x)$, $\text{rms}(\mathbf{d}_y)$, and $\text{rms}(\mathbf{d}_z)$, in the left panel; Δp_{\max} , Δp_x , Δp_y , and Δp_z , in the right panel) that describe the STA affecting the eight and seven skin-markers on the scapula and arm, respectively, during the movement. Outliers are also depicted.



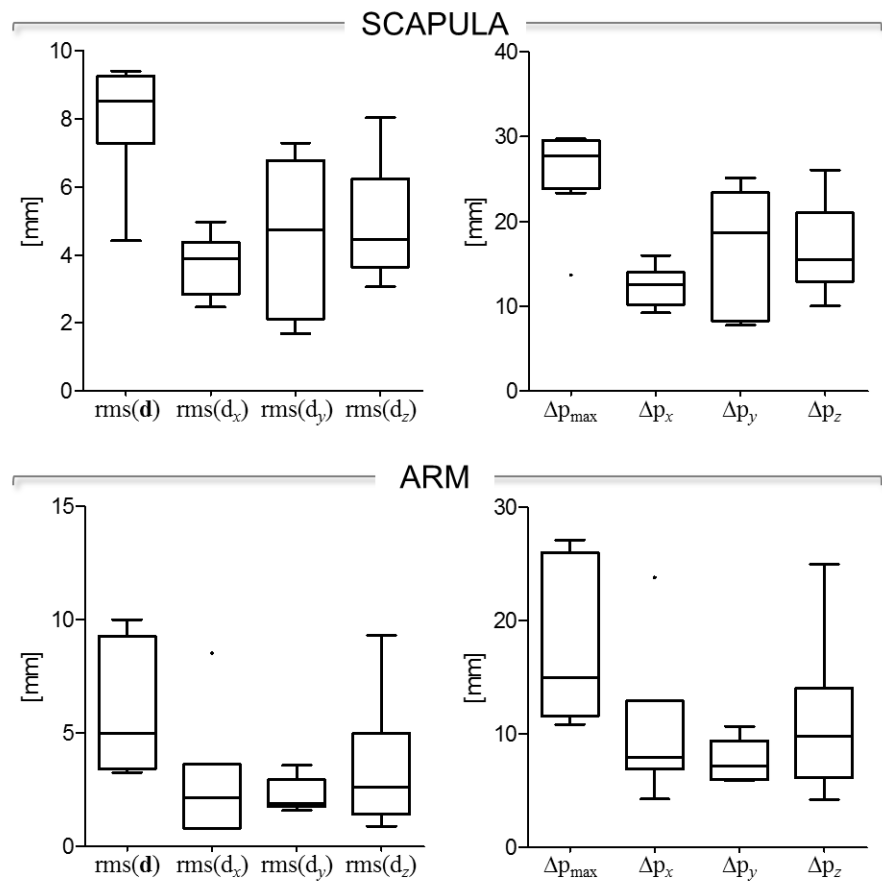
970
971
972
973
974
975
976
977

Figure 74 – FLEXION. Magnitude of the instantaneous displacement of the eight and seven skin-markers glued on the scapula (a) and arm (b) represented in the relevant ACS. c) Relevant shoulder kinematics calculated using the $X_t Z_f' Y_h''$ sequence (Bonnefoy-Mazure et al., 2012): rotation around the X_t axis of the thorax corresponding to the shoulder elevation (blue); rotation around the floating Z_f' axis corresponding to the shoulder flexion/extension (red); rotation around the Y_h'' axis of the humerus corresponding to the shoulder axial rotation (green). Superior elevation, flexion and internal rotations are positive.



978
979
980
981
982
983

Figure 75 – EXTENSION. Humeral (a) and scapular (b) ACSs, relevant ALs, and arm and scapula skin-marker trajectories (represented in red and blue, respectively). The axes of the ACSs are represented in red, green, and blue for the x (antero/posterior, div = 50 mm), y (superior/inferior, div = 50 mm), and z (right/left, div = 50 mm) directions, respectively.



984
985
986
987
988

Figure 76 – EXTENSION. Box-plots of the eight parameters ($\text{rms}(\mathbf{d})$, $\text{rms}(\mathbf{d}_x)$, $\text{rms}(\mathbf{d}_y)$, and $\text{rms}(\mathbf{d}_z)$, in the left panel; Δp_{\max} , Δp_x , Δp_y , and Δp_z , in the right panel) that describe the STA affecting the eight and seven skin-markers on the scapula and arm, respectively, during the movement. Outliers are also depicted.

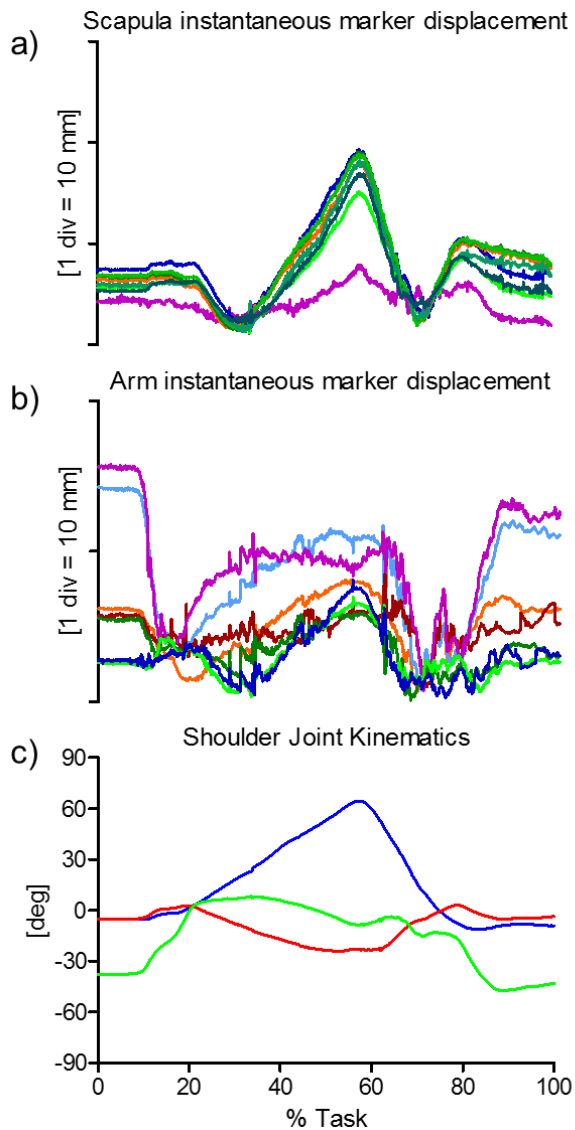


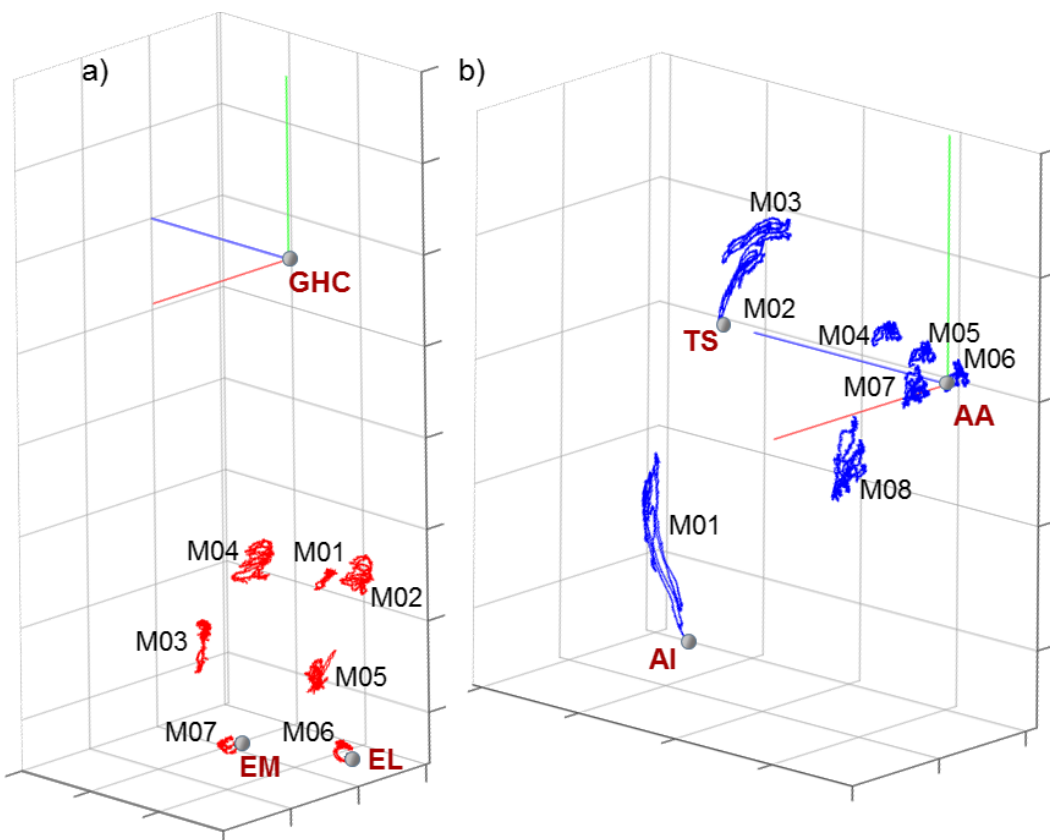
Figure 77 – EXTENSION. Magnitude of the instantaneous displacement of the eight and seven skin-markers glued on the scapula (a) and arm (b) represented in the relevant ACS. c) Relevant shoulder kinematics calculated using the $X_t Z_f' Y_h''$ sequence (Bonnefoy-Mazure et al., 2012): rotation around the X_t axis of the thorax corresponding to the shoulder elevation (blue); rotation around the floating Z_f' axis corresponding to the shoulder flexion/extension (red); rotation around the Y_h'' axis of the humerus corresponding to the shoulder axial rotation (green). Superior elevation, flexion and internal rotations are positive.

2.8.2. Data samples 26-31: daily living activities

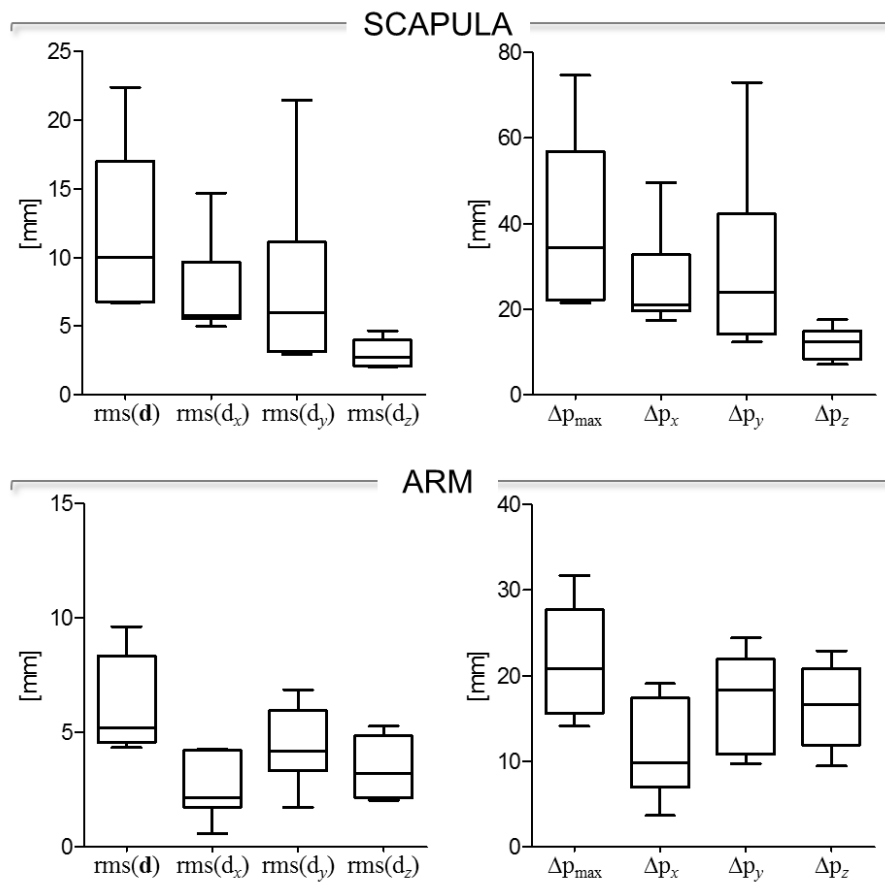
Subject characteristics - A healthy male subject 27 y.o. Height = 1.65 m, mass = 57 kg.

Motor task description - All trials started with the arm relaxed at the side with thumb pointing forward referred to as neutral axial rotation. The subject was asked to mimic hair combing, ball throwing, eating, gleno-humeral functional movements, punching in a bag, reaching back. The gleno-humeral functional movements consisted of successive maximum arm elevations, circumductions and arm sweeping.

1005 *STA characteristics* - Skin-marker trajectories in the scapula and arm ACSs are depicted in
 1006 Fig. 78, 81, 84, 87, 90, 93, for hair combing, ball throwing, eating, gleno-humeral functional
 1007 movements, punching, and reaching with the hand the middle of the opposite side of the back,
 1008 respectively. Unfiltered data were used. Statistical data describing the STAs are shown in
 1009 Figs. 79, 82, 85, 88, 91, 94, for hair combing, ball throwing, eating, gleno-humeral functional
 1010 movements, punching, and reaching back, respectively. For each motor task, the magnitude of
 1011 the instantaneous displacement of scapula and arm skin-markers along with the shoulder joint
 1012 angular kinematics are depicted in Figs. 80, 83, 86, 89, 92, 95, for hair combing, ball
 1013 throwing, eating, gleno-humeral functional movements, punching, and reaching back,
 1014 respectively.

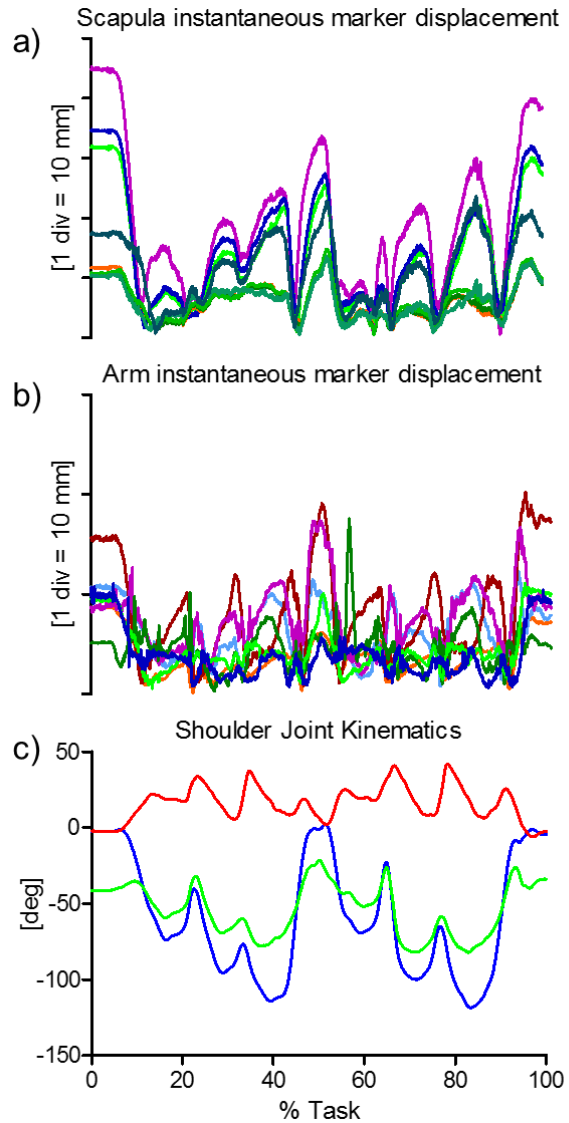


1015
 1016 **Figure 78 – HAIR COMBING.** Humeral (a) and scapular (b) ACSs, relevant ALs, and arm and
 1017 scapula skin-marker trajectories (represented in red and blue, respectively). The axes of the ACSs are
 1018 represented in red, green, and blue for the x (antero/posterior, div = 50 mm), y (superior/inferior, div =
 1019 50 mm), and z (right/left, div = 50 mm) directions, respectively.
 1020
 1021



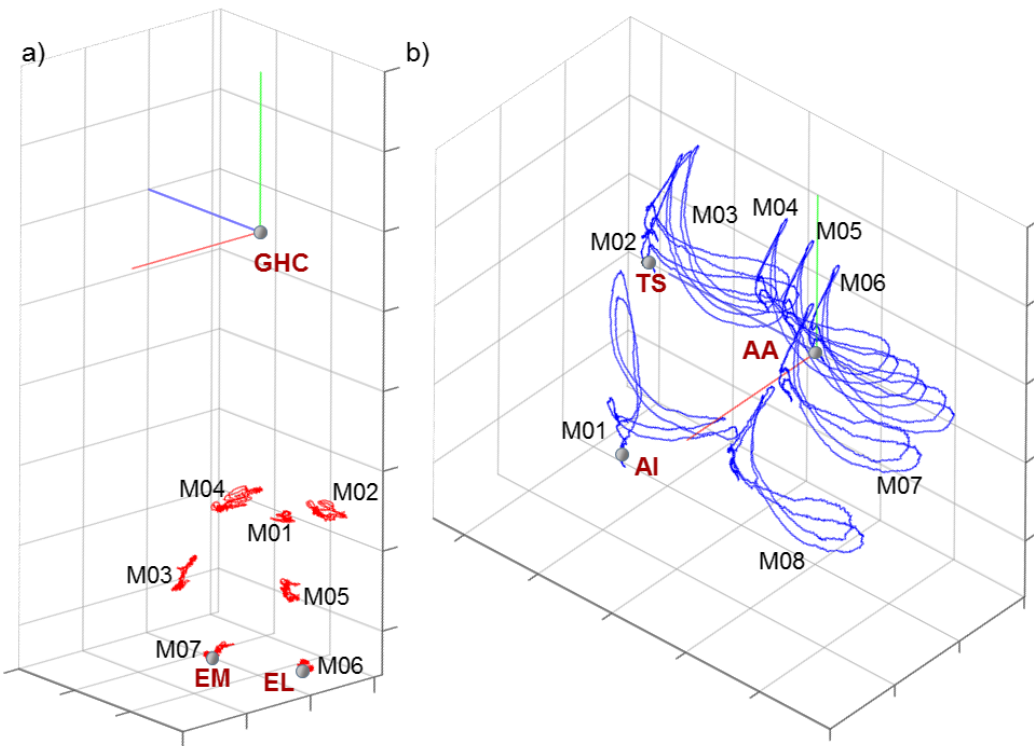
1022

1023 **Figure 79 – HAIR COMBING.** Box-plots of the eight parameters ($\text{rms}(\mathbf{d})$, $\text{rms}(\mathbf{d}_x)$, $\text{rms}(\mathbf{d}_y)$, and
1024 $\text{rms}(\mathbf{d}_z)$, in the left panel; Δp_{\max} , Δp_x , Δp_y , and Δp_z , in the right panel) that describe the STA affecting
1025 the eight and seven skin-markers on the scapula and arm, respectively, during the movement. Outliers
1026 are also depicted.

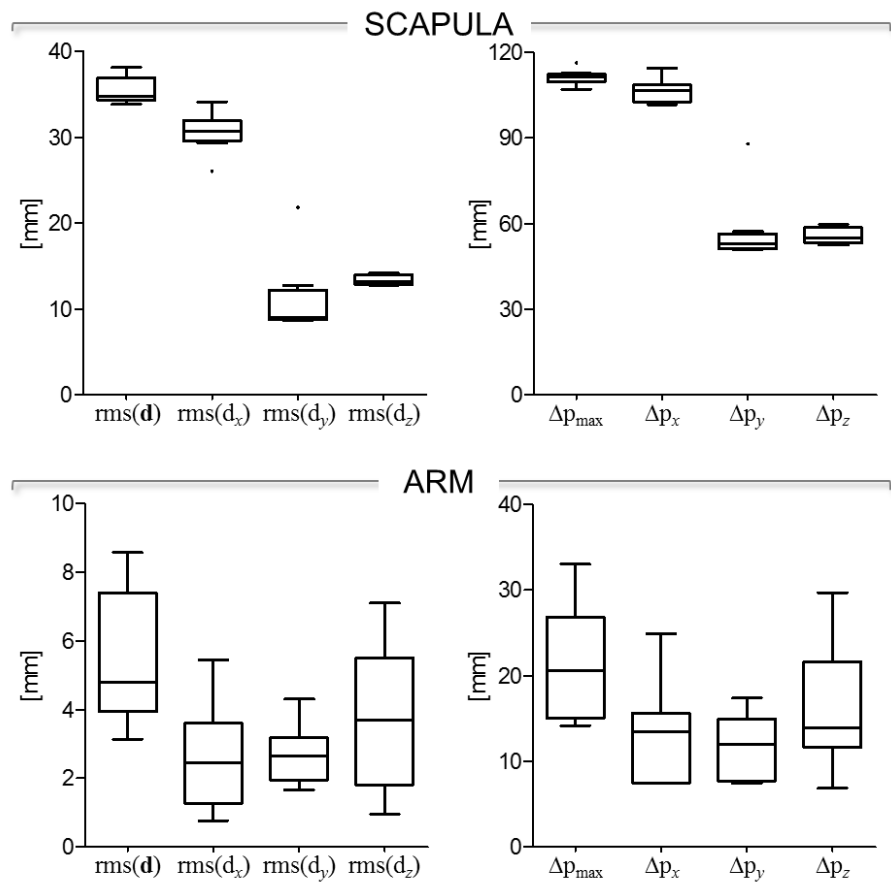


1027
1028
1029
1030
1031
1032
1033
1034

Figure 80 – HAIR COMBING. Magnitude of the instantaneous displacement of the eight and seven skin-markers glued on the scapula (a) and arm (b) represented in the relevant ACS. c) Relevant shoulder kinematics calculated using the $X_t Z_f' Y_h''$ sequence (Bonnefoy-Mazure et al., 2012): rotation around the X_t axis of the thorax corresponding to the shoulder elevation (blue); rotation around the floating Z_f' axis corresponding to the shoulder flexion/extension (red); rotation around the Y_h'' axis of the humerus corresponding to the shoulder axial rotation (green). Superior elevation, flexion and internal rotations are positive.

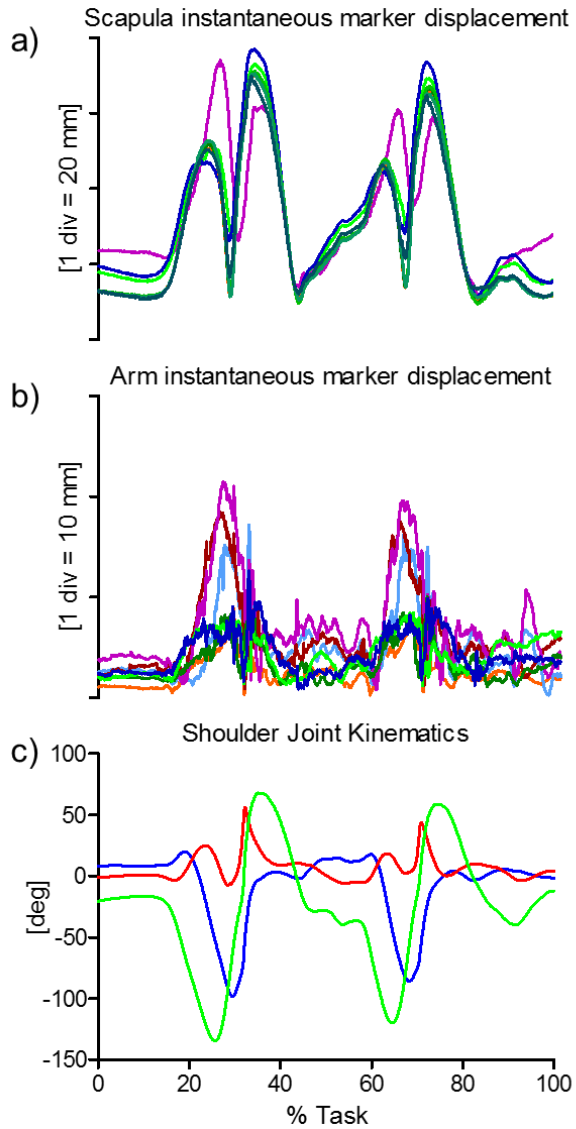


1035
1036 **Figure 81 – BALL THROWING.** Humeral (a) and scapular (b)
1037 ACSs, relevant ALs, and arm and
1038 scapula skin-marker trajectories (represented in red and blue, respectively). The axes of the ACSs are
1039 represented in red, green, and blue for the x (antero/posterior, div = 50 mm), y (superior/inferior, div =
1040 50 mm), and z (right/left, div = 50 mm) directions, respectively.
1041



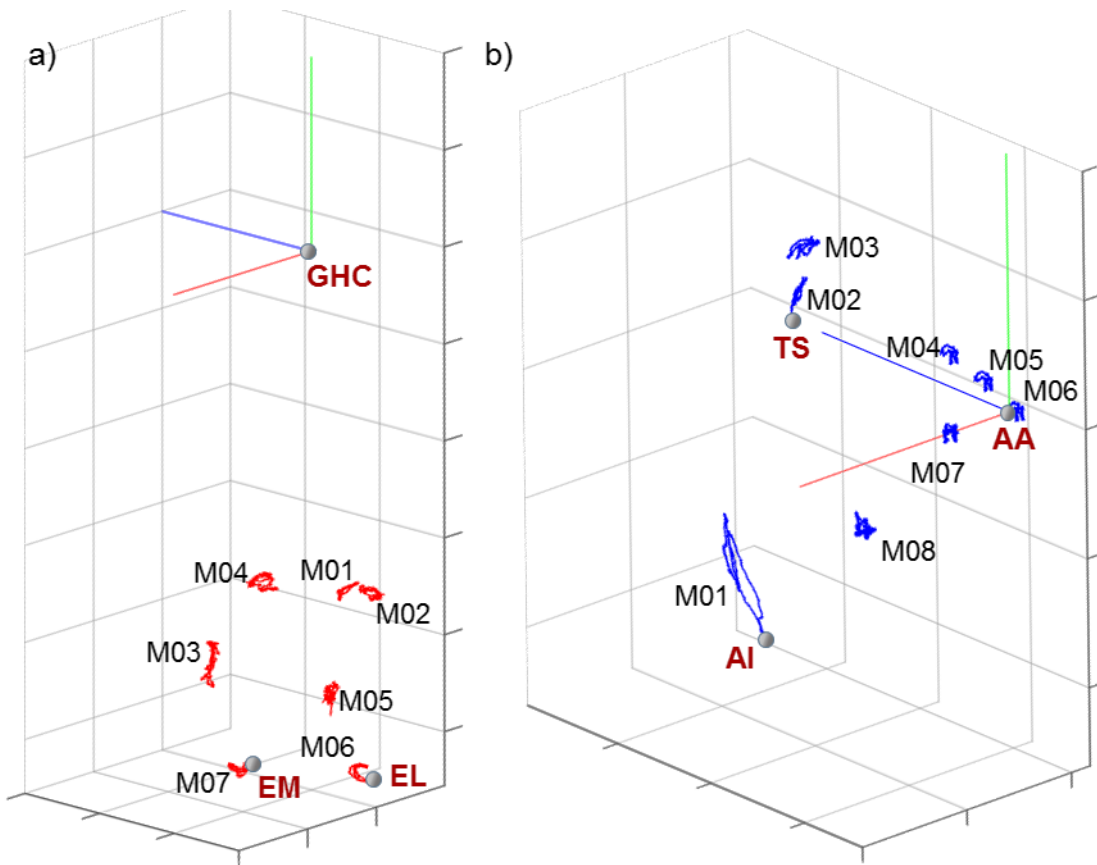
1042

1043 **Figure 82 – BALL THROWING.** Box-plots of the eight parameters (rms(d), rms(dx), rms(dy), and
 1044 rms(dz), in the left panel; Δp_{\max} , Δp_x , Δp_y , and Δp_z , in the right panel) that describe the STA affecting
 1045 the eight and seven skin-markers on the scapula and arm, respectively, during the movement. Outliers
 1046 are also depicted.



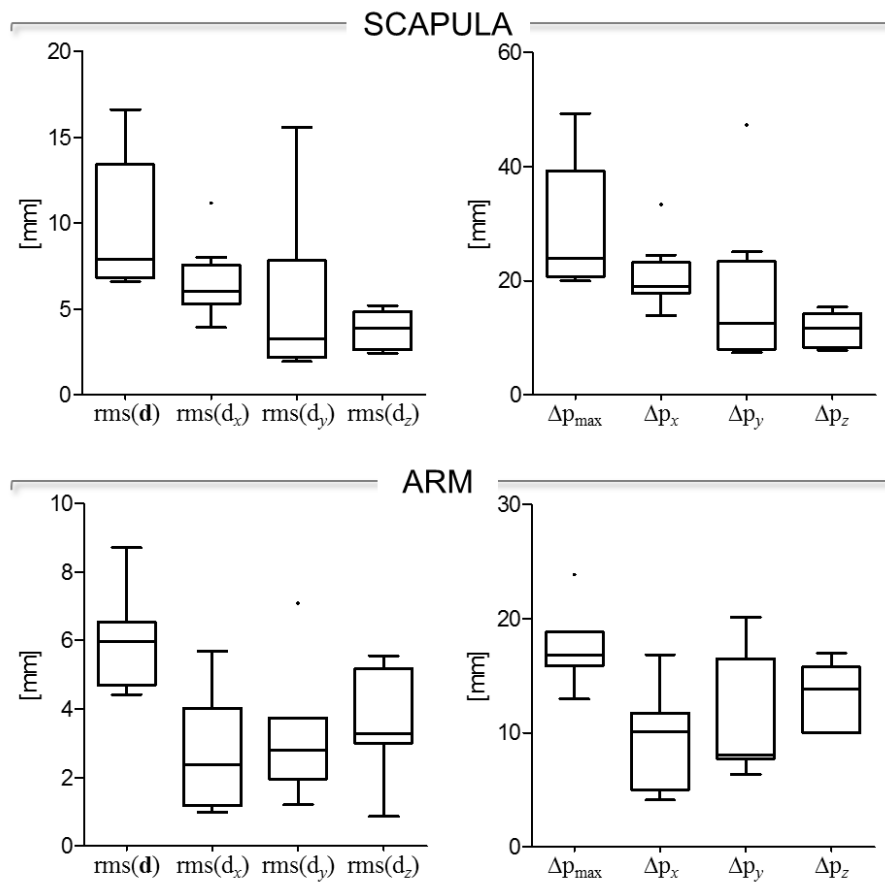
1047
 1048 **Figure 83 – BALL THROWING.** Magnitude of the instantaneous displacement of the eight and seven
 1049 skin-markers glued on the scapula (a) and arm (b) represented in the relevant ACS. c) Relevant
 1050 shoulder kinematics calculated using the X_t Z_{f'} Y_{h''} sequence (Bonnefoy-Mazure et al., 2012): rotation
 1051 around the X_t axis of the thorax corresponding to the shoulder elevation (blue); rotation around the
 1052 floating Z_{f'} axis corresponding to the shoulder flexion/extension (red); rotation around the Y_{h''} axis
 1053 of the humerus corresponding to the shoulder axial rotation (green). Superior elevation, flexion and
 1054 internal rotations are positive.

1055



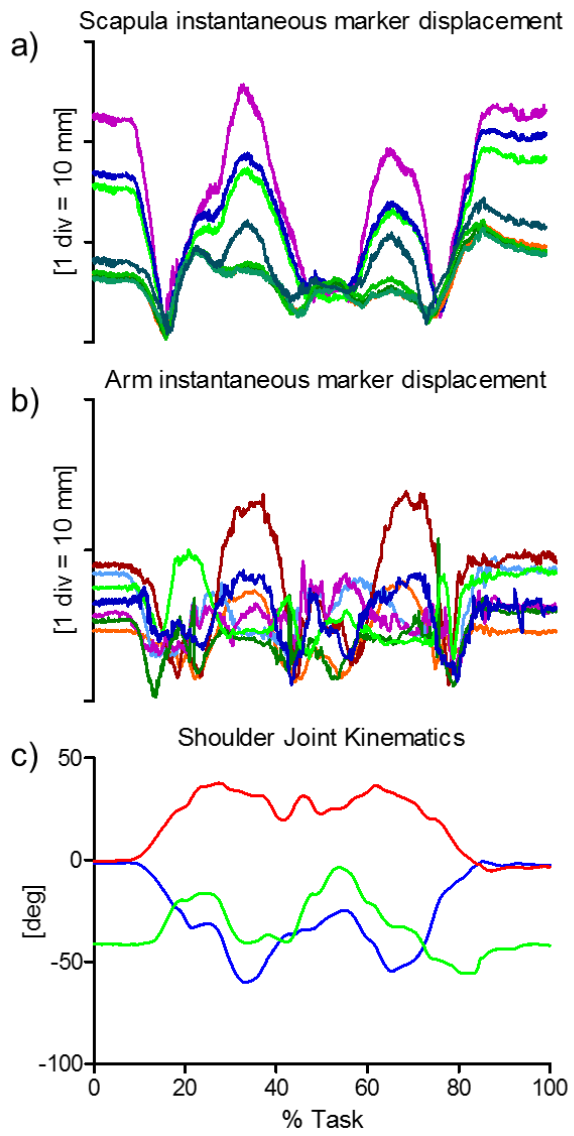
1056
 1057
 1058
 1059
 1060
 1061
 1062

Figure 84 – EATING. Humeral (a) and scapular (b) ACSs, relevant ALs, and arm and scapula skin-marker trajectories (represented in red and blue, respectively). The axes of the ACSs are represented in red, green, and blue for the x (antero/posterior, div = 20 mm), y (superior/inferior, div = 50 mm), and z (right/left, div = 50 mm) directions, respectively.



1063

1064 **Figure 85 – EATING.** Box-plots of the eight parameters (rms(d), rms(d_x), rms(d_y), and rms(d_z), in the
1065 left panel; Δp_{max}, Δp_x, Δp_y, and Δp_z, in the right panel) that describe the STA affecting the eight and
1066 seven skin-markers on the scapula and arm, respectively, during the movement. Outliers are also
1067 depicted.



1068
1069
1070
1071
1072
1073
1074
1075

Figure 86 – EATING. Magnitude of the instantaneous displacement of the eight and seven skin-markers glued on the scapula (a) and arm (b) represented in the relevant ACS. c) Relevant shoulder kinematics calculated using the $X_t Z_f' Y_h''$ sequence (Bonnefoy-Mazure et al., 2012): rotation around the X_t axis of the thorax corresponding to the shoulder elevation (blue); rotation around the floating Z_f' axis corresponding to the shoulder flexion/extension (red); rotation around the Y_h'' axis of the humerus corresponding to the shoulder axial rotation (green). Superior elevation, flexion and internal rotations are positive.

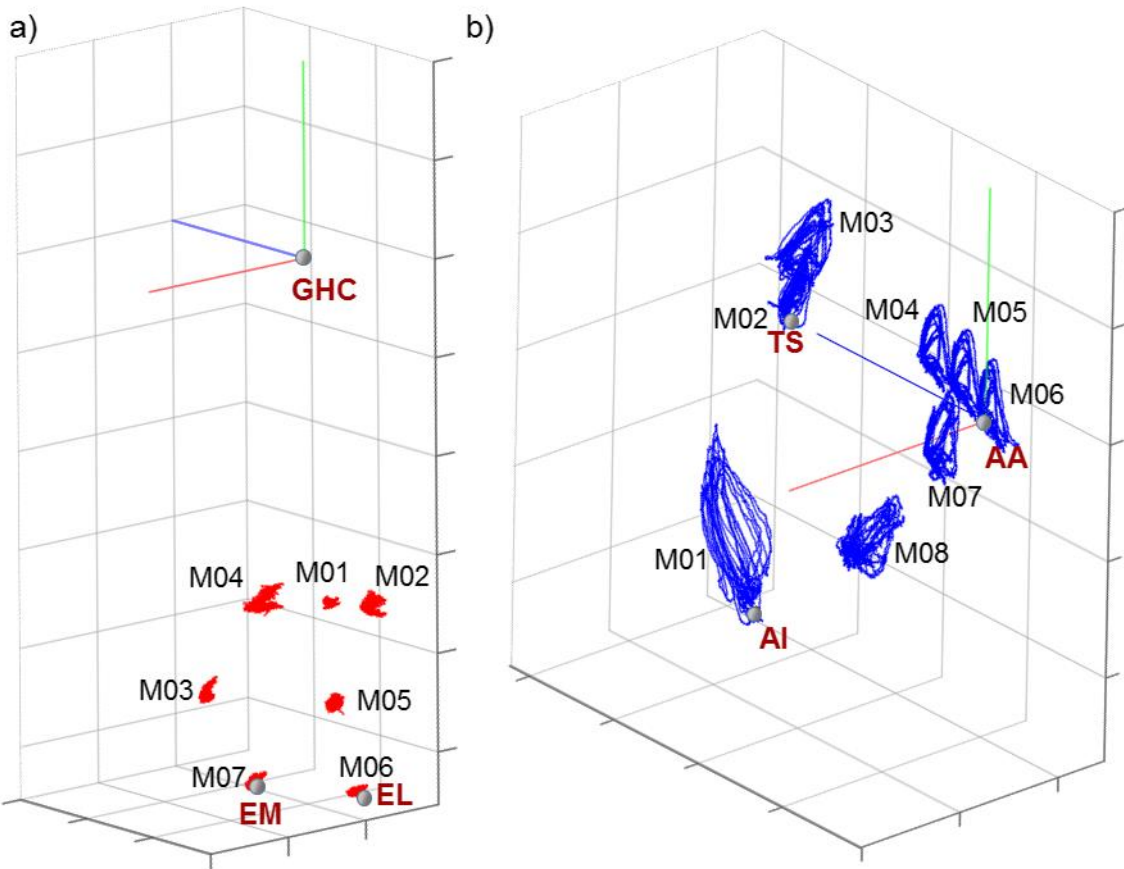
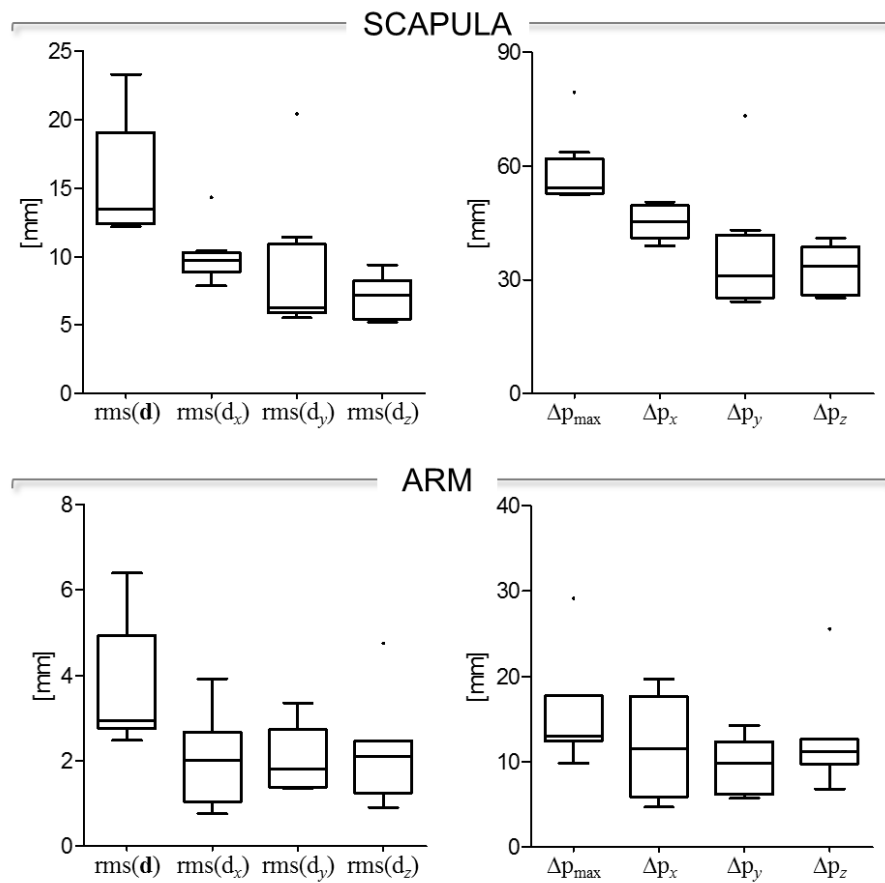


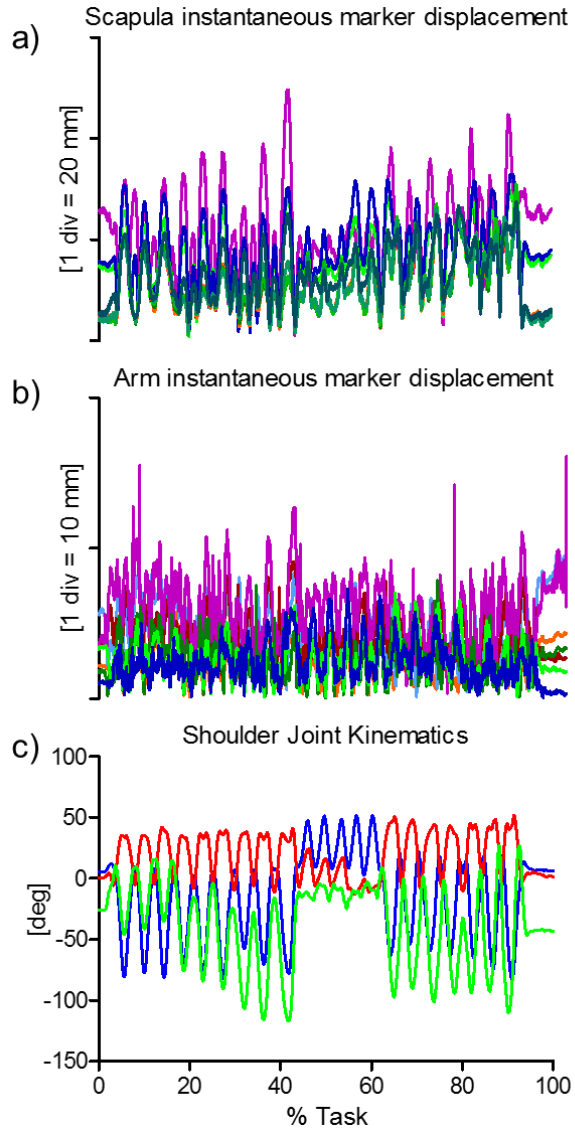
Figure 87 – GLENO-HUMERAL FUNCTIONAL MOVEMENTS. Humeral (a) and scapular (b) ACSs, relevant ALS, and arm and scapula skin-marker trajectories (represented in red and blue, respectively). The axes of the ACSs are represented in red, green, and blue for the x (antero/posterior, div = 50 mm), y (superior/inferior, div = 50 mm), and z (right/left, div = 50 mm) directions, respectively.

1076
1077
1078
1079
1080
1081
1082
1083



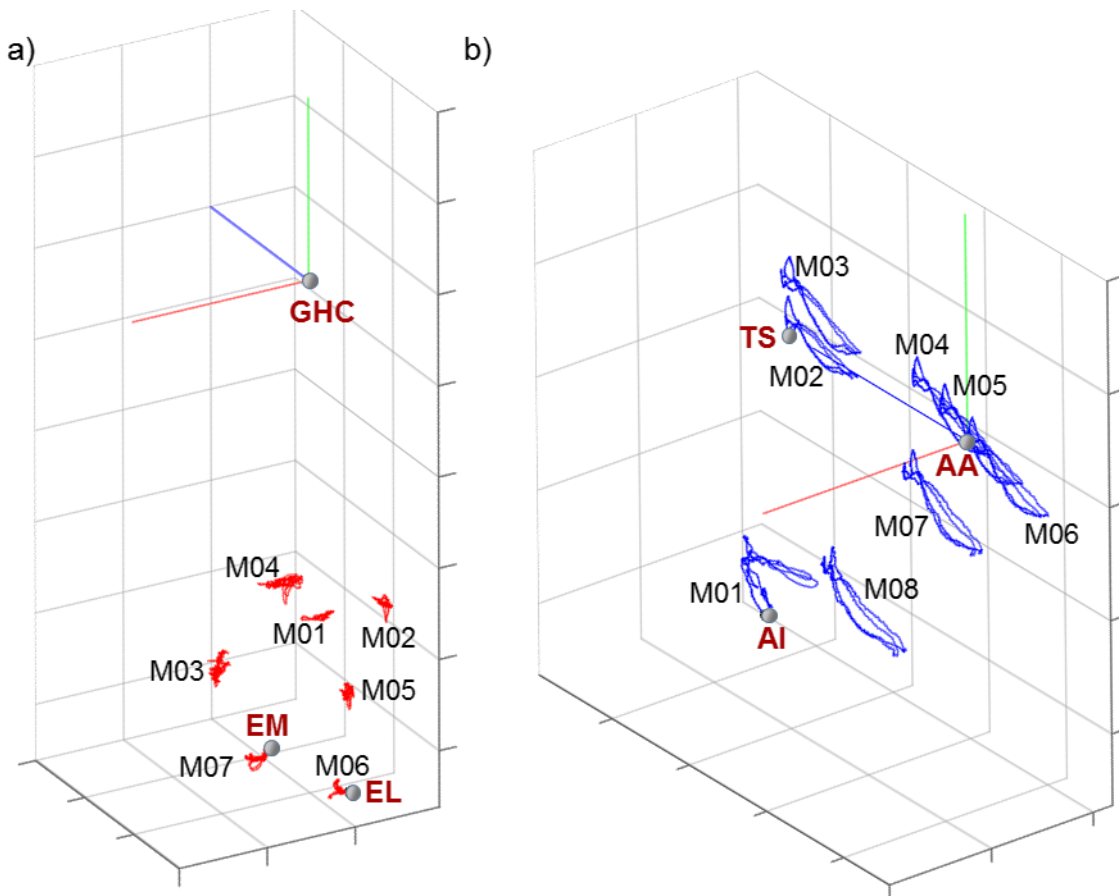
1084

1085 **Figure 88 – GLENO-HUMERAL FUNCTIONAL MOVEMENTS.** Box-plots of the eight parameters
 1086 ($\text{rms}(\mathbf{d})$, $\text{rms}(\mathbf{d}_x)$, $\text{rms}(\mathbf{d}_y)$, and $\text{rms}(\mathbf{d}_z)$, in the left panel; Δp_{\max} , Δp_x , Δp_y , and Δp_z , in the right panel)
 1087 that describe the STA affecting the eight and seven skin-markers on the scapula and arm, respectively,
 1088 during the movement. Outliers are also depicted.

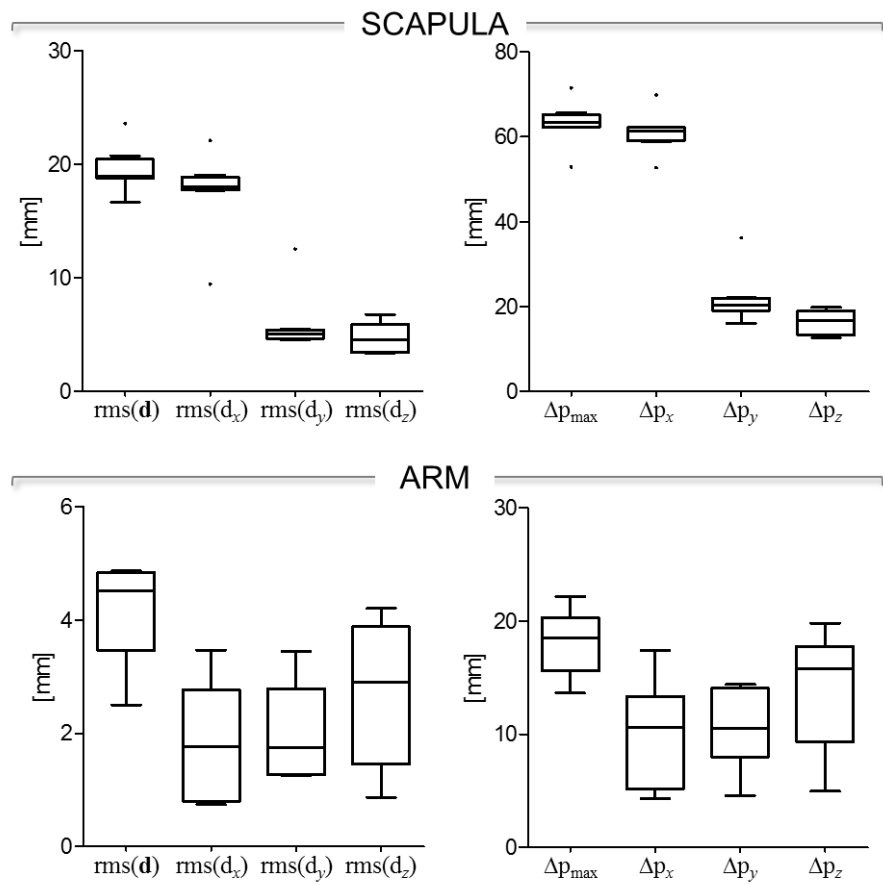


1089
1090
1091
1092
1093
1094
1095
1096

Figure 89 – GLENO-HUMERAL FUNCTIONAL MOVEMENTS. Magnitude of the instantaneous displacement of the eight and seven skin-markers glued on the scapula (a) and arm (b) represented in the relevant ACS. c) Relevant shoulder kinematics calculated using the $X_t Z_f' Y_h''$ sequence (Bonnefoy-Mazure et al., 2012): rotation around the X_t axis of the thorax corresponding to the shoulder elevation (blue); rotation around the floating Z_f' axis corresponding to the shoulder flexion/extension (red); rotation around the Y_h'' axis of the humerus corresponding to the shoulder axial rotation (green). Superior elevation, flexion and internal rotations are positive.

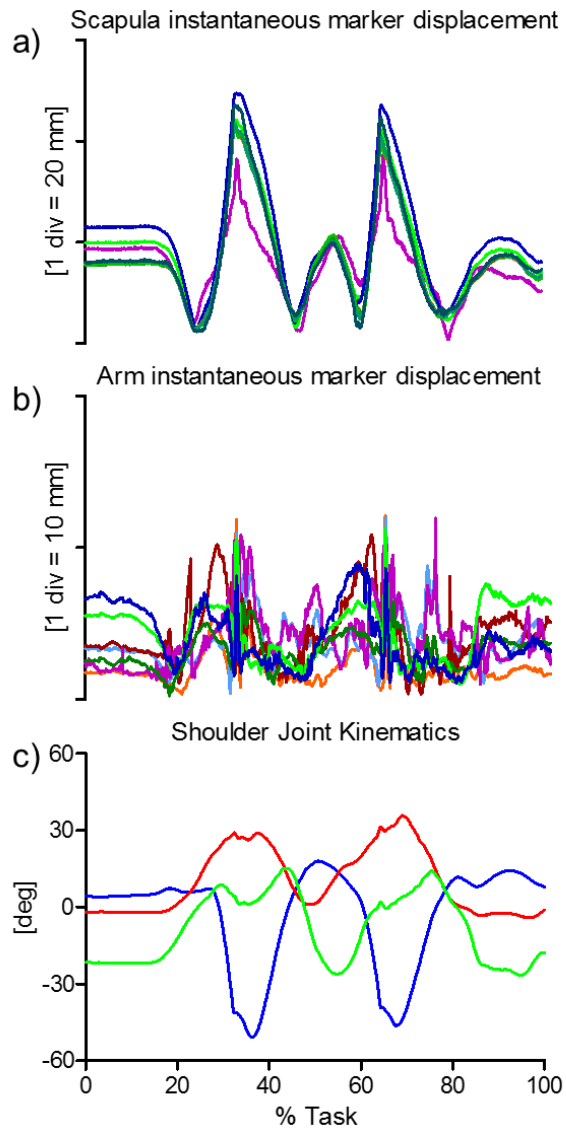


1097
 1098 **Figure 90 – PUNCHING.** Humeral (a) and scapular (b) ACSs, relevant ALs,
 1099 and arm and scapula
 1100 skin-marker trajectories (represented in red and blue, respectively). The axes of the ACSs are
 1101 represented in red, green, and blue for the x (antero/posterior, div = 50 mm), y (superior/inferior, div =
 1102 50 mm), and z (right/left, div = 50 mm) directions, respectively.
 1103



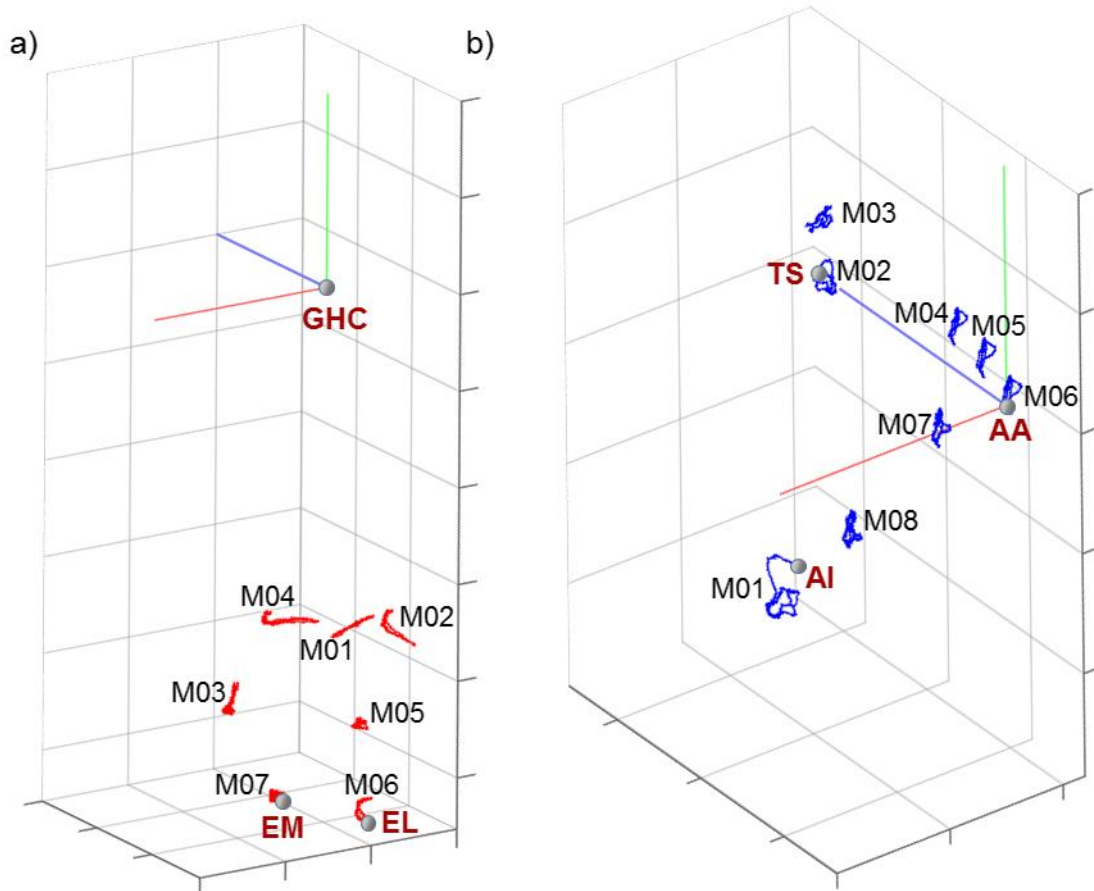
1104

1105 **Figure 91 – PUNCHING.** Box-plots of the eight parameters ($\text{rms}(\mathbf{d})$, $\text{rms}(\mathbf{d}_x)$, $\text{rms}(\mathbf{d}_y)$, and $\text{rms}(\mathbf{d}_z)$, in
 1106 the left panel; Δp_{\max} , Δp_x , Δp_y , and Δp_z , in the right panel) that describe the STA affecting the eight and
 1107 seven skin-markers on the scapula and arm, respectively, during the movement. Outliers are also
 1108 depicted.



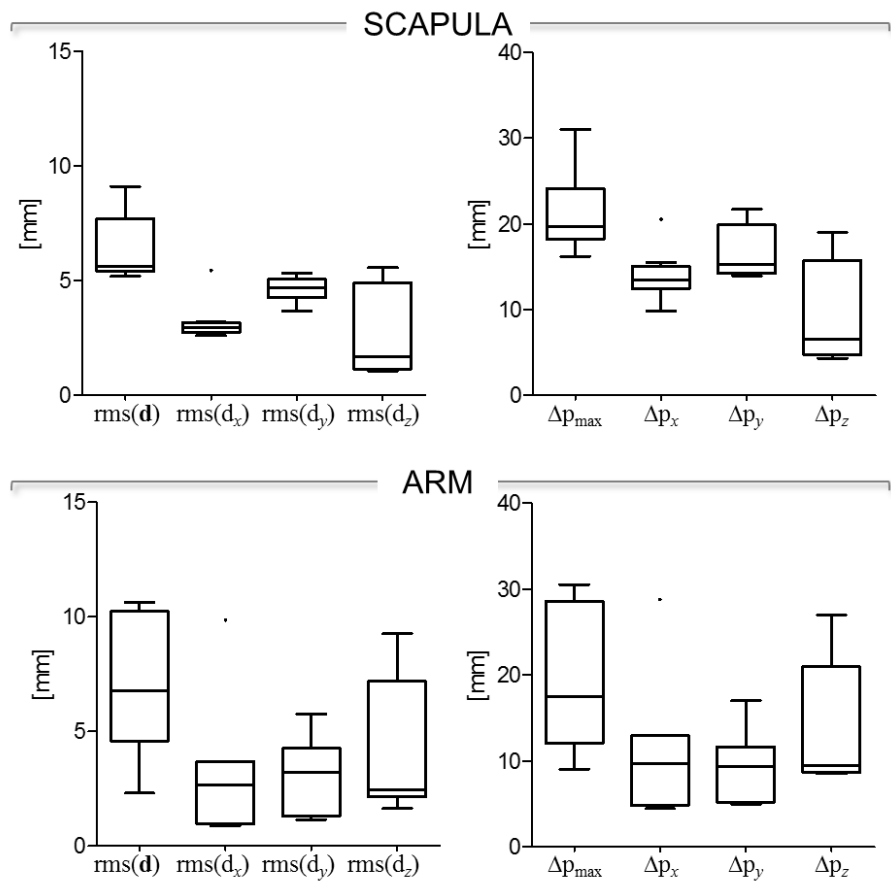
1109
1110
1111
1112
1113
1114
1115
1116

Figure 92 – PUNCHING. Magnitude of the instantaneous displacement of the eight and seven skin-markers glued on the scapula (a) and arm (b) represented in the relevant ACS. c) Relevant shoulder kinematics calculated using the $X_t Z_f' Y_h''$ sequence (Bonnefoy-Mazure et al., 2012): rotation around the X_t axis of the thorax corresponding to the shoulder elevation (blue); rotation around the floating Z_f' axis corresponding to the shoulder flexion/extension (red); rotation around the Y_h'' axis of the humerus corresponding to the shoulder axial rotation (green). Superior elevation, flexion and internal rotations are positive.



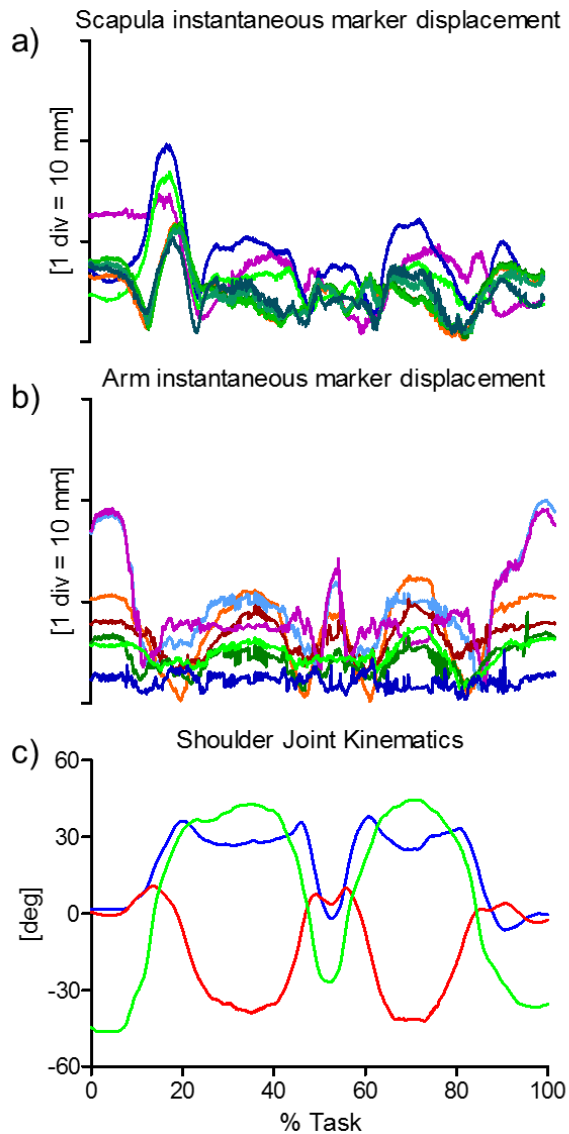
1117
1118
1119
1120
1121
1122

Figure 93 – REACHING BACK. Humeral (a) and scapular (b) ACSs, relevant ALs, and arm and scapula skin-marker trajectories (represented in red and blue, respectively). The axes of the ACSs are represented in red, green, and blue for the x (antero/posterior, div = 50 mm), y (superior/inferior, div = 50 mm), and z (right/left, div = 50 mm) directions, respectively.



1123

1124 **Figure 94 – REACHING BACK.** Box-plots of the eight parameters ($\text{rms}(\mathbf{d})$, $\text{rms}(\mathbf{d}_x)$, $\text{rms}(\mathbf{d}_y)$, and
1125 $\text{rms}(\mathbf{d}_z)$, in the left panel; Δp_{\max} , Δp_x , Δp_y , and Δp_z , in the right panel) that describe the STA affecting
1126 the eight and seven skin-markers on the scapula and arm, respectively, during the movement. Outliers
1127 are also depicted.



1128
1129
1130
1131
1132
1133
1134
1135

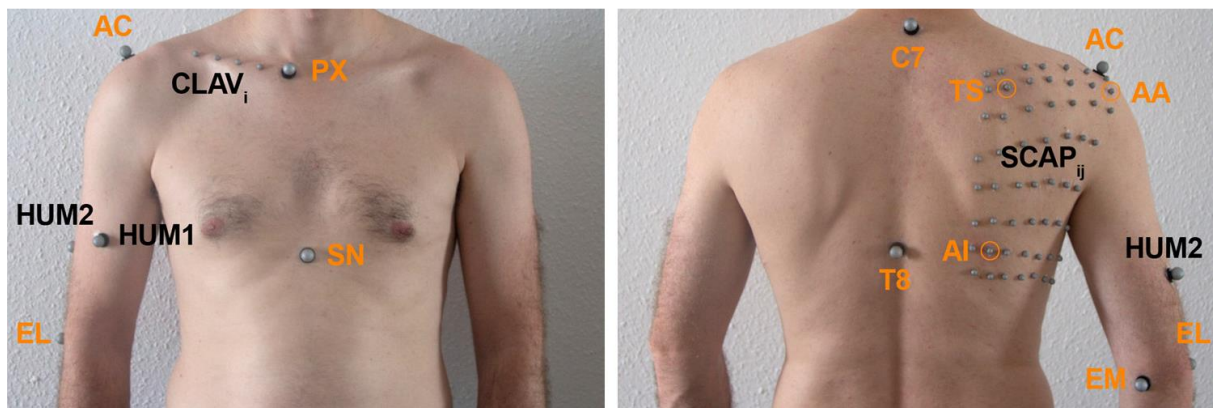
Figure 95 – REACHING BACK. Magnitude of the instantaneous displacement of the eight and seven skin-markers glued on the scapula (a) and arm (b) represented in the relevant ACS. c) Relevant shoulder kinematics calculated using the X_t Z_f' Y_h'' sequence (Bonnefoy-Mazure et al., 2012): rotation around the X_t axis of the thorax corresponding to the shoulder elevation (blue); rotation around the floating Z_f' axis corresponding to the shoulder flexion/extension (red); rotation around the Y_h'' axis of the humerus corresponding to the shoulder axial rotation (green). Superior elevation, flexion and internal rotations are positive.

1136

1137 2.9. *In-vivo data from ARTANIM*

1138 *Scientific articles of reference* - A detailed description of the original data set can be found
1139 in Charbonnier et al (2014).

1140 *Experimental data description* - Four markers (\varnothing 14 mm) were attached to the thorax
1141 (sternal notch, xiphoid process, C7 and T8 vertebra, and four (\varnothing 14 mm) on the upper arm –
1142 two placed on anatomical landmarks (LE_H and ME_H) and two as far as possible from the
1143 deltoid. For the scapula, 1 marker (\varnothing 14 mm) was fixed on the acromion. In addition, the
1144 scapula was covered with a regular grid of 56 markers (\varnothing 6.5 mm) (Fig. 96).
1145



1146 Fig. 2. Marker placement, including markers placed on anatomical landmarks (orange) and technical markers (black). PX= xiphoid process, SN = sternal notch, AC = acromion,
1147 TS= trigonum spinae, AA= angulus acromialis, AI= angulus inferior, EL = lateral epicondyle, EM = medial epicondyle.

1148 **Figure 96** – Experimental markers setup, including markers placed on anatomical landmarks (orange)
1149 and technical markers (black). Landmark names are described in Table 3.3. Markers HUM1 and
1150 HUM2 correspond to markers M01 and M02 of the arm segment, markers placed on EL and EM
1151 landmarks were named M03 and M04, respectively.
1152

1153 *Anatomical coordinate system definitions* - Both humerus and scapular ACSs were
1154 determined according to the definitions proposed in Wu et al. (2005). The glenohumeral joint
1155 centre was calculated using a sphere-fitting method.
1156

1157 *Measurement specifications* - The instantaneous markers position was reconstructed using
1158 a 8-camera stereophotogrammetric system (VICON MX40S) acquiring at 120 sample/s.

1159 *Ground truth* - Kinematic data were collected using an X-ray fluoroscopy unit
1160 (MultiDiagnostEleva, Philips Medical Systems, Netherlands) operating at 30 sample/s. Prior
1161 to data collection, the fluoroscopy system was calibrated for image distortion and
1162 radiographic projection parameters using a calibration object. A calibration frame was also
1163 acquired with 10 non-coplanar retroreflective markers, visible in both systems, to compute the
1164 pose of the CS of the stereophotogrammetric system relative to the fluoroscopy CS. The 3D
1165 MRI-based model of the scapula and of the humerus were acquired from a 1.5 T HDxT MRI
system. The 3D poses of the scapula and humerus were obtained using a 3D-to-2D shape-

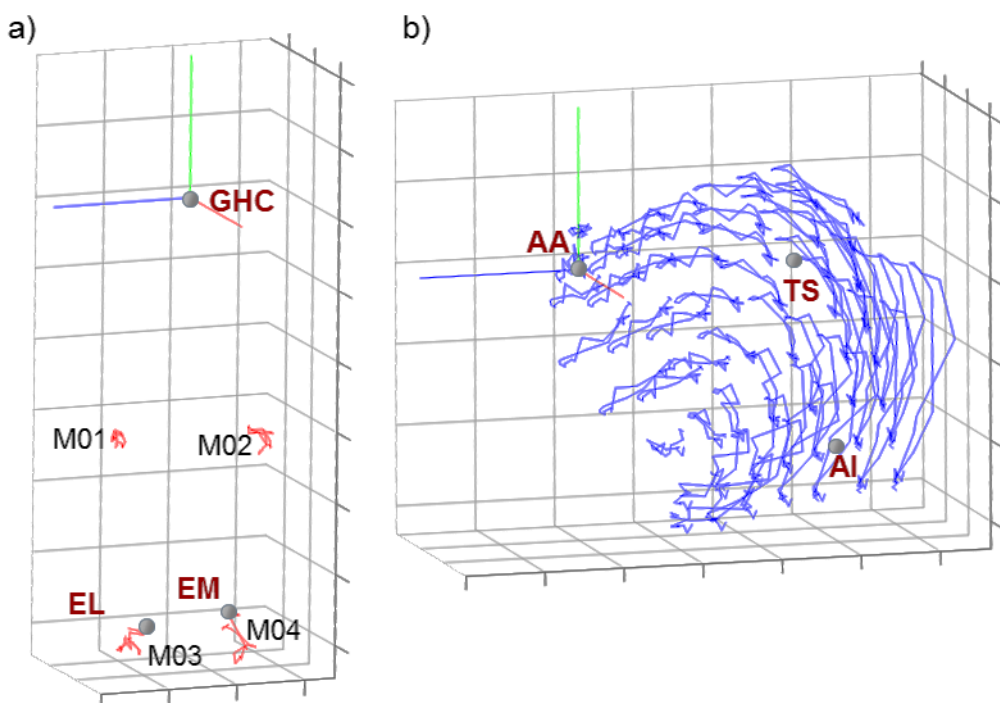
1166 matching technique using a custom software. A previous validation study (Moro-Hoka et al.,
1167 2007) had shown that best-case accuracy for fluoroscopy measurements was 0.53 mm for in-
1168 plane translation (parallel to image plane), 1.6 mm for out-of-plane translation (perpendicular
1169 to image plane), and 0.54 deg for rotation in all planes.

1170 *2.9.1. Data samples 22,24: Arm flexion and arm elevation in the scapular plane*

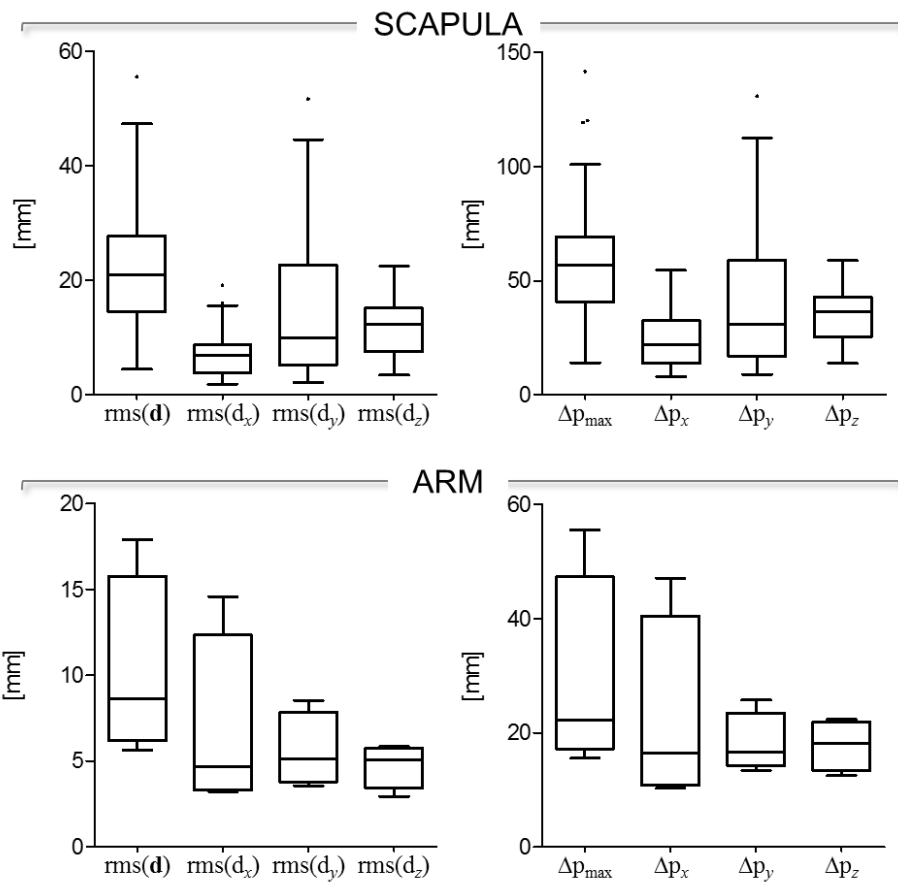
1171 *Subject characteristics* - A healthy male subject 25 y.o. Height = 1.80 m, weight = 80 kg.

1172 *Motor task description* - the following shoulder motions were analyzed: 3 consecutive arm
1173 flexions from neutral to maximum flexion, and 3 consecutive elevation from neutral to
1174 maximum abduction in the scapular plane.

1175 *STA characteristics* - Skin-marker trajectories in the scapula and arm ACSs are depicted in
1176 Fig. 97, 100, for arm flexion and arm elevation in the scapular plane, respectively.
1177 Stereophotogrammetric data were acquired at 120 Hz and then down-sampled to 30 Hz.
1178 Statistical data describing the STAs are shown in Figs. 98, 101, for arm flexion and arm
1179 elevation in the scapular plane, respectively. For each motor task, the magnitude of the
1180 instantaneous displacement of scapula and humerus skin-markers along with the shoulder
1181 joint angular kinematics is depicted in Figs. 99, 102, for arm flexion and arm elevation in the
1182 scapular plane, respectively.

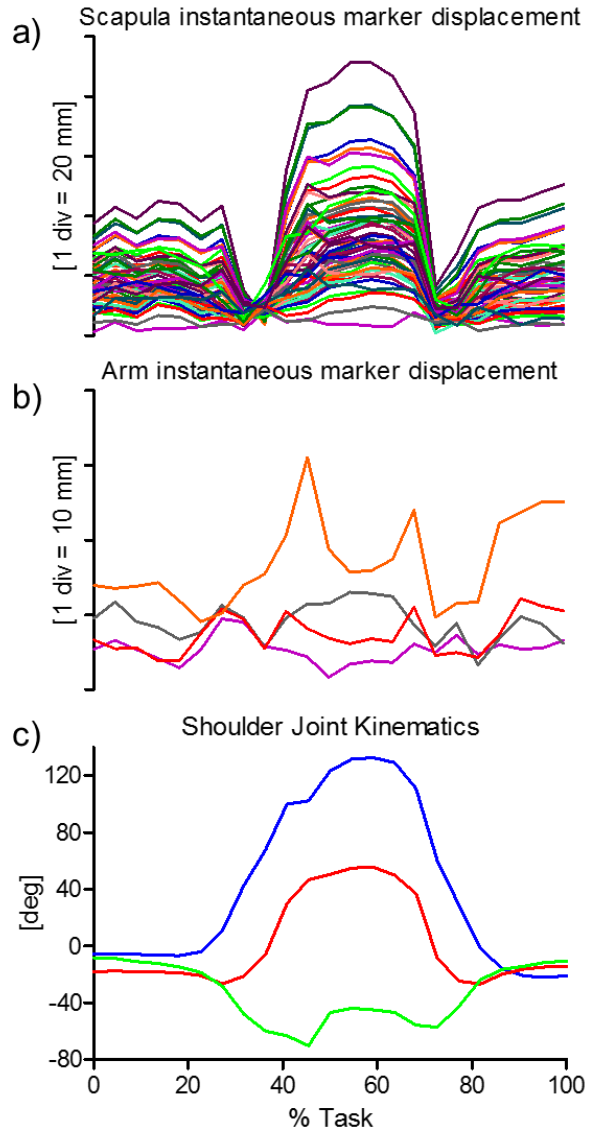


1183
1184 **Figure 97 – FLEXION.** Humerus (a) and scapular (b) ACSs, relevant ALs, and arm and scapula skin-
1185 marker trajectories (represented in red and blue, respectively). The axes of the ACSs are represented in
1186 red, green, and blue for the x (antero/posterior, div = 50 mm), y (superior/inferior, div = 50 mm), and z
1187 (right/left, div = 50 mm) directions, respectively.
1188



1189

1190 **Figure 98 – FLEXION.** Box-plots of the eight parameters (rms(d), rms(d_x), rms(d_y), and rms(d_z), in
 1191 the left panel; Δp_{max}, Δp_x, Δp_y, and Δp_z, in the right panel) that describe the STA affecting the fifty-
 1192 seven and four skin-markers on the scapula and arm, respectively, during the movement. Outliers are
 1193 also depicted.



1194
1195
1196
1197
1198
1199
1200
1201

Figure 99 – FLEXION. Magnitude of the instantaneous displacement of the fifty-seven and four skin-markers glued on the scapula (a) and arm (b) represented in the relevant ACS. c) Relevant shoulder kinematics calculated using the $X_t Z_f Y_h''$ sequence (Bonnefoy-Mazure et al., 2012): rotation around the X_t axis of the thorax corresponding to the shoulder elevation (blue); rotation around the floating Z_f axis corresponding to the shoulder flexion/extension (red); rotation around the Y_h'' axis of the humerus corresponding to the shoulder axial rotation (green). Superior elevation, flexion and internal rotations are positive.

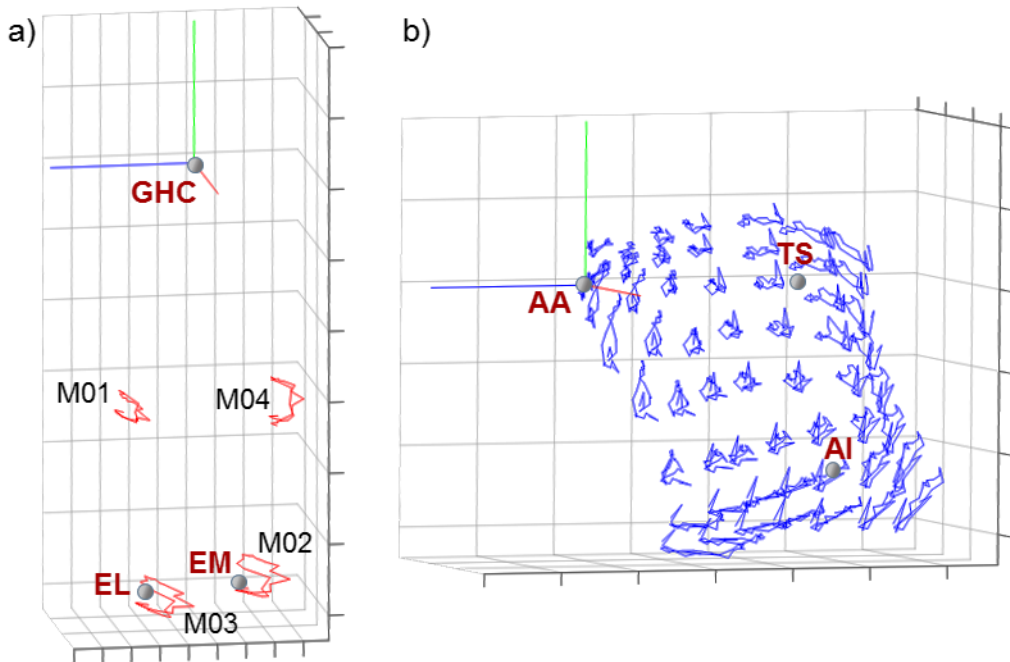
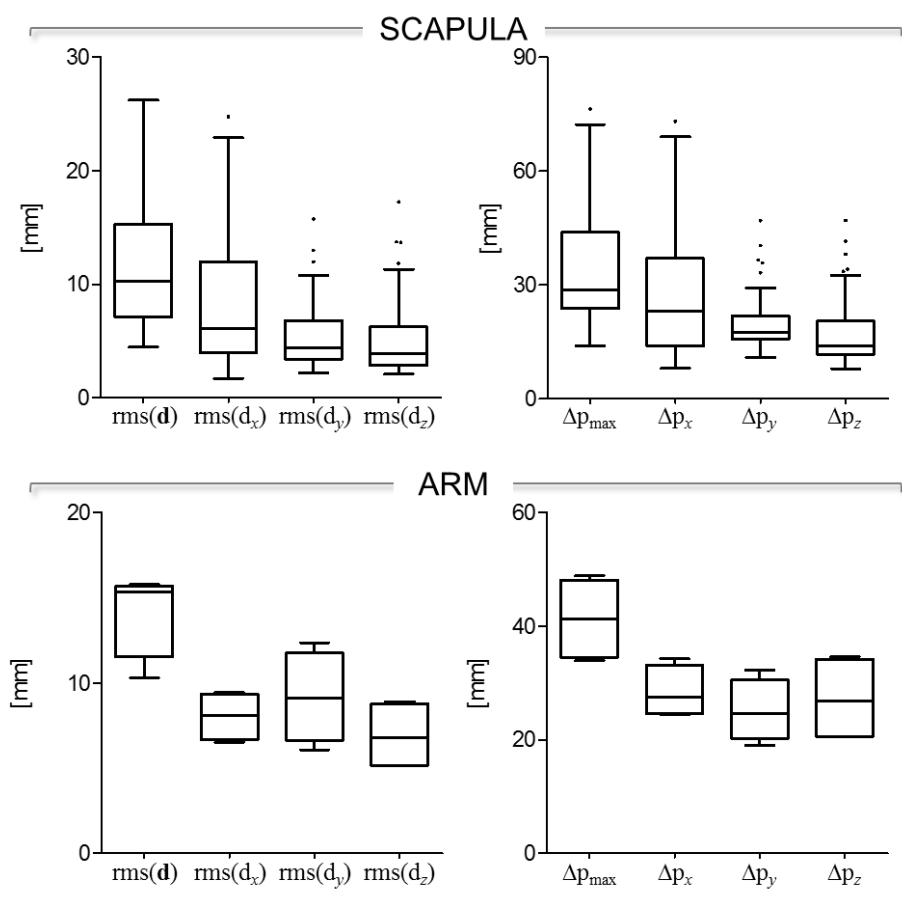


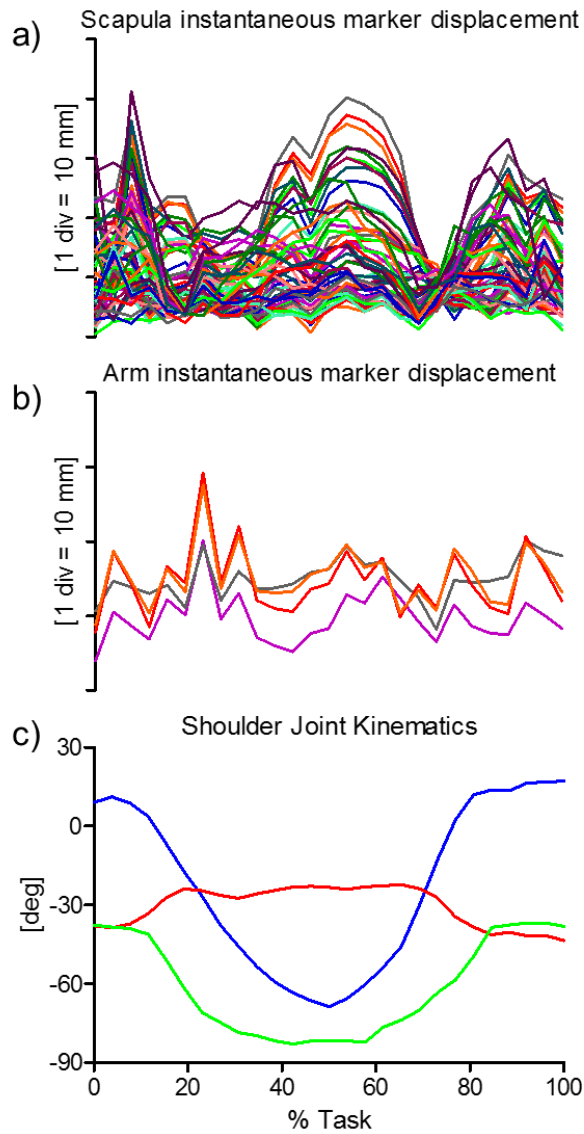
Figure 100 – ABDUCTION. Humerus (a) and scapular (b) ACSs, relevant ALs, and arm and scapula skin-marker trajectories (represented in red and blue, respectively). The axes of the ACSs are represented in red, green, and blue for the x (antero/posterior, div = 50 mm), y (superior/inferior, div = 50 mm), and z (right/left, a) div = 20 mm; b) div = 50 mm) directions, respectively.

1202
1203
1204
1205
1206
1207
1208



1209

1210
 1211 **Figure 101** – ABDUCTION. Box-plots of the eight parameters ($\text{rms}(\mathbf{d})$, $\text{rms}(d_x)$, $\text{rms}(d_y)$, and $\text{rms}(d_z)$,
 1212 in the left panel; Δp_{\max} , Δp_x , Δp_y , and Δp_z , in the right panel) that describe the STA affecting the fifty-
 1213 seven and four skin-markers on the scapula and arm, respectively, during the movement. Outliers are
 also depicted.



1214
 1215 **Figure 102** – ABDUCTION. Magnitude of the instantaneous displacement of the fifty-seven and four
 1216 skin-markers glued on the scapula (a) and arm (b) represented in the relevant ACS. c) Relevant
 1217 shoulder kinematics calculated using the $X_t Z_f' Y_h''$ sequence (Bonnefoy-Mazure et al., 2012): rotation
 1218 around the X_t axis of the thorax corresponding to the shoulder elevation (blue); rotation around the
 1219 floating Z_f' axis corresponding to the shoulder flexion/extension (red); rotation around the Y_h'' axis
 1220 of the humerus corresponding to the shoulder axial rotation (green). Superior elevation, flexion and
 1221 internal rotations are positive.

1222

1223 3. *Data storing and exchange: the lexicon*

3.1. Dataset description

1225 Data were stored according to the same lexicon into Matlab structures, named datasets, each
1226 consisting of:

1. an *info* field, of type text, which contains general information concerning the experiment, the experimental set up, possible problems in the dataset, and on the subject/trial/task characteristics
 2. several *subject* fields, one for each subject, containing specific subject information and numeric data

1232

3.1.1. Dataset name

1234 The dataset name has the following format:

1235 dataset provider name motor task name

1236 where:

1237 provider name indicates the institution owner of the data (see Table
1238 {owner})

1241 Example:

1242 dataset_FOROIT_hipFunct

1243

3.1.2. Data information

1245 The information listed below were included, when available, in the *info* field. These
1246 information are general to the dataset, specific problems relative to specific subjects are
1247 detailed at the subject level.

1248 The following format was used:

1249 contact person person who acquired/organized the data

1250 experiment day day/month/year of original data acquisition

1251 experiment location location of original data acquisition

1252	motor task description	details on the task under analysis (e.g. speed; tread and rise when step or seat are used; type of footwear, see relevant Table).
1255	number of subjects	
1256	number of trials per subject	
1257	body segments	
1258	number of markers per segment	indicating the number decided in the experiment design
1259		
1260	marker location	a general description of the location (frontal, distal, etc)
1261	reference data source	short details on how bone pose was determined (pin, fluoroscopy, sampling frequency of the reference data, etc.)
1262		
1263		
1264	subject/specimen	stating if it was <i>in-vivo</i> or <i>ex-vivo</i>
1265	anatomical coordinate system	definition adopted for each segment (to be brief reference to literature can be used)
1266		
1267	measurement errors	if experiments were carried out to assess measurement errors, information on them is provided here.
1268		
1269	data processing	if normalized data are provided as supplementary trials, information on normalization is provided here. Similarly, if interpolated data are provided to cope with occlusions, on interpolation is provided here.
1270		
1271		
1272		
1273	sampling frequency	indicating the sampling frequency of the system providing the skin kinematics (sampling frequency of the reference data source are indicated along with other information on the relevant measurement system).
1274		
1275		
1276		

1277 Example:

1278 dataset_FOROIT_hipFunct.info

1279 CONTACT PERSON: VALENTINA CAMOMILLA; EXPERIMENT DATE AND LOCATION: NIZZA
1280 2006; MOTOR TASK DESCRIPTION: STAR-ARC MOVEMENT; NUMBER OF SUBJECTS: 1;
1281 NUMBER OF TRIALS PER SUBJECT: 1; TYPE OF SEGMENTS: RIGHT LOWER LIMB AND PELVIS;
1282 NUMBER OF MARKERS PER SEGMENT: 12 ON THE THIGH AND 4 ON THE SHANK; MARKER

1283 LOCATION: THIGH AND SHANK ANTERIOR ASPECT; REFERENCE DATA SOURCE: PIN MARKERS;
1284 EX-VIVO; ANATOMICAL COORDINATE SYSTEM DEFINITION ADOPTED FOR EACH SEGMENT:
1285 CAPPOZZO 1995 ET AL.

1286

3.1.3. Measurement units

1288 The default assumption for the units of measurement used to report data is the reported in the
1289 following section. Any difference with respect to this standard should be state in the *info*
1290 section of each dataset.

1291 Time Unit s

1292 Linear Kinematic Unit mm for lengths

1293 Angular Kinematic Unit rad for angles

1294 Mass Inertia Unit kg for body mass

1295

3.2. Subject description

3.2.1. Subject name

1298 The subject name has the following format:

1299 subjNumber

1300 where only the number can sequentially change. Each number is described by two characters
1301 (e.g., please specify 01 instead of 1). The root “subj” must be used for all subjects. Additional
1302 information on a possible subject identifier is to be included in the info field.

3.2.2. Subject information

1304 The information listed below were included, when available, in the *info* field, to provide an
1305 identification for the subject in addition to basic anthropometric measures and age and sex.
1306 These information are general to the subject, specific problems relative to specific trials are
1307 detailed at the trial level.

1308 The following format was used:

1309 ref_code is an string uniquely identifying the patient within the institution of
1310 the creator of the file

1311 pathology identifies a patient pathology, if any (see Table {pathology})

1312 age is the patient's age (in years) at the date of the experiment

1313 sex is the patient's gender (M or F)
1314 body_mass is the patient's body mass
1315 stature is the patient's stature
1316 other Other information. For example: anatomical measures available for
1317 the subject. Supplementary details if the patient wears a prosthesis
1318 or an orthosis.

1319 Example:

```
1320        dataset_FOROIT_hipFunct.subj01.info.ref_code  
1321        '2301'  
1322        dataset_FOROIT_hipFunct.subj01.info.pathology  
1323        'abled body'  
1324        dataset_FOROIT_hipFunct.subj01.info.age  
1325        6  
1326        dataset_FOROIT_hipFunct.subj01.info.sex  
1327        'M'  
1328        dataset_FOROIT_hipFunct.subj01.info.body_mass  
1329        70  
1330        dataset_FOROIT_hipFunct.subj01.info.stature  
1331        1750  
1332        dataset_FOROIT_hipFunct.subj01.info.other  
1333        'segment geometry: diameters of the proximal, median, and distal sections of the thigh  
1334        are 161, 123, 105 mm, respectively'
```

1335

1336 *3.2.3. Warning*

1337 A brief description of the experimental problems, if any, should be reported with reference to
1338 the trial numbers. Write "none" if the subject is complete.

1339 Example:

```
1340        dataset_FOROIT_hipFunct.subj03.warning  
1341        'For trial03, no markers are available for the shank.'
```

1343 *3.2.4. Subject data*

1344 The trials available for each specific subject are included in the subject field. For the posture
1345 trial, if available, use the number 00.

1346 Example:

1347 **dataset_FOROIT_hipFunct.subj03.trial03**

1348

1349 In the trial field, each body segment is reported separately and contains both time invariant
1350 and time variant data for the specific body segment (use names as in Table {segment}):

1351 warning A brief description of the experimental problems, if any, at the
1352 body segment level. Write "none" if data are complete. If there
1353 are missing fields, state it here.

1354 mrk.Mxx This field contains a set of subfields, one for each marker M01,
1355 M02, M03 etc. Marker coordinates are provided in the
1356 anatomical coordinate system (antero-posterior, x; superior-
1357 inferior, y; left-right, z). Data dimension for each marker: [Nx3]

1358 (mrk_raw.Mxx) Optional. This field contains a set of subfields, one for each
1359 marker M01, M02, M03 etc. When skin-marker trajectories
1360 presented gaps smaller than 0.35 s that were filled using a partial
1361 Procrustes superimposition approach (Grimpampi et al., 2014)
1362 or larger gaps that were not filled, original marker coordinates
1363 are also provided in this field. The latter coordinates are
1364 provided in the anatomical coordinate system (antero-posterior,
1365 x; superior-inferior, y; left-right, z). Data dimension for each
1366 raw marker: [Nx3]

1367

1368 ALs.ALnames Anatomical landmarks named as in Cappozzo 1995/ISB
1369 convention reported in Table {anat_landmk} (antero-posterior,
1370 x; superior-inferior, y; right-left, z). Data dimension for each
1371 landmark: [3x1]

1372 gRa Rotation matrix of the segment anatomical coordinate system
1373 with respect to the global coordinate system. Each row contains

1406 In case vast portions of the dataset were interpolated due to occlusion problems, raw
1407 data were stored using NaN as missed frame identifier. However, interpolated data can be
1408 stored as supplementary field in the subject data structure. Information on interpolation
1409 procedures must be stored in the data processing field of the data information.

1410 Example:

1411 **dataset_FOROIT_hipFunct.subj01.trial03.L_thigh.gRa_int**
1412 [2423x9]
1413 **dataset_FOROIT_hipFunct.subj01.trial03.L_thigh.gta_int**
1414 [2423x3]
1415 **dataset_FOROIT_hipFunct.subj01.trial03.L_thigh.mrk_int**
1416 [2423x3]
1417

1418 **3.3. Tables**

1419 Table {owner}

1420	<i>Ecole Polytechnique Fédérale de Lausanne, Laboratory of</i>	
1421	<i>Movement Analysis and Measurement</i>	LMAM
1422	<i>Fondation Artanim</i>	ARTANIM
1423	<i>National Taiwan University</i>	NTU
1424	<i>Simulation et Modélisation du Mouvement</i>	S2M
1425	<i>Università degli Studi di Roma "Foro Italico"</i>	FOROIT
1426	<i>University of Bologna</i>	UNIBO
1427	<i>University of Melbourne</i>	UNIMELB
1428	<i>University of Ohio</i>	CSUOHIO
1429	<i>University of Ottawa</i>	OTTAWA

1430 Table {motortask}

1431	<i>walking:</i>	walking
1432	<i>cutting:</i>	cutting
1433	<i>hopping:</i>	hopping
1434	<i>treadmill walking:</i>	treadmillWalking
1435	<i>step up & down:</i>	stepUp
1436	<i>functional hip joint centre determination:</i>	hipFunct
1437	<i>hip axial rotation:</i>	hipAxialRot
1438	<i>hip and knee flexion & extension:</i>	hipKneeFlex
1439	<i>knee extension against gravity:</i>	kneeAgainstGravity
1440	<i>sit-to-stand:</i>	sit2stand
1441	<i>knee flexion & extension:</i>	kneeFlex
1442	<i>running:</i>	running
1443	<i>arm adduction:</i>	armAdd
1444	<i>arm abduction (scapular plane):</i>	armAbd
1445	<i>arm flexion:</i>	armFlex
1446	<i>arm extension:</i>	armExt
1447	<i>hair combing:</i>	hairComb
1448	<i>ball throwing:</i>	ballThrowing
1449	<i>eating:</i>	eating
1450	<i>punching:</i>	punching
1451	<i>reach the back:</i>	behindBackReach
1452	<i>functional gleno-humeral centre determination:</i>	glenoHumeralFunct

1453 Table {footwear}

1454	<i>barefoot:</i>	BF
1455	<i>training shoes:</i>	TS
1456	<i>other:</i>	OT

1457 Table {pathology}

1458	<i>able-bodied:</i>	AB
1459	joint implant	
1460	<i>hip:</i>	IH
1461	<i>knee:</i>	IK
1462	<i>ankle:</i>	IA
1463	joint disease	
1464	<i>hip:</i>	JH
1465	<i>knee:</i>	JK
1466	<i>ankle:</i>	JA
1467	amputee	
1468	<i>hip disarticulation:</i>	HD
1469	<i>above-knee:</i>	AK
1470	<i>through knee:</i>	TK
1471	<i>below-knee:</i>	BK
1472	<i>through ankle:</i>	TA
1473	<i>foot:</i>	FO
1474	<i>other:</i>	OT

1475 Table {side}

1476	<i>left:</i>	L
1477	<i>irrelevant:</i>	I
1478	<i>right:</i>	R

1479 Table {segment}

1480	<i>Thorax</i>	
1481	<i>L_clavicle</i>	
1482	<i>L_scapula</i>	
1483	<i>L_humerus</i>	
1484	<i>R_clavicle</i>	
1485	<i>R_scapula</i>	
1486	<i>R_humerus</i>	
1487	<i>pelvis</i>	
1488	<i>L_thigh</i>	
1489	<i>L_shank</i>	
1490	<i>L_foot</i>	
1491	<i>R_thigh</i>	
1492	<i>R_shank</i>	
1493	<i>R_foot</i>	

1494 Table {anat_landmk}

1495	<i>Thorax</i>	
1496	<i>incisura jugularis:</i>	IJ

1497	<i>xiphoid process:</i>	PX
1498	<i>spinous process of the 8th thoracic vertebra:</i>	T8
1499	<i>spinous process of the 7th cervical vertebra:</i>	C7
1500	<i>sternal notch:</i>	SN
1501	Clavicle	
1502	<i>sternal extremity of the clavicle:</i>	SC
1503	<i>acromial extremity of the clavicle:</i>	AC
1504	Scapula	
1505	<i>angulus inferior:</i>	AI
1506	<i>trigonum spinae:</i>	TS
1507	<i>angulus acromialis:</i>	AA
1508	Humerus	
1509	<i>glenohumeral joint centre:</i>	GHC
1510	<i>lateral epicondyle of the humerus:</i>	EL
1511	<i>medial epicondyle of the humerus:</i>	EM
1512	Pelvis	
1513	<i>right anterior superior iliac spine:</i>	RASIS
1514	<i>left anterior superior iliac spine:</i>	LASIS
1515	<i>right posterior superior iliac spine:</i>	RPSIS
1516	<i>left posterior superior iliac spine:</i>	LPSIS
1517	Femur	
1518	<i>centre of the femoral head:</i>	FH
1519	<i>greater trochanter external surface:</i>	GT
1520	<i>medial epicondyle:</i>	ME
1521	<i>lateral epicondyle:</i>	LE
1522	<i>antero-lateral apex of the patellar surface ridge:</i>	LP
1523	<i>antero-medial apex of the patellar surface ridge:</i>	MP
1524	<i>adductor tubercle:</i>	AT
1525	<i>most distal point of the lateral condyle:</i>	LC
1526	<i>most distal point of the medial condyle:</i>	MC
1527	TibiaFibula	
1528	<i>prominence of the tibial tuberosity:</i>	TT
1529	<i>apex of head of the fibula:</i>	HF
1530	<i>most medial ridge of the medial tibial plateau:</i>	MR
1531	<i>most lateral ridge of the medial lateral plateau:</i>	LR
1532	<i>Gerdy's tubercle:</i>	YT
1533	<i>distal apex of the medial malleolus:</i>	MM
1534	<i>distal apex of the lateral malleolus:</i>	LM
1535	Foot	
1536	<i>upper ridge of the calcaneus posterior surface:</i>	CA
1537	<i>sustentaculum tali:</i>	ST

1538	<i>tuberosity of navicular bone:</i>	TN
1539	<i>dorsal aspect of first metatarsal head:</i>	FM
1540	<i>dorsal aspect of second metatarsal head:</i>	SM
1541	<i>dorsal aspect of fifth metatarsal head:</i>	VM
1542	<i>tuberosity of fifth metatarsal bone:</i>	VT
1543	<i>peroneal trochlea:</i>	PT
1544		

1545 **4. MATLAB code example**

1546 **4.1. Main script**

```
1547 % -----
1548 %% 
1549 % Reference:
1550 % Cereatti et al. (2017). Standardization proposal of soft tissue artefact
1551 % description and data exchange for data sharing in
1552 % human motion measurements. To be published
1553 %
1554 % Grimpampi et al. (2014). Metrics for describing soft-tissue artefact and
1555 % its effect on pose, size, and shape of marker
1556 % clusters. IEEE Trans. Biomed. Eng. 61, 362-367.
1557 %
1558 %%
1559
1560 % Version: 1.1
1561 % Tecla Bonci
1562 % Life and Health Sciences, Aston University, Birmingham, UK
1563 %
1564 % Interuniversity Centre of Bioengineering of the Human
1565 Neuromusculoskeletal
1566 % system, University of Rome "Foro Italico", Rome, Italy
1567 %
1568 % 2016 Dec 29
1569 %
1570 -----
1571 clear all
1572 close all
1573 clc
1574
1575 % select the dataSample_*.mat of interest
1576 [a,b] = uigetfile ('*.mat');
1577 data = load([b,a]);
1578 dataSample = fieldnames(data);
1579 disp(strcat('Load data: ',dataSample))
1580 Seg = fieldnames(data.(dataSample{1}).subj01.trial01);
1581
1582 %% 3D Skin marker trajectories - ACS and ALs - PLOTS
1583 t = [0 0 0]';
1584 R = eye(3);
1585 scale = 100; % scale factor for the axes dimension
1586 linewidth = 2;
1587
1588 % A graph is created for each segment in the structure
1589 for seg = 1:size(Seg,1)
1590
1591     % Skin-marker trajectories in the ACS
1592     % Check that mrk coordinates are available
1593     check =
1594     strcmp(fieldnames(data.(dataSample{1}).subj01.trial01.(Seg{seg})), 'mrk');
1595     if find(check)
1596         figure('Name',strcat((Seg{seg}), ' mrk + ALs -
1597 ARF'), 'NumberTitle','off')
1598         set3Dview
1599         hold on
1600         mrk =
1601         fieldnames(data.(dataSample{1}).subj01.trial01.(Seg{seg}).mrk);
```

```

1602
1603     for i =1:size(mrk,1)
1604         hold on
1605         mrkNow =
1606         data.(dataSample{1}).subj01.trial01.(Seg{seg}).mrk.(mrk{i});
1607         plot3d_tb(mrkNow,'b',5)
1608     end
1609 end
1610
1611 % ACS
1612 my3Dplot(t,R,scale,linewidth)
1613
1614 % Check that AL coordinates are available
1615 check =
1616 strcmp(fieldnames(data.(dataSample{1}).subj01.trial01.(Seg{seg})), 'ALs');
1617 if find(check)
1618     mrk =
1619     fieldnames(data.(dataSample{1}).subj01.trial01.(Seg{seg}).ALs);
1620     for i =1:size(mrk,1)
1621         mrkNow =
1622         data.(dataSample{1}).subj01.trial01.(Seg{seg}).ALs.(mrk{i});
1623         plot3d_tb(mrkNow,'.k',30)
1624         text(mrkNow(1,1),mrkNow(2,1),mrkNow(3,1),...
1625             strcat('\leftarrow -',(mrk{i})), 'FontSize',10)
1626     end
1627 end
1628 axis equal
1629 end
1630
1631 %% STA Parameters for each segment calculated as detailed in the manuscript
1632 for seg = 1:size(Seg,1)
1633     check =
1634     strcmp(fieldnames(data.(dataSample{1}).subj01.trial01.(Seg{seg})), 'mrk');
1635     if find(check)
1636         mrk =
1637         fieldnames(data.(dataSample{1}).subj01.trial01.(Seg{seg}).mrk);
1638         [rmsd, deltap, d] =
1639         STA_Parameters(data.(dataSample{1}).subj01.trial01.(Seg{seg}).mrk,mrk');
1640
1641         figure('Name',strcat('rms(d) and delta p -
1642 ',(Seg{seg})), 'NumberTitle', 'off')
1643         subplot(121)
1644         boxplot([rmsd.mod,rmsd.x, rmsd.y, rmsd.z],
1645 'Labels',{'rms(d)', 'rms(d_x)', 'rms(d_y)', 'rms(d_z)'})
1646         title('rms(d)', 'fontWeight', 'bold', 'FontSize', 14);
1647         ylabel('[mm]', 'FontSize', 12);
1648
1649         subplot(122)
1650         boxplot([deltap.max, deltap.x, deltap.y,
1651 deltap.z], 'Labels',{'deltap_max','deltap_x','deltap_y','deltap_z'})
1652         title('delta p', 'fontWeight', 'bold', 'FontSize', 14);
1653         ylabel('[mm]', 'FontSize', 12);
1654
1655         figure('Name', 'Instantaneous displacement
1656 vector', 'NumberTitle', 'off')
1657         title(strcat('Instantaneous displacement vector -
1658 ',(Seg{seg})), 'fontWeight', 'bold', 'FontSize', 14);
1659         set3Dview
1660         hold on
1661         mrk = fieldnames(d);

```

```

1662     cc = hsv(size(mrk,1));
1663     for i =1:size(mrk,1)
1664         hold on
1665         plot3(d.(mrk{i}) (:,1),d.(mrk{i}) (:,2),d.(mrk{i}) (:,3), '-',
1666 'MarkerSize',2,'color',cc(i,:))
1667     end
1668     xlabel('x [mm]')
1669     ylabel('y [mm]')
1670     zlabel('z [mm]')
1671 end
1672 end
1673
1674

```

1675 ***4.2. Functions***

1676

```

1677 % -----
1678 %% STA Parameters for each segment calculated as detailed in the Cereatti
1679 et al.(2017)
1680 % INPUT
1681 % STA (Structure) Skin-marker trajectories (M01, M02,...)
1682 represented in the relevant ACS
1683 % Each marker trajectory is [nx3]
1684 % mrk (3x3) Name of the skin-markers
1685 %
1686 % OUTPUT
1687 % d Instantaneous displacement vector
1688 % rmsd Root mean square amplitude (rmsd.mod) and its
1689 % components (rmsd.x, rmsd.y, rmsd.z)
1690 % deltap Peak-to-peak amplitude, maximum value (deltap.max)
1691 % and relevant components (deltap.x, deltap.y,
1692 deltap.z)
1693 %
1694 %%
1695
1696 function [rmsd, deltap, d] = STA_Parameters(STA, mrk)
1697
1698 for j = 1:size(mrk,2)
1699     STAnow = STA.(mrk{j});
1700     n = size(STAnow,1);
1701     for k = 1:n
1702         STAvect (k,:) = STAnow(k,:);
1703         STAvectx (k,1) = STAnow(k,1);
1704         STAvecty (k,1) = STAnow(k,2);
1705         STAvectz (k,1) = STAnow(k,3);
1706     end
1707
1708     pmeanx = mean(STAvectx);
1709     pmeany = mean(STAvecty);
1710     pmeanz = mean(STAvectz);
1711
1712     for k = 1:n
1713         D(k,1) = norm(STAvect(k,:) - mean(STAnow));
1714         d.(mrk{j})(k,:) = STAvect(k,:) - mean(STAnow);
1715
1716         dx(k,1) = STAvectx(k,1) - pmeanx;
1717         dy(k,1) = STA vecty(k,1) - pmeany;

```

```

1718     dz(k,1) = STAvectz(k,1) - pmeanz;
1719 end
1720
1721 rmsd.mod(j,1) = rms(D);
1722 rmsd.x(j,1) = rms(dx);
1723 rmsd.y(j,1) = rms(dy);
1724 rmsd.z(j,1) = rms(dz);
1725
1726 % Deltap max
1727 P = STAnow;
1728 [M N] = size(P); % Number of points and number of dimensions
1729
1730 % METHOD 1 (quick, without loops)
1731
1732 if M < 500
1733     % Distances between pairs of points
1734     P = shiftdim(P, -1);      % (1×M×N)
1735     P2 = reshape(P, [M 1 N]); % (M×1×N)
1736     dd = bsxfun(@minus, P, P2); % Distance vectors (M×M×N)
1737     dd = magn(dd, 3); % Scalar distances (M×M)
1738
1739     % Row and column containing maximum value in DD
1740     [dd, rows] = max(dd); % (1×M)
1741     [Deltap, column] = max(dd); % (1×1)
1742
1743 % METHOD 2 (slower, but requires a much smaller amount of memory)
1744 else
1745     dd = zeros(M-1, 1);
1746     ii2 = zeros(M-1, 1);
1747     for i = 1 : (M-1)
1748         next = (i+1) : M;
1749         Deltap = bsxfun(@minus, P(i,:), P(next,:)); % Distances (M-i1×N)
1750         Deltap = magn(Deltap, 2); % Scalar distances (M-i1×1)
1751         [dd(i), j] = max(Deltap);
1752         ii2(i) = i + j;
1753     end
1754
1755     [Deltap, i1] = max(dd);
1756 end
1757
1758 deltap.max(j,1) = Deltap;
1759
1760 deltap.x(j,1) = (max(STAnow(:,1))- min(STAnow(:,1)));
1761 deltap.y(j,1) = (max(STAnow(:,2))- min(STAnow(:,2)));
1762 deltap.z(j,1) = (max(STAnow(:,3))- min(STAnow(:,3)));
1763
1764 end

```

```

1765 % -----
1766 %% Plotting 3-D reference frame axes defined by t and R
1767 %     t (3x1)          Origin position
1768 %     R (3x3)          Orientation of the axes (each column of the
1769 %                         matrix represents an axis)
1770 %     scale (1x1)       Scale factor for axes dimension
1771 %
1772 % The axes are plotted using the following convention:
1773 %     x-axis --> red line
1774 %     y-axis --> green line
1775 %     z-axis --> blue line
1776 % -----
1777 %%
1778
1779 function my3Dplot(t,R,scale,linewidth)
1780     e = t*ones(1,3)+scale*R;
1781
1782     plot3([t(1),e(1,1)], [t(2),e(2,1)], [t(3),e(3,1)], 'r-
1783     ', 'Linewidth', linewidth);
1784     plot3([t(1),e(1,2)], [t(2),e(2,2)], [t(3),e(3,2)], 'g-
1785     ', 'Linewidth', linewidth);
1786     plot3([t(1),e(1,3)], [t(2),e(2,3)], [t(3),e(3,3)], 'b-
1787     ', 'Linewidth', linewidth);
1788 end
1789
1790

```

1791 **References**

- 1792 Abdel-Aziz, Y.I., Karara, H.M., 1971. Direct linear transformation from comparator
1793 coordinates into object space coordinates in close range photogrammetry. In ASP Symp.
1794 Close Range Photogrammetry, pp. 1-19. American Society of Photogrammetry, Falls Church.
- 1795 Akbarshahi, M., Schache, A.G., Fernandez, J.W., Baker, R., Banks, S., Pandy, M.G., 2010.
1796 Non-invasive assessment of soft-tissue artifact and its effect on knee joint kinematics during
1797 functional activity. *J Biomech* 43, 1292–301.
- 1798 Andersen, M.S., Damsgaard, M., Rasmussen, J., Ramsey, D.K., Benoit, D.L., 2012. A
1799 linear soft tissue artefact model for human movement analysis: proof of concept using in vivo
1800 data. *Gait Posture* 35, 606-11.
- 1801 Baltzopoulos, V., 1995. A video fluoroscopy method for optical distortion correction and
1802 measurement of knee-joint kinematics, *Clin Biomech* 10, 85–92.
- 1803 Banks, S.A., Hodge, W.A., 1996. Accurate measurement of three dimensional knee
1804 replacement kinematics using single-plane fluoroscopy. *IEEE Trans. Biomed. Eng.* 43, 638–
1805 649.
- 1806 Barré, A., Thiran, J.-P., Jolles, B.M., Theumann, N., Aminian, K., 2013. Soft tissue artifact
1807 assessment during treadmill walking in subjects with total knee arthroplasty. *IEEE Trans*
1808 *Biomed Eng* 60, 3131–3140.
- 1809 Barré A., Jolles B.M., Theumann N., Aminian, K., 2015. Soft tissue artifact distribution on
1810 lower limbs during treadmill gait: Influence of skin markers' location on cluster design. *J*
1811 *Biomech* 48, 1965-71.
- 1812 Begon, M., Monnet, T., Lacouture, P., 2007. Effects of movement for estimating the hip
1813 joint centre. *Gait Posture* 25, 353-359.
- 1814 Benoit, D.L., Ramsey, D.K., Lamontagne, M., Xu, L., Wretenberg, P., Renström, P., 2006.
1815 Effect of skin movement artifact on knee kinematics during gait and cutting motions
1816 measured in vivo. *Gait Posture*. 24, 152-64.
- 1817 Besl, P.J., McKay, H.D., 1992. A method for registration of 3-D shapes. *IEEE Trans PAMI*
1818 14, 239–256.
- 1819 Bonci, T., Camomilla, V., Dumas, R., Chèze, L., & Cappozzo, A., 2014. A soft tissue
1820 artefact model driven by proximal and distal joint kinematics. *J Biomech* 47(10), 2354-2361.

- 1821 Bonnefoy-Mazure, A., Slawinski, J., Riquet, A., Lévèque, J. M., Miller, C., & Cheze, L.,
1822 2010. Rotation sequence is an important factor in shoulder kinematics. Application to the elite
1823 players' flat serves. *J Biomech*, 43(10), 2022-2025.
- 1824 Cappozzo, A., Della Croce, U., Catani F, Leardini, A., 1994a. Anatomical Frame
1825 Definition and Determination. CAMARC II Internal Report.
- 1826 Charbonnier, C., Chagué, S., Kolo, F.C., Chow, J.C.K., Lädermann, A., 2014. A patient-
1827 specific measurement technique to model shoulder joint kinematics. *Orthop Traumatol Surg*
1828 *Res* 100, 715–719.
- 1829 Dal Maso, F., Raison, M., Lundberg, A., Arndt, A., Begon, M., 2014. Coupling between
1830 3D displacements and rotations at the glenohumeral joint during dynamic tasks in healthy
1831 participants. *Clin Biomech* 29, 1048–55.
- 1832 Dal Maso F., Blache Y., Raison M., Lundberg A., Begon, M., 2016. Glenohumeral joint
1833 kinematics measured by intracortical pins, reflective markers, and computed tomography: A
1834 novel technique to assess acromiohumeral distance. *J Electromyog Kinesiol* 29, 4-1
- 1835 Della Croce, U., Cappozzo, A., 2000. A spot check for estimating stereophotogrammetric
1836 errors. *Med. Biol. Eng. Comput.* 38, 260-266.
- 1837 Eckhoff, D.G., Bach, J.M., Spitzer, V.M., Reinig, K.D., Bagur, M.M., Baldini, T.H.,
1838 Flannery, N.M.P., 2005. Three-dimensional mechanics, kinematics, and morphology of the
1839 knee viewed in virtual reality. *J Bone Joint Surg.* 87, 71–80.
- 1840 Gronenschild, E., 1997. The accuracy and reproducibility of a global method to correct for
1841 geometric image distortion in the X-ray imaging chain. *Med Phys* 24, 1875–1888.
- 1842 Hatze, H., 1988. High-precision three-dimensional photogrammetric calibration and object
1843 space reconstruction using a modified DLT approach. *J. Biomech* 21, 533-538.
- 1844 Lu, T.W., Tsai, T.Y., Kuo, M.Y., Hsu, H.C., Chen, H.L., 2008. In vivo three-dimensional
1845 kinematics of the normal knee during active extension under unloaded and loaded conditions
1846 using single-plane fluoroscopy. *Med Eng Phys* 30, 1004–1012.
- 1847 Miranda, D.L., Rainbow, M.J., Leventhal, E.L., Crisco, J.J., Fleming, B.C., 2010.
1848 Automatic determination of anatomical coordinate systems for three-dimensional bone
1849 models of the isolated human knee. *J Biomech* 43, 1623-6.
- 1850 Moro-oka, T.A., Hamai, S., Miura, H., Shimoto, T., Higaki, H., Fregly, B.J., Iwamoto, Y.,
1851 Banks, S.A., 2007. Can magnetic resonance imaging-derived bone models be used for
1852 accurate motion measurement with single-plane three-dimensional shape registration. *J Ortho*
1853 *Res* 25, 867–72.

- 1854 Paul, J.P., 1992. Terminology and Units. Deliverable n. 4, C.E.C. Program AIM, Project
1855 A-2002, CAMARC-II.
- 1856 Penney, G.P., Weese, J., Little, J.A., Desmedt. P., Hill, D.L.G., Hawkes, D.J. 1998. A
1857 comparison of similarity measures for use in 2D–3D medical image registration, IEEE T Med
1858 Imaging, 17, 586–595.
- 1859 Ramsey, D.K., Wretenberg, P.F., Benoit, D.L., Lamontagne, M., Nemeth, G., 2003.
1860 Methodological concerns using intra-cortical pins to measure tibiofemoral kinematics. Knee
1861 Surg Sport Tr A 11, 344–9.
- 1862 Soderkvist, I. and Wedin, P.A., 1993. Determining the movements of the skeleton using
1863 well-configured markers. J. Biomech 26, 1473-1477.
- 1864 Winter, D.A., 1990. Biomechanics and Motor Control of Human Movement. J. Wiley,
1865 New York.
- 1866 Wood, G.A. and Marshall, R.N., 1986. The accuracy of DLT extrapolation in three-
1867 dimensional film analysis. J. Biomech 9, 781-785.
- 1868 Wu, G., van der Helm, F.C.T., Veeger, H.E.J., Makhsous, M., Van Roy, P., Anglin, C.,
1869 Nagels, J., Karduna, A.R., McQuade, K., Wang, X., Wernerl, F.W., Buchholz, B., 2005. ISB
1870 recommendation on definitions of joint coordinate systems of various joints for the reporting
1871 of human joint motion–Part II: shoulder, elbow, wrist and hand. J. Biomech 38, 981–992